Analytical Considerations for Residual Stress Best Practices and Case Studies

July 2018

FORWARD

The fatigue life benefits of engineered residual stress processes such as cold expansion of fastener holes and laser shock peening are well known and have been demonstrated by test in countless applications over the past few decades. Typical USAF methodologies do not directly account for the effects of residual stress and consequently often do not accurately replicate the fatigue life improvement from these processes. This, and the lack of in-situ process validation, have contributed to the USAF hesitation to take advantage of these benefits in damage tolerance analyses. Recently, AFRL and the A-10 and T-38 Aircraft Structural Integrity Program (ASIP) offices have engaged in a concerted effort to move to a physics based analytical approach to account for engineered residual stress in Damage Tolerance Assessments (DTAs).

To support this initiative, a specific task under the A-10 ASIP Modernization VI TLPS program, PWS 3.6.4 Crack Growth Analyses in Residual Stress Fields, was established with Northrop Grumman and Hill Engineering LLC to continue development of a fundamental analytical framework for incorporation of engineered residual stress. One key aspect of this initiative is to provide best practices, lessons learned, and case studies to the larger community. This best practices and case studies document is specifically developed to meet this initiative. This initial release establishes a framework, with the opportunity to add additional information and case studies from the community as methods mature and develop.

This document is broken down into specific chapters. Chapter I provides an introduction to fatigue, damage tolerance, residual stress, residual stress determination techniques, and historical analytical approaches to incorporate residual stress. Chapter II provides details on analytical processes used to incorporate residual stress into damage tolerance assessments. Chapter III provides details for other considerations, such as fatigue testing, non-destructive inspections, and risk assessment considerations. Chapter IV provides benchmark cases for baseline comparisons analysts can use to compare their predictions. Chapter V details several case studies where engineered residual stress has been incorporated into damage tolerance assessments.

As weapon systems continue to age, sharpened analytical tools are paramount to sustain and efficiently manage these USAF fleets. Engineered residual stress, and the ability to accurately predict their benefits (and limitations), must be a part of the structural integrity engineer’s toolkit.

ACKNOWLEDGEMENTS

Appreciation is expressed to all those that contributed to the development of this best practices document, in particular the A-10 ASIP and analysis teams as well as Hill Engineering and Northrop Grumman.

TABLE OF CONTENTS

LIST OF FIGURES

LIST OF TABLES

LIST OF ABBREVIATIONS AND ACRONYMS

The following is a list of all acronyms and abbreviations likely used in this document:

ASIP	Aircraft Structural Integrity Program
CDRL	Contract Deliverable Requirements List
Cx	Cold expansion
DTA	Damage Tolerance Assessment
FMEA	Failure Modes and Effects Analysis
FSMP	Force Structural Maintenance Plan
HAFB	Hill Air Force Base
IAW	In Accordance With
IFS	Initial Flaw Size
Mod III	Modernization III program
Mod V	Modernization V program
LPB	Low Plasticity Burnishing
LSP	Laser Shock Peening
NGC	Northrop Grumman Corporation
NGAS	Northrop Grumman Aircraft Systems
NGTS	Northrop Grumman Technical Systems
PWS	Performance Work Specification
RS	Residual stress
SPO	System Program Office
SSI	Scheduled Structural Inspection
TLPS	Thunderbolt Life-cycle Program Support
USAF	United States Air Force

CHAPTER I - INTRODUCTION

1. *HISTORY OF FATIGUE*

Fatigue is the process of progressive degradation of a material subjected to fluctuating stress and strains, and often involves the development and propagation of cracks. Given the right conditions, cracks can nucleate, propagate, and ultimately result in fracture of the component or structure. Our understanding of failure mechanisms, and the related design philosophies, have evolved over time. Traditional design focused on static strength capability, however, failures in the early 1800s indicated components exposed to cyclic loads were failing well below static load limits. Schutz[1] provides a comprehensive overview of the history of fatigue, which highlights the key individuals and events that molded our understanding of fatigue failures (paraphrased below). The earliest identified fatigue investigations began with Albert[2] who was a Royal Hannoverian “Oberbergrat” (civil servant for mines). He published the first fatigue test results, as he sought to understand failures of conveyor chains in service in the Clausthal mines. The term “fatigue” was first mentioned by the Englishman Braithwaite in 1854[3], where he describes many service failures of brewery equipment, water pumps, propeller shafts, crankshafts, railway axles, levers, cranes, etc. Allowable stress for fatigue loaded components are also discussed in his paper. In this period of time, many disastrous railroad accidents due to fatigue occurred; for example, on 5 October 1842, a locomotive axle broke at Versailles, claiming the lives of 60 people[4]. The failures became so prevalent that an English newspaper reported the “most serious railway accident of the week”. The majority of these cases were due to fatigue failures of axles, couplings, and rails claiming many lives.

In Germany in the 1850s and 1860s, Wohler investigated the cyclical failure behavior of railway axles. He focused on measuring the service loads of railway axles with deflection gages he designed himself as well as developing many laboratory fatigue tests using cyclic loading. Ultimately, his work culminated into characterizing stress versus life (S-n) diagrams, demonstrating how fatigue life decreases with increased stress amplitude. These experiments were considered the first systematic investigation of fatigue, and Wohler has often been considered the “father” of systematic fatigue tests. Continuing Wohler’s classical work, Gerber, Goodman, and others investigated the influence of mean stress on fatigue behavior. Bauschinger in 1886 demonstrated a change in the elastic limit by often repeated stress cycles, coined the Bauschinger effect, which formed the basis for the hypotheses of Manson and Coffin in the 1950s which are still utilized today in the field of Low Cycle Fatigue. These investigations established the foundation of understanding cyclic softening and hardening of metals.

In the early 1900s, a great deal of research contributed to the understanding of fatigue mechanisms. Of significance was Griffith’s publication[5] of his theoretical calculations and experiments on brittle failure of glass. He found that the strength of glass was related to the size of microscopic cracks in the material. This fundamental understanding established the foundation for fracture mechanics as we know it today. In the 1920s Palmgren[6] developed a damage accumulation hypothesis for fatigue life predictions under variable amplitude loading. Langer[7] and Miner[8] published similar work on damage accumulation, resulting in the Palmgren-Miner linear damage model prevalent today.

The 1950s introduced the age of commercial jet air transportation, with the de Havilland “Comet”, introduced as the first commercial jet aircraft of the western world. This introduction also ushered in the need to understand the influence of fatigue. The Comet experienced multiple in-service failures of the fuselage at “square” window cutouts. Small fatigue cracks nucleated and propagated from the corners of the windows and ultimately caused the catastrophic failure of the fuselage. In 1958, the USAF experienced (5) catastrophic failures of B-47s as a result of fatigue. These failures identified several shortcomings in design, notably material selection, management of stress concentrations, and fail-safe concepts. They also highlighted considerations for full-scale testing, establishing the foundation for full-scale fatigue test methods still utilized today. Fail-safe and safe-life design considerations became more common. This also brought about the advent of closed-loop servohydraulic test systems, which allowed better simulation of fatigue loading.

In 1958, Irwin[9] built upon Griffith’s work and introduced the stress intensity factor (K) as the determining factor for static strength in a cracked state. If K reaches a certain point, the critical fracture toughness, rapid fracture occurs. This finding was the birth of Linear Elastic Fracture Mechanics (LEFM). In the early 1960s, ASTM began forming focused committees on the subjects of Fatigue and Fracture and have contributed immensely to the standardization of methods. Also, at the same time, Paris[10] showed an empirical relationship between the fatigue crack growth rate, da/dN, and the stress intensity factor range, ΔK through the mid-range of the crack growth data.

In the late 1960s, the catastrophic crash of a USAF F-111 aircraft after only 100 flight hours of service was the catalyst for the inception of damage tolerance design requirements. The F-111 failure was a result of utilization of high strength materials with limited tolerance for cracks. A pre-existing crack in a wing attach lug, manufactured from D6AC ultra high strength steel, undetected during manufacturing, grew to failure and resulted in loss of the aircraft. This failure highlighted the need to recognize the existence of flaws in the material and incorporate damage tolerant materials into aircraft designs. As a result, in 1974 the USAF formally adopted damage tolerance requirements for the design of new military aircraft, with the issue of MIL-A-83444.

Damage tolerance is defined as the ability of a structure that contains cracks or anomalies in the material to resist fracture. This design philosophy assumes that there are inherent cracks in the material and fracture mechanics analysis and testing are used to determine whether these cracks will grow to a critical size resulting in fracture of the part. The objective of the damage tolerance approach is to detect cracks in critical parts before they propagate to failure. The three key elements required by the damage tolerance design philosophy are the fatigue crack growth behavior, residual strength, and nondestructive inspections. As shown in Figure 1, the combination of these three elements ensures the structural reliability of components.

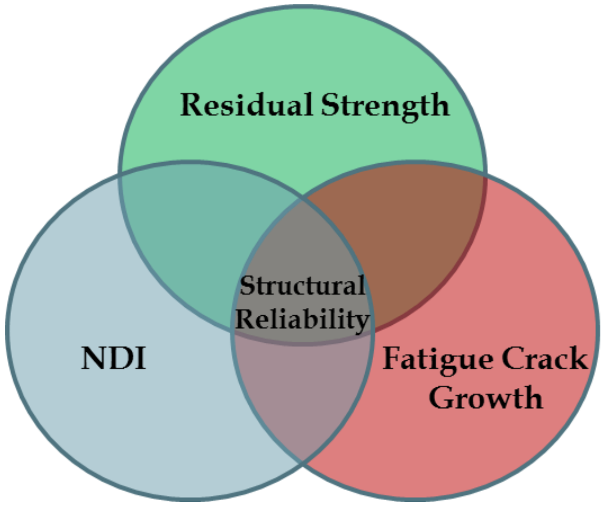

Figure 1 – Fundamental elements of damage tolerance

Recent fatigue research has focused on Holistic Structural Integrity (HOLSIP) concepts, considering all factors that influence the integrity of materials and structures, augmenting and enhancing the traditional safe life and damage tolerance paradigms. Physics based approaches accounting for both cyclic and time dependent environmental effects in assessing structural integrity are a primary focus.

The basic material microstructure and surface integrity resulting from manufacturing are built into physics-based models in conjunction with other intrinsic and extrinsic factors such as residual stress, environmental/chemical exposure, maintenance damage, and age degradation in service[11].

2. *RESIDUAL STRESS*

The idea of inducing a residual compressive stress into the surface of a part to improve its strength and durability is not new. Ancient sword makers aggressively hammered and worked weapons to improve their strength. Village blacksmiths practiced the art of surface working in making wagon and buggy springs, axles, and other heavily loaded parts. Similarly, mill and ship shafts were cold worked by the application of small rollers at high pressure after machining because of the greater strength that was known to result[12]. Within recent years, surface compressive residual stress has been used to improve the fatigue characteristics of components. Processes such as shot peening, laser shock peening (LSP), and cold expansion of holes have been implemented to improve fatigue characteristics at different locations in parts. Compressive residual stress has been implemented to mitigate the effects of FOD damage, fatigue, fretting fatigue, stress corrosion cracking, corrosion fatigue, etc.

What is a residual stress? Stephens[13] defines residual stress as “self-equilibrating stress” because they are in equilibrium within the part and “residual stress” because they remain from a previous operation. ASTM E6 defines residual stress as the “stress in a body which is at rest and in equilibrium and at uniform temperature in the absence of external and mass forces.”

Management of residual stress, whether a direct result of manufacturing processes or engineered into the design, is no doubt a critical component to efficient structural integrity management moving into the future. Residual stress is present in most manufactured parts and its impact on manufacturing conformance (part distortion) and long-term fatigue durability cannot be understated.

3. *RESIDUAL STRESS INDUCING PROCESSES*

Residual stress is introduced by many common mechanical and thermal processes. Its introduction can be intentional, as is the case for cold expanded fastener holes, or inadvertent, as is the case of differential cooling during welding, grinding, or heat treatment of thick sections. The affected region can vary from very shallow (shot peening) to near surface (laser shock peening) to through the bulk of the material (forming).

3.1. *Mechanical methods*

When external forces acting on a body create inhomogeneous plastic deformation the resulting elastic "spring back" creates residual stress. The permanent strains induced in the plastically deformed regions of the part are in direct competition with the elastically strained regions of the part, creating internal self-equilibrating strains and stress. Figure 2 details a simple example of the bent beam, identifying the plastic and elastic regions of the part and resulting residual stress after unloading[14]. In all cases of residual stress, there are always compensating compressive and tensile components creating equilibrium in the part. You cannot have one without the other.

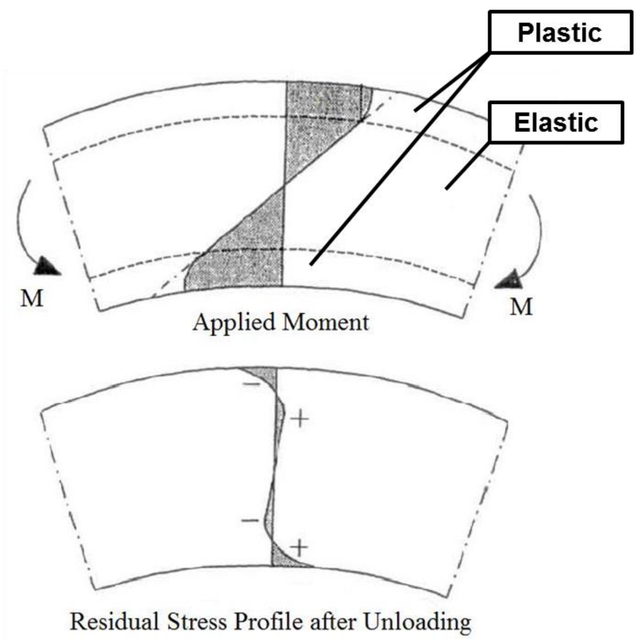

Figure 2 – Inhomogeneous plastic deformation

Many mechanical methods, whether intentional or as an artifact of a manufacturing process, can create residual stress. Of particular importance are the methods that have been developed throughout the years to tailor compressive residual stress to gain fatigue, durability, and damage tolerant benefits. The primary techniques include shot peening, surface rolling (threads), Low Plasticity Burnishing

(LPB), Cold Expansion (Cx) of fastener holes, and Laser Shock Peening (LSP). Residual stress can also be created during production forming processes.

3.1.1. ***Shot peening***

Shot peening was discovered by accident in the automotive industry during research and development to improve the fatigue life of valve springs. By the late 1930’s, highway and engine speeds had increased significantly and valve springs could not keep up with the pace. As a result, the automotive industry was researching methods to improve the fatigue life of valve springs. During testing and research, General Motors discovered that valve springs blast cleaned with round steel shot had a marked improvement in fatigue life. This was the origin of shot peening as we know it. Walz[15] wrote a brochure on the fatigue life of springs detailing the influence of shot-peening time, shot size, type of peening machining, etc.

Shot peening is a process used to produce a compressive residual stress in the surface of a part by mean of impacting the surface with shot (round metallic, glass, or ceramic) with force sufficient to create plastic deformation (depiction shown in Figure 3). Each piece of shot acts as a tiny peening hammer, imparting into the surface a small indentation[16].

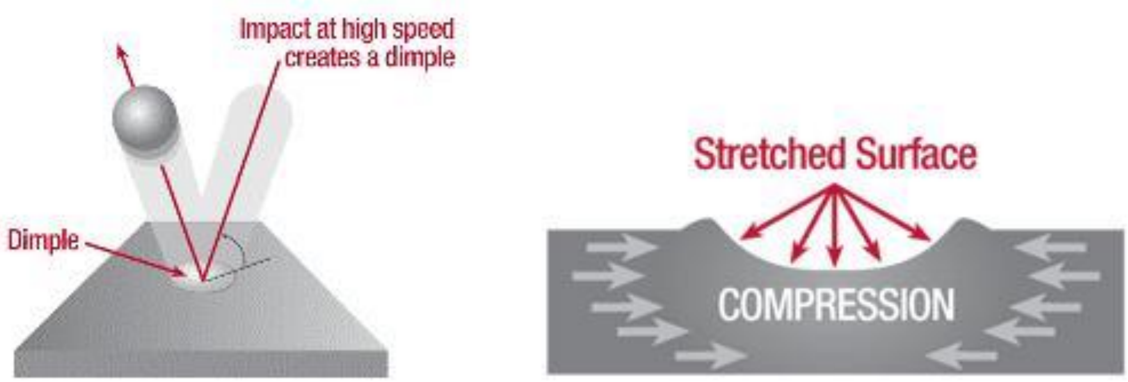

Figure 3 – Illustration of Shot Peening Process[16]

3.1.2. ***Surface rolling***

Surface rolling is the second most widely used mechanical process producing beneficial residual stress, most notably to form threads for bolts and screws. Heywood[17] had reported a 50 percent increase in fatigue life for high strength steel bolts with rolled threads compared to cut or ground threads. Rolling is also used to produce compressive residual stress in the fillets of components such as crankshafts, axles, gear teeth, turbine blades, and between the shank and head of bolts[13].

3.1.3. ***Low plasticity burnishing***

Low plasticity burnishing (LPB) is a CNC controlled process in which a high modulus ball is rolled over a metal surface with a high normal force (Figure 4). The contact stress in the metal caused by the ball plastically deforms the surface of the metal and induce surface residual compressive stress. The ball is supported in a spherical hydrostatic bearing and the machine tool's coolant is used to pressurize the bearing and "float the ball". The tool path and normal force can be controlled to give a prescribed residual stress profile in the surface of the metal. As stated by Migala and Jacobs[18], LPB can produce residual compressive stress as deep as 0.040" (1mm) into the surface of the material with very low coldwork (equivalent true plastic strain), less than 5%. Also, the LPB process has the added benefit of smoothing out the surface finish – a mirror finish can be achieved in some cases.

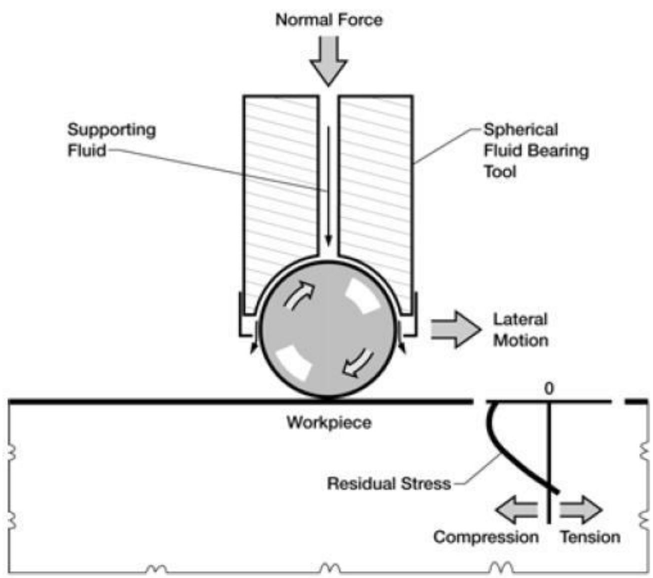

Figure 4 – Low Plasticity Process Schematic[18]

3.1.4. ***Cold expanded fastener holes***

By far, the most frequent source of fatigue problems in aircraft structures are fastener holes. Manufacturing and other defects are common at holes and during aircraft operation the adverse effects of these defects is magnified by high stress concentrations associated with holes, which leads to fatigue cracks. Several methods were developed to try to mitigate these effects. The most common, split-sleeve cold expansion, conceived by Boeing Company and later developed by Fatigue Technology Incorporated (FTI), involves pulling a tapered mandrel, pre-fitted with a lubricated split sleeve, through the hole (Figure 5). The mandrel and sleeve are designed to generate a prescribed amount of radial plastic deformation, which creates a state of biaxial residual compressive stress spanning between one radius to one diameter beyond the edge of the hole.

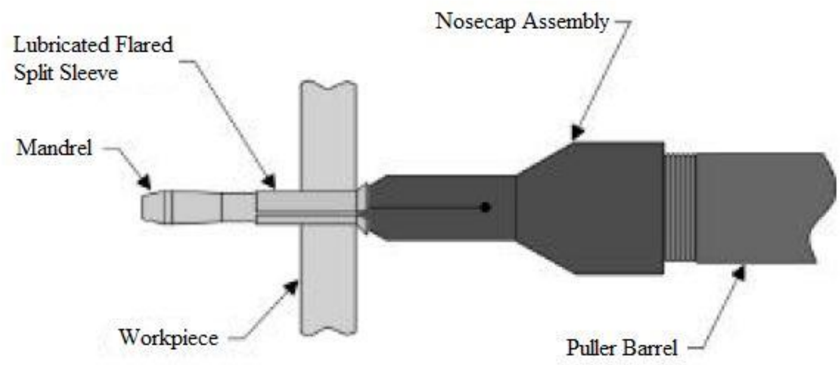

Figure 5 – The FTI Split Sleeve Cold Expansion System[19]

A similar method, patented by West Cost Industries in 1983, does not use disposable sleeves. Instead it uses a longitudinally split mandrel, allowing it to partially collapse to facilitate insertion into the hole. A small pilot is pushed through the inner diameter of the mandrel, retaining the splits of the mandrel in a solid position as it is withdrawn back through the hole, creating a compressive stress radially around the hole.

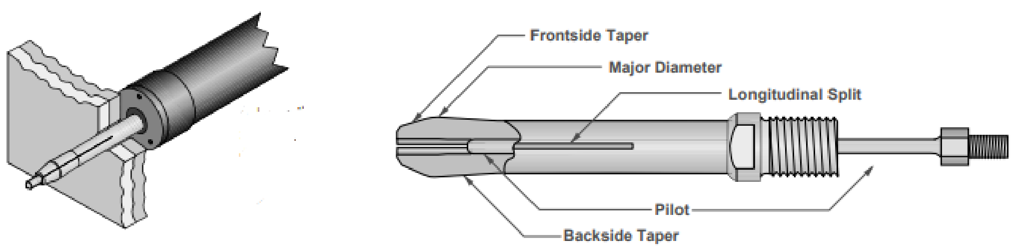

Figure 6 – The WCI Split Mandrel Cold Expansion System[20]

3.1.5. ***Laser shock peening***

Laser peening is an emerging surface treatment technology that was developed during the late 1960's and early 1970's[21,22,23] and has recently emerged as a viable commercial practice[24]. Like other similar surface treatments, laser peening is used to generate compressive residual stress on the surface of a part. This has been shown to inhibit failures caused by fatigue[25] and stress corrosion cracking[26]. The depth of residual stress produced by laser peening (typically >0.04 inch[24,25] or 1 mm) is significantly greater than that produced by other processes (e.g., shot peening produces compressive residual stress to a few thousandths of an inch[27]), which provides added performance gains.

To fix ideas, it is useful to describe the laser peening process (Figure 7). First, a protective layer is applied to the surface; this is called the ablative layer because its surface is ablated off during treatment. Typical ablative layer materials include opaque tape or paint[28]. Next, a transparent inertial tamping layer is applied over the ablative layer, which acts to confine the expansion of the high-pressure plasma to be generated by a laser pulse and greatly increases the effectiveness of the laser peening treatment[29]. A stream of flowing water is typically used for the inertial tamping layer. After these two surface layers are in place, the laser peening process can be carried out.

Laser peening uses a pulsed laser to generate high-pressure plasma on a small region of the part surface. The laser is fired at the material and the photons in the laser beam pass through the transparent inertial tamping layer and are absorbed by the opaque ablative layer forming a high-pressure plasma. The expansion of the plasma is confined by the inertial tamping layer, which further increases the pressure on the surface. This causes a shock wave to travel through the material resulting in plastic deformation (and eventually compressive residual stress).

Laser peening is applied in a spot by spot manner with typical spot dimensions ranging from around 0.04 inch on a side[30] up to 0.40 inch[25] (round or rectangular). Multiple layers of laser peening are commonly used to help ensure that there is uniform coverage and to increase the depth of the compressive residual stress[31]. A layer of laser peening refers to a nominal 100% coverage of the treatment area with a slight overlap between successive spots. In most cases the ablative layer is replaced between peening layers.

Notable damage tolerance benefits have been realized for LSP versus traditional shot peen methods. Figure 8 details a comparative study of LSP versus shot peening implemented on the leading edge of a F101-GE-102 fan blade. For this particular application, LSP demonstrated an approximate 2x life increase over high intensity shot peening.

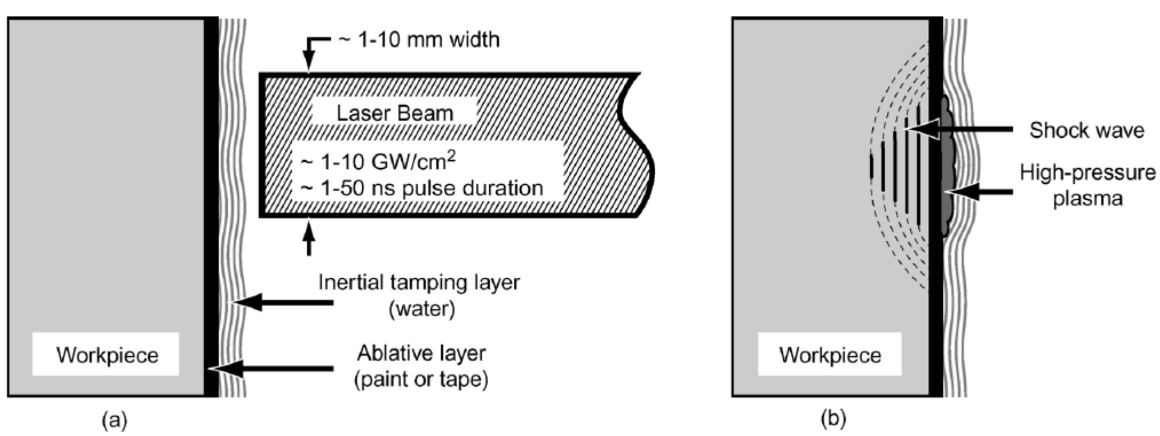

Figure 7 – Schematic of Laser Peening Process

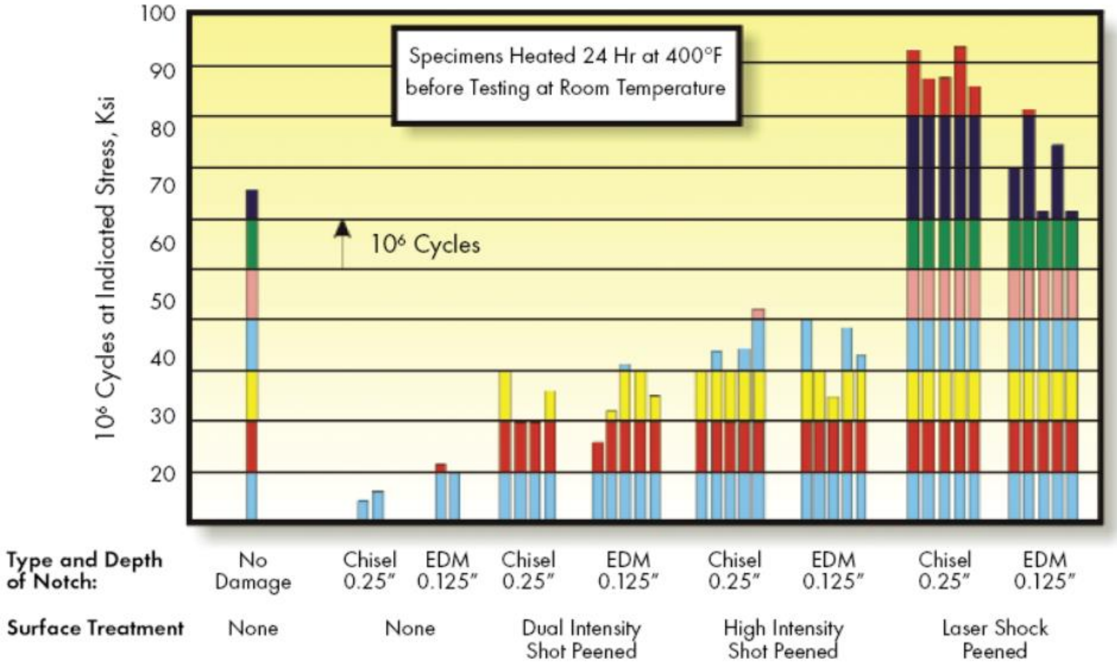

Figure 8 – Comparison of Laser Peen and Shot Peen Processes on the Leading Edge of F101-GE-102 Fan Blade[32]

3.1.6. ***Manufacturing processes***

Various forming processes are utilized in the production of parts. During these processes, the material is plastically deformed to produce desired shapes, grain orientation, or strength properties. During forming operations, no material is removed, the material is deformed and/or displaced. Forming process examples include forging, extruding, rolling, hot forming, cold forming, and peen forming. Residual stress is a primary design factor for forming operations. If left unconsidered, this stress will often cause manufacturing distortion problems and can result in long-term fatigue failures.

Forging, rolling, and other metal production processes (including additive manufacturing) are intended to produced desirable material properties, however, can often create residual stress. Process steps, such as those for 7000 series aluminum: solution heat treatment, quench, cold work stress relieving, and artificial age can each contributed to residual stress. There residual stress can cause significant, and often unexpected, distortion of material as a part is machined from its preform (forging or plate).

For example, Figure 9 shows the distribution of residual stress through the thickness of a typical stress relieved 7000 series aluminum plate. Even though the magnitude is small, on the order of ±20 MPa (3 ksi) in the rolling direction and ±10 MPa (1.5 ksi) in the long transverse direction, residual stress in rolled plate may cause significant distortion. Furthermore, residual stress can concentrate at machined features in the final part, like fillets and holes, and negatively affect fatigue and corrosion performance.

The fabrication of integral components can use high speed milling, where high material removal rates result from a combination of high spindle speeds and high feed rates. At the present time, one of the biggest limitations of high speed milling of integral structures is distortion. Gross distortions, like that in Figure 10, arise from residual stress in the preform (forging or plate), which redistribute as material is removed. In addition, the machining process itself induces residual stress in a thin surface layer, which can drive additional distortion in areas of thin cross section.

For illustrative purposes, a residual stress analysis was performed to quantify the expected distortion of a fictional, but representative, aerospace part (Figure 11) when machined from a plate containing the initial residual stress shown in Figure 9. The analysis shows that there is significant distortion of the machined part from these relatively low levels of residual stress (Figure 12). The distortion arises because the part is asymmetric about the thickness of the plate, which is a common layout for integral structure. Small stresses cause large distortion because of the significant amount of material removed during machining, the lack of stiffness of the part relative to out of plane bending, and the out of plane bending caused by the remaining residual stress. The illustrative analysis confirms that small residual stress can produce significant distortion, and that available analysis tools can predict the scale of such distortions.

Excessive distortion is a concern for aerospace part production and can lead to the introduction of fit-up stress during assembly, which can result in improper joints/connections, and can result in parts being rejected.

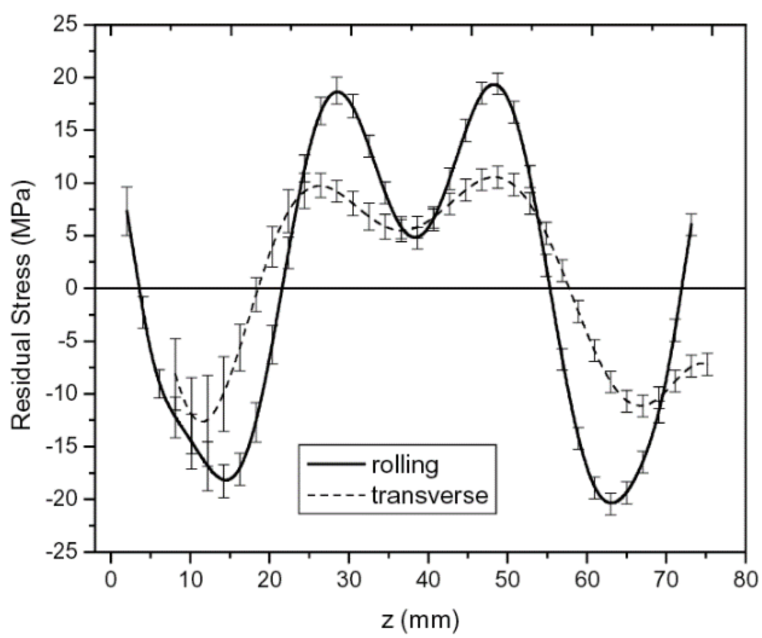

Figure 9 – Representative bulk residual stress distribution in a 3.0-inch-thick plate of 7050-T7451 measured using the slitting method [Prime and Hill 2002]

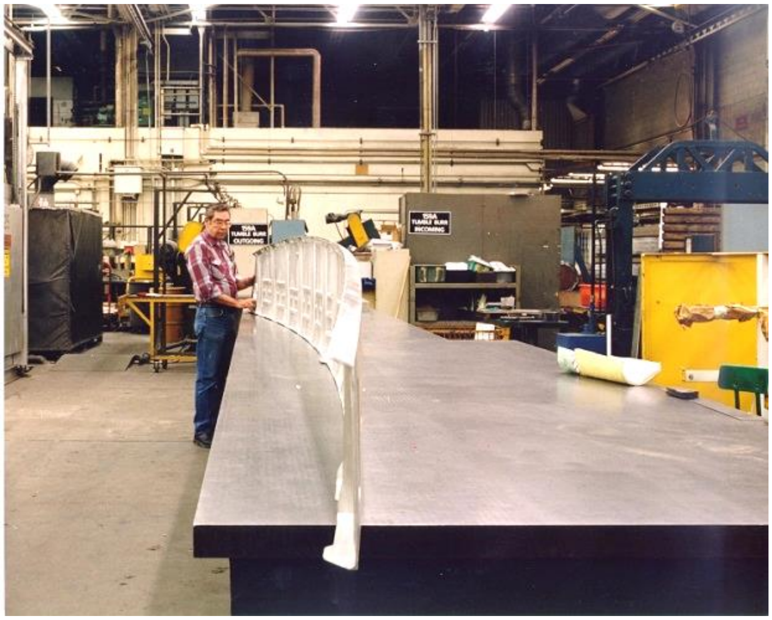

Figure 10 – Photograph of a distorted part produced by high speed milling

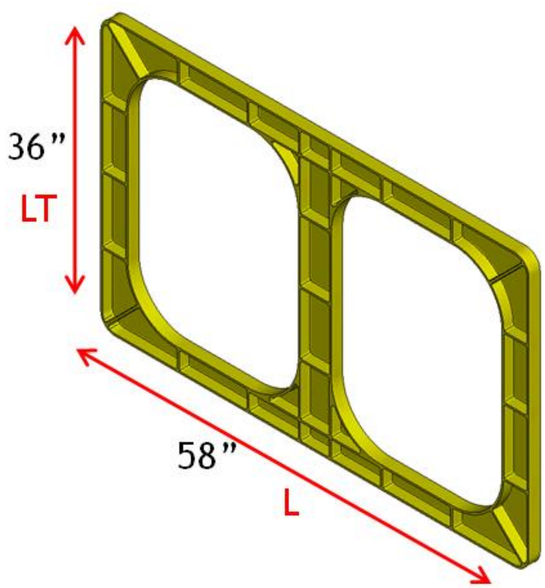

Figure 11 – Illustration of a simplified aerospace component used for scoping analysis

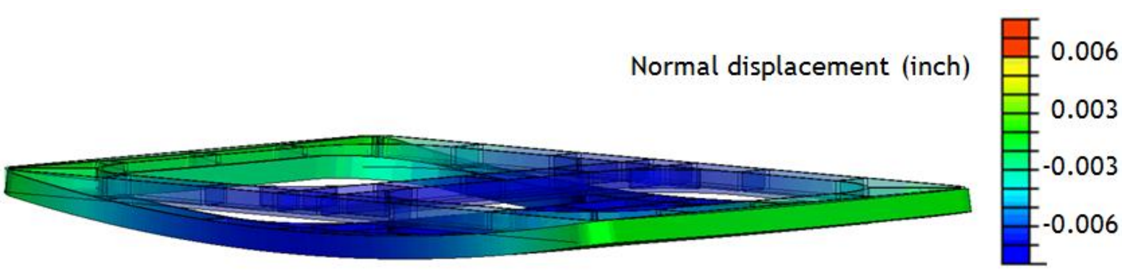

Figure 12 – Illustration of distortion resulting from removal of the simplified aerospace component from aluminum plate containing typical levels of residual stress (deformations exaggerated)

3.1.7. ***Mechanical methods – key characteristics***

Each of the residual stress-inducing mechanical methods has their own unique applicability, resultant residual stress, and effects on part distortion as well as its impact on associated durability and damage tolerance. A brief summary of these key characteristics is detailed in Table 1.

Table 1 – Mechanical methods - key characteristics

Mechanical Method	Typical Applications	Typical Depth of Residual Stress	Durability Impact	Damage Tolerance Impact
Shot Peening	Widespread – Surface of Parts	~ 0.002” - 0.008”	Yes	Minimal
Surface Rolling	Rolled Threads, Gear Teeth, Fillets	~ 0.04”	Yes	Yes
Low Plasticity Burnishing	Fan Blades, Radii	~ 0.04”	Yes	Yes
Cx Holes	Critical Fastener Holes	~ 1 radius	Yes	Yes
Laser Shock Peening	Critical Geometric Features	~ 0.04”	Yes	Yes
Manufacturing Processes	Widespread – Part Manufacturing	Surface to Full Field	Yes	Yes

3.2. *Thermal methods*

Thermal processes are often a key component in the process steps to manufacture parts. These processes might include casting, forging, hot-rolling, injection molding, welding, quenching and tempering, hardening, and carburizing. For all of these processes, controlling temperature and cooling rates impacts the microstructure, strength properties, and residual stress within the component. For residual stress, the primary driver is differential cooling during solidification and cooldown of metal. As the material contracts during cooling, if it's not fairly uniform throughout the component residual strain and stress result. Extensive focus is given to controlling cooling to mitigate part warpage and residual stress.

3.3. *Other methods – manufacturing (machining, grinding, etc.)*

Manufacturing of parts can sometime have unintended impacts on part distortion and/or residual stress. Several notable examples include residual stress induced by aggressive machining or grinding of parts. In a basic sense, these processes are akin to the thermal methods discussed above, where the aggressive processes create excessive heat that exceeds the temperature that results in microstructural changes for the particular material. Also, as a side note, other deleterious effects such as embrittlement, heat affected zone, recast layer, and microcracking can occur as a result of aggressive manufacturing methods.

3.4. *Plastic deformation, strain hardening, and residual stress relaxation*

As discussed in the previous section, mechanical methods create residual stress as a result of inhomogeneous plastic deformation. This plastic deformation impacts the material on a microstructural level, creating elongated grains, increased dislocation density and entanglement, and re-orientation of the grains relative to the direction of applied stress. Figure 13 details an example of the change in dislocation density with increased plastic deformation. The net effect is an increase in stored internal energy and strain hardening of the material. This is particularly important when considering stress relaxation, which can occur at "elevated temperatures". Stress relaxation is a function of stored internal energy and percent cold work and is most likely to occur in steep residual stress gradients near the surface and areas of higher amounts of plastic distortion and internal energy.

Figure 14 illustrates a comparison of residual stress profiles and percent coldwork distributions for an Inconel 718 steel surface processed using shot peening, laser shock peening, and low plasticity burnishing methods. The residual stress profile for shot and gravity peening compared to laser shock peening and low plasticity burnishing has similar maximum residual stress but their residual stress profile depths are much shallower. The percent coldwork was determined using x-ray diffraction line broadening, which indicates a greater percent coldwork at the surface for shot peen versus the other processes. As a result, residual stress inducing processes such as shot peening are comparably more susceptible to residual stress relaxation at "elevated temperatures" versus processes that produce relatively deeper residual stress profiles and less coldwork at the surface of the material.

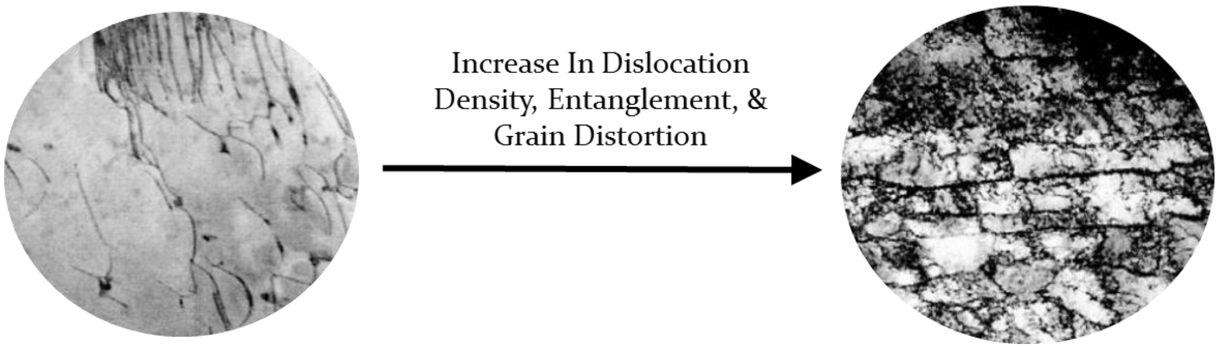

Figure 13 – Example of Change in Dislocation Density with Increased Plastic Deformation[33]

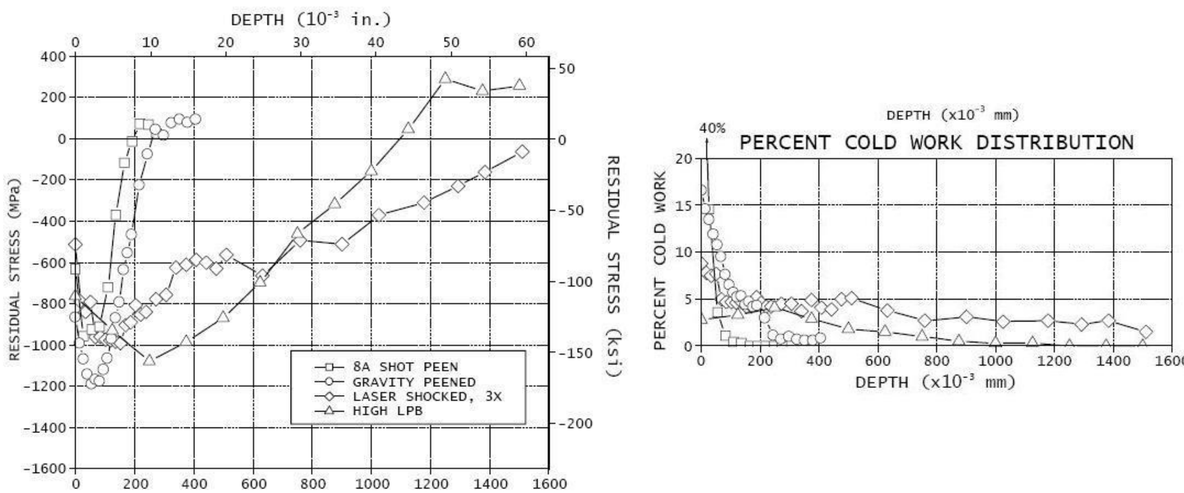

Figure 14 – Residual Stress and % Cold Work Profiles for Several Residual Stress Processes[34]

4. *RESIDUAL STRESS DETERMINATION*

4.1. *Residual stress determination overview*

Residual stress cannot be measured directly. Typical approaches measure strains or deformation then calculate residual stress profiles based on relevant assumptions and models. Residual stress determination techniques can be classified into three main categories: diffraction (neutron, x-rays), mechanical (cut, deform), and other methods (Barkhausen noise, ultrasonic, thermoelastic, photoelastic). Each category and specific technique has advantages and disadvantages. It is important to select the method/s that are best suited for the needs of the application. Consideration should be given to the following parameters:

- Part geometry (e.g., shape, size, access, and handling)
- Residual stress field quantities to be measured (e.g., spatial locations and components of the residual stress tensor)
- Expected features in the residual stress distribution (e.g., gradients, 2D and 3D spatial variations)
- Required accuracy/uncertainty
- Depth of residual stress to be measured
- Material properties (e.g., isotropic, anisotropic, spatial property variations, microstructural complications)
- Potential environmental and material hazards
- Acceptable level of permanent changes to the part (e.g., cutting and etching)
- Required equipment
- Processing time/throughput
- Cost/effort
- Portability

4.2. *Residual stress determination techniques*

Many methods currently exist for the determination of residual stress. A brief discussion of the more common techniques and their strengths and limitations are provided below. Residual stress determination method selection is an important consideration. Each method has a unique effective range, which must be carefully considered in the context of the desired outcome and follow-on usage.

4.2.1. *Contour*

The contour method is a residual stress measurement technique for mapping two-dimensional distributions of residual stress over a plane in a body. The contour method is illustrated using a two-dimensional body (for simplicity), but the measurement principle applies to three dimensional bodies. Figure 15 provides a conceptual framework for the contour method principle.

The contour method is based on the principle of superposition. The residual stress in the original body, $\sigma^a(x,z)$, (state a) is equal to the sum of the residual stress remaining in the body after it has been cut in half, $\sigma^b(x,z)$, (state b) and the residual stress induced by forcing the deformed cut surface back to an assumed cut plane, $\sigma^c(x,z)$, (state c).

$$\sigma^a(x,z) = \sigma^b(x,z) + \sigma^c(x,z) \tag{1}$$

The residual stress for state c, $\sigma^c(x,z)$, is equivalent to the residual stress that was released/redistributed during sectioning and is determined through the contour method experimental process (cutting the body, measuring the displacements, and imposing those displacements on a finite element model of the body).

The residual stress for state a, $\sigma^a(x,z)$ (original residual stress), is of primary interest and can be computed from Equation (1) using the residual stress in state c and known information about the residual stress in state b. Specifically, the free-surface boundary condition on the cut face in state b ensures that the normal component of stress over the cut surface in state (b) is zero

$$\sigma^b_{zz}(x,0) = 0 \tag{2}$$

Substituting Equation (2) into Equation (1) gives a relation between the released residual stress in state (c) and the original residual stress in state (a) on the cut plane (z = 0)

$$\sigma^a_{zz}(x,0) = \sigma^c_{zz}(x,0) \tag{3}$$

Since the residual stress for state (c) is known (from the contour method experiment) Equation (1) provides a means to compute the original residual stress (a) normal to the measurement plane.

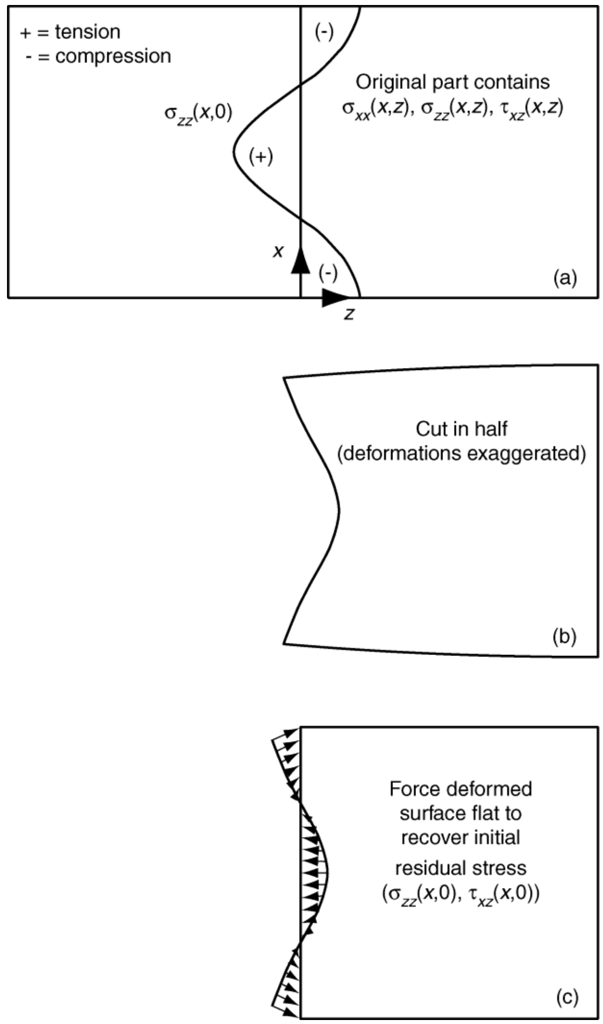

Figure 15 – Conceptual images of contour method.

4.2.2. *Hole drilling*

The incremental hole drilling method is a residual stress measurement technique for generating in-plane residual stress versus depth profiles from the material surface. In the hole drilling method, a hole is incrementally extended into a body containing residual stress. The strain released with each incremental hole depth is measured using a strain gage rosette placed around the hole. The measured strain versus hole depth data are used to calculate the residual stress that was initially in the part through an elastic inverse solution. Hole drilling measurements are often performed in the field, on a variety of structures, and in very tight spaces.

4.2.3. *Ring core*

The ring core method is very similar to incremental hole drilling. Both measure in-plane residual stress versus depth from the material surface by removing material and recording strain at a nearby location. In the ring core method, an annular groove is incrementally extended into a body containing residual stress, whereas hole drilling a hole is incrementally extended into the specimen. The strain released with each incremental groove depth is measured using a strain gage rosette placed around the hole. The measured strain versus hole depth data are used to calculate the residual stress that was initially in the part through an elastic inverse solution.

4.2.4. *Slitting*

The slitting method is a technique for generating a profile of residual stress versus depth from the material surface. In the slitting method, a slit is incrementally extended into a body containing residual stress. The strain released with each incremental slit depth is measured using strain gages placed at strategic locations. Common strain gage locations include on the face near the entry of the slit and on the bottom face directly below the slit. The measured strains versus slit depth data are used to calculate the residual stress that was initially in the part through an elastic inverse solution. Figure 16 provides a conceptual image of the slitting method.

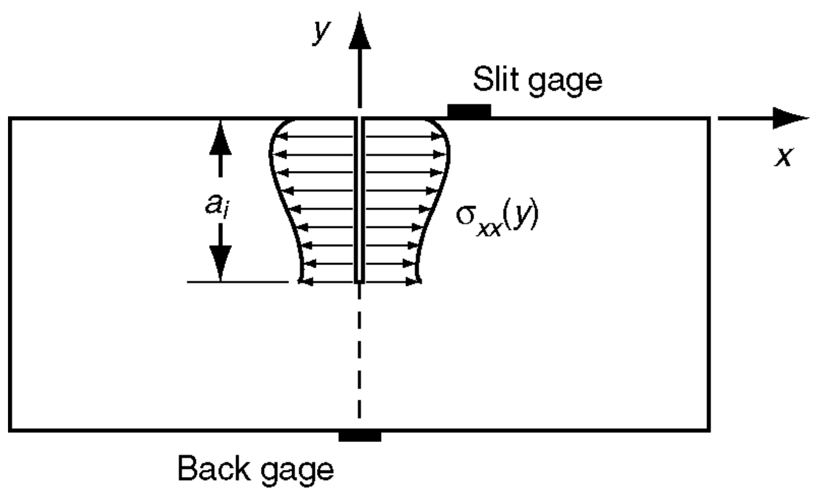

Figure 16 – Conceptual image of slitting method.

4.2.5. *X-ray diffraction with layer removal*

Conventional x-ray diffraction (and associated layer removal for depth profiling) is a common technique for the determination of residual stress. This technique uses the diffraction patterns produced by x-rays interacting with the material crystal lattice to quantify the inter-atomic lattice spacing, which is indicative of the strain state at the measurement site.

Conventional x-rays can only penetrate to a depth of a few microns, so the measurement technique is limited to near surface residual stress measurement. Since the measurements are limited to the surface, a simplifying plane stress assumption can be employed to calculate residual stress. The plane stress assumption eliminates the need to measure unstressed lattice spacing and allows stress to be calculated using only the lattice spacing measurements at several angles.

X-ray diffraction requires a large number of randomly oriented grains within the sampling volume to achieve a useful result. Many modern aerospace materials have relatively large microstructure or preferential grain orientations (texture) that can cause errors. When this occurs, the technique produces inconsistent results with large measurement-to-measurement variability or is simply unusable.

4.2.6. *High energy X-ray diffraction*

High energy X-ray diffraction uses much higher energy x-rays (e.g., a synchrotron source) than those used in conventional X-ray diffraction, which allows the x-rays to penetrate much deeper into the specimen (tens of mm). The x-ray penetration depth allows stress to be measured further into the sample but eliminates the plane stress assumption used in conventional X-ray diffraction. Without the plane stress assumption, all the principal strains need to be measured, which can be problematic because synchrotron X-ray diffraction requires shallow diffraction angles (difficult to pass through large samples).

The strain values are typically determined by comparing the lattice spacing in the specimen to reference stress-free coupons. This requires cutting up the specimen into small, residual stress free, bits (e.g., comb). As was the case for conventional X-ray diffraction, synchrotron X-ray diffraction requires a large number of randomly oriented grains (i.e., no large grains or preferentially grain orientations).

4.2.7. *Neutron diffraction*

Neutron diffraction is similar to high energy X-ray diffraction in that it also uses high energy particles (neutrons instead of x-rays) and can penetrate deep into the material (many tenths of in). Similar to high energy X-ray diffraction, all the principal strains need to be measured and are determined by comparing the lattice spacing in the specimen to reference stress-free coupons. The diffraction angle is typically around 90°, so it is less problematic to measure all the needed strain components compared with high energy X-ray diffraction. As with the other diffraction techniques, neutron diffraction requires a large number of randomly oriented grains (i.e., no large grains or preferentially grain orientations). The gage volume for neutron diffraction is typically on the order of 0.075 to 0.200 in, which makes it difficult to quantify residual stress features with a small length scale.

4.3. *Strengths/Weaknesses of each technique*

Each technique has its own strengths and weaknesses and should be considered for a particular application. Table 2 provides a brief overview of the strengths and weaknesses of the techniques described in the previous section.

Table 2 – Strengths and weaknesses of various residual stress measurement techniques

Measurement Technique	Strengths	Weaknesses
XRD with layer	Portable equipment	Significantly affected by

removal		microstructure variations Less repeatable than other techniques
Neutron Diffraction	2D mapping of multiple components Bulk residual stress	Difficult to obtain (limited facilities) Significantly affected by microstructure variations
Hole Drilling	Portable equipment ASTM standard Near-surface measurement Multiple stress components	Less repeatable than other techniques
Ring Core	Portable equipment Near-surface measurement Multiple stress components	Large averaging volume
Contour	2D mapping of residual stress Bulk residual stress	Difficult to resolve sharp stress gradients
Slitting	Excellent measurement repeatability	Limited to select geometry classes

4.4. *ERSI open hole Cx residual stress determination experiments*

In 2017 a research program was developed that would allow for cross-validation of residual stress determination methods and for the validation of finite element simulations of the Cold Expansion (Cx) process. For this program two aluminum alloys were selected, 2024-T351 and 7075-T651. The level of applied expansion was varied from the “Low” end of the FTI specification at 3.16% to the “High” end at 4.16%. This would allow for the capture of the effect of applied expansion on the residual stress and strain fields. Material for these coupons was provided by the A-10 ASIP Office and were machined at AFRL. Strain gages were installed by FTI and the Cx process was performed at SwRI.

Multiple strain measurement methods were used during the Cx process, including Digital Image Correlation (DIC), a fiber optic system called LUNA, and strain gages. An image of the test setup overlaid with the DIC results is shown in Figure 17. In addition to the strain measurements that were performed during the Cx process, four of the coupons (each representing one of the specific test conditions) all followed a series of post-Cx residual stress determination processes. The first process focused on Energy-Dispersive X-ray Diffraction (ED-XRD) accomplished at the Argonne National Lab. The second process focused on surface X-ray Diffraction (XRD) accomplished at the National Research Council (NRC) – Canada, with a specific focus to compare to the in-process DIC, LUNA, and strain gage data. The final process involved destructive contour results to quantify the residual stress on the assumed crack plane.

Data reduction and comparisons between the surface strain measurements and the data from the advanced proton sources is currently in process. Additionally, FTI is currently developing finite element models that represent these specific conditions, to include the sleeve clocking orientation and applied expansion. This work is planned to be published as a first in a series of papers building to the development of a validation process for FEA simulations of the Cx process and a summary of results will be included within this document.

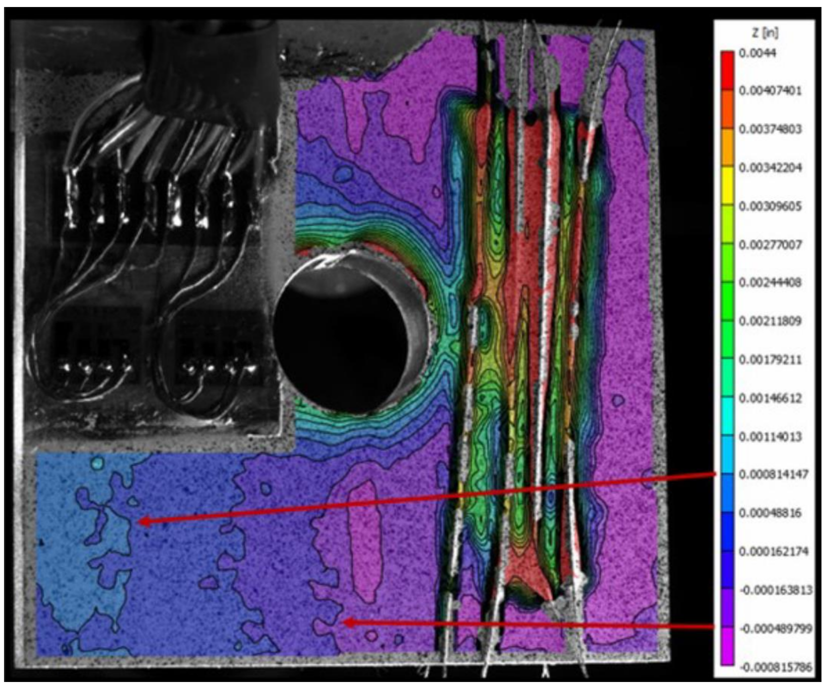

Figure 17 – ERSI open hole Cx residual stress setup detailing DIC, LUNA, and strain gage installations.

5. *GUIDING POLICY AND REQUIREMENTS*

The majority of the guiding policy related to the consideration of residual stress in structural analysis, albeit limited, centers around fastened joints, interference fasteners, and cold expanded holes. For the Department of Defense (DoD), several references are relevant for inclusion of residual stress in durability or damage tolerance analysis:

Department of Defense (DoD) Joint Service Specification Guide (JSSG) 2006 for Aircraft Structures[35]:

<u>*Durability Guidance:*</u>

> *The beneficial effects of interference fasteners, cold expanded holes, shot peening, or other specific joint design and assembly procedures may be used in achieving the durability analysis requirements. For durability fracture mechanics analysis, the limits of the beneficial effects to be used in design should be no greater than the benefit derived by assuming a 0.005-inch radius corner flaw at one side of an as manufactured, non-expanded hole containing a neat fit fastener in a non-clamp-up joint.*

The guidance also specifies using a 0.05-inch radius corner flaw at non-cold expanded holes.

<u>*Damage Tolerance Guidance:*</u>

> *Beneficial effects of life enhancement processes must be approved by the procuring activity.*
>
> *To maximize safety of flight and to minimize the impact of potential manufacturing errors, it should be a goal to achieve compliance with the damage tolerant requirements of this specification without considering the beneficial effects of specific joint design and assembly procedures such as interference fasteners, cold expanded holes, or joint clamp-up. In general, this goal should be considered as a policy but exceptions can be considered on an individual basis. The limits of the beneficial effects to be used in design should be no greater than the benefit derived by assuming a 0.005-inch radius corner flaw at one side of an as-manufactured, non-expanded hole containing a neat fit fastener in a non-clamped-up joint. In any exception, the burden of proof of compliance by analysis, inspection, and test is the responsibility of the contractor.*

Policy guidance from other entities (FAA, etc.) is limited to non-existent, but often refers back to the DoD JSSG 2006 guidance of a reduced initial flaw size. Notable examples include established inspection intervals for the Boeing 757 and 767 aircraft.

Recently, the USAF published a structures bulletin entitled “Testing and Evaluation for Utilization of an Empirical Method to Establish the Beneficial Effects of

Cold Expanded Fastener Holes for Damage Tolerance."[36] The intent of this structures bulletin was to further clarify the appropriate methods to empirically correlate a reduced initial flaw size. The structures bulletin specifically states its limited applicability to the reduced initial flaw size approach and refers to "other analysis methods" that are physics based for establishing the beneficial effects from residual stress. The bulletin provides guidance for damage tolerance testing and the follow-on correlation to test to established reduced initial flaw size limits, not to exceed 0.005-inch. The bulletin also addresses the limitations in JSSG and MIL-A-83444 (Airplane Damage Tolerance Requirements, 2 July 1974):

> *The reason for inclusion of the 0.005-inch limit is to provide protection for the possibility that not all critical locations were properly processed and/or assembled and that validated Non-Destructive Inspection (NDI) methods did not exist to verify the process was completed per design. These issues still exist today, although NDI methods are being developed and evaluated.*

This perceived risk has been a significant roadblock for taking advantage of the beneficial effects from residual stress. Recent programs have focused on this aspect of the problem and are developing inspection methods and data collection that go above and beyond the current requirements (example, FTIs check gages, etc.) to mitigate this perceived risk. These developments are discussed later in the quality assurance section of the document.

Recent initiatives have focused on moving beyond the reduced initial flaw size approach above, often referred to as "partial credit", to a "full credit" approach directly incorporating engineered residual stress. The path to "full credit" has hinged around the development of three key technology aspects: 1) a validated damage tolerance analysis (DTA) method that appropriately accounts for the presence of residual stress on crack growth, 2) a validated non-destructive inspection (NDI) method that can detect cracks in the presence of residual stress, and 3) a validated non-destructive evaluation (NDE) method that can verify the presence of compressive residual stress.[37] Figure 18 highlights that each of these three technology aspects is key to full credit for Cx. Many of these key factors are primary initiatives of the Engineered Residual Stress Implementation (ERSI) working group and are detailed throughout this document.

A draft structures bulletin with specific details related to the "full credit" process is currently in development. This structures bulletin focused on the DTA methods and QA processes that are necessary to take credit for initial DTA inspection requirements. Follow-on research and development methods are necessary to address NDE methods for in-service Cx holes before "full credit" can be accounted for in recurring inspection intervals.

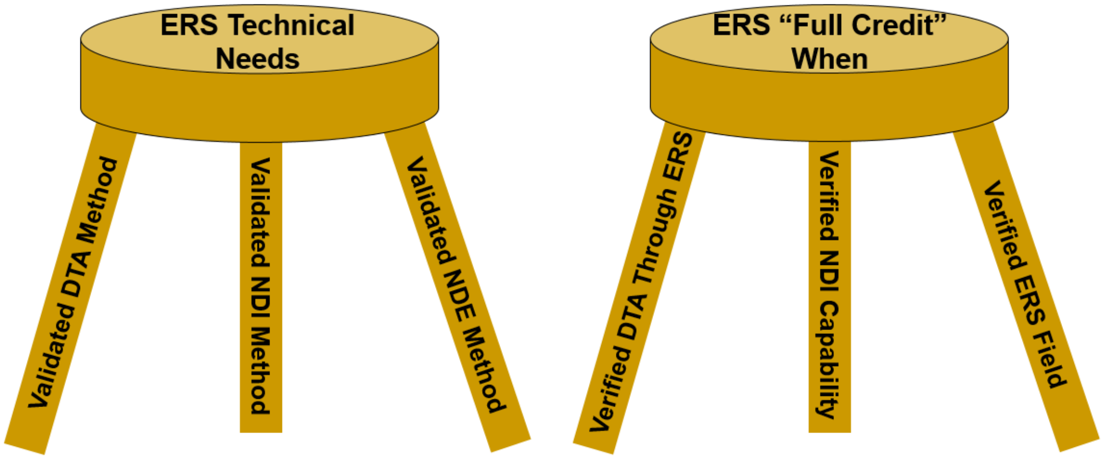

Figure 18 – The role of three technology aspects in supporting full credit for engineered residual stress (ERS) processes like cold expanded (Cx) holes.[37]

In the current version of the Air Force Structures Bulletin, In-Service Inspection Crack Size Assumptions for Metallic Structures[38], guidance on the applicability and limitations of non-destructive inspection (NDI) techniques such as eddy current, penetrant, and ultrasonics have been incorporated.

6. *HISTORICAL MODELING APPROACHES*

There's no doubt, the history of incorporating residual stress into analytical fatigue predictions has been fraught with struggles. There are endless sources of experimental results[39,40,41,42,43,44,45,49,51] demonstrating the fatigue life benefits from engineered residual stress processes, most notably cold expansion of fastener holes. Jones[59] provides a thorough overview of the evolution of analytical methods for cold expanded fasteners holes, with specific conclusions and recommendations for improved predictions.

6.1. *Stress life (S-N) comparisons*

Early investigations focused on characterizing life benefits in terms of stress life (S-N) behavior based on coupon test results. Figure 19 is a typical example in the literature detailing the life benefits of shot-peening notched coupons. Figure 20 details damage tolerance comparisons of precracked fastener holes for baseline open holes versus cold expanded fastener holes utilizing split and solid sleeves. Coupon test programs established the foundation for empirically based approaches for accounting for beneficial durability or damage tolerance impact resulting from residual stress. Major OEMs developed design factors to account for processes such as shot peening and cold expansion.

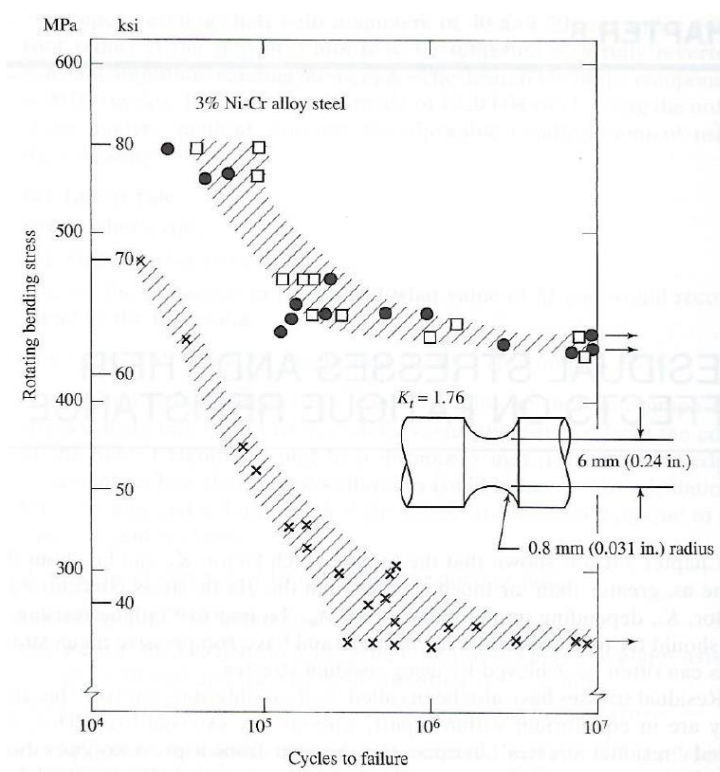

Figure 19 – S-N Behavior of Smooth, Notched Unpeened, and Notched Peened Specimens (●) Smooth, Polished, (x) Notched, (□) Notched, Shot-peened[13].

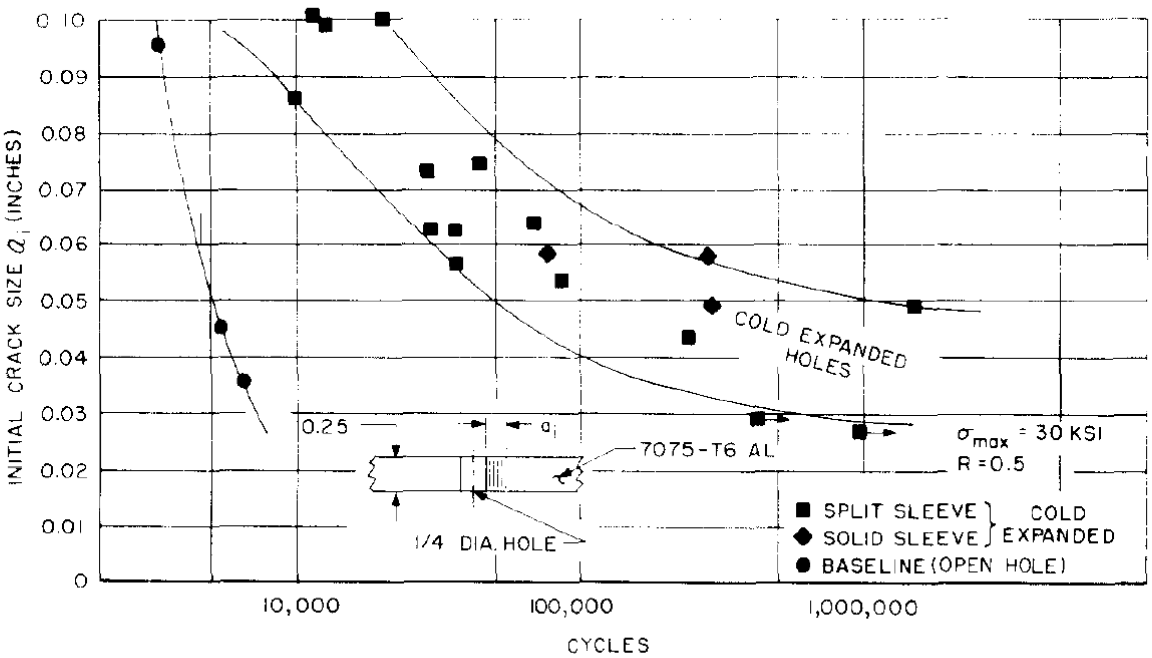

Figure 20 – Cold Expanded Hole (Split and Solid Sleeve) Test Results Relative to Baseline Open Hole Coupons[40]

6.2. *Reduced initial flaw size*

As discussed in the guiding policy section, JSSG 2006 allows the use of a reduced Initial Flaw Size (IFS) in fracture mechanics-based durability and damage tolerance analyses to account for the beneficial impacts of processes such as shot peening and cold expanded fastener holes. This allowance established a common practice in the USAF and DoD to reduce the IFS for these processes.

As discussed in the USAF Damage Tolerance Design Handbook, the reduced IFS is generally derived by “back” extrapolating the flaw population in a structure to obtain the initial flaw population. This initial flaw population is used to develop an effective IFS. This effective IFS must be validated through some form of testing.

Figure 21 illustrates the fatigue life prediction differences between an IFS of 0.05-inch and 0.005-inch. By assuming a smaller IFS in the damage tolerance analysis, the fatigue life prediction is increased resulting in increased initial inspection requirements. In the example shown, the fatigue life prediction was increased by approximately four times (4x).

The problem with this philosophy, however, is that the selected IFS is often an arbitrary selection and does not address location specific information such as part geometry, material, loading sequence, etc. It does not incorporate the variability in the fatigue life of a part due to changes in the coldwork process conditions, i.e. percent interference, lubrication, etc. It provides an arbitrary prediction of the fatigue life benefits that are gained by cold expanding structural holes and often grossly under-predicts the actual fatigue life benefits.

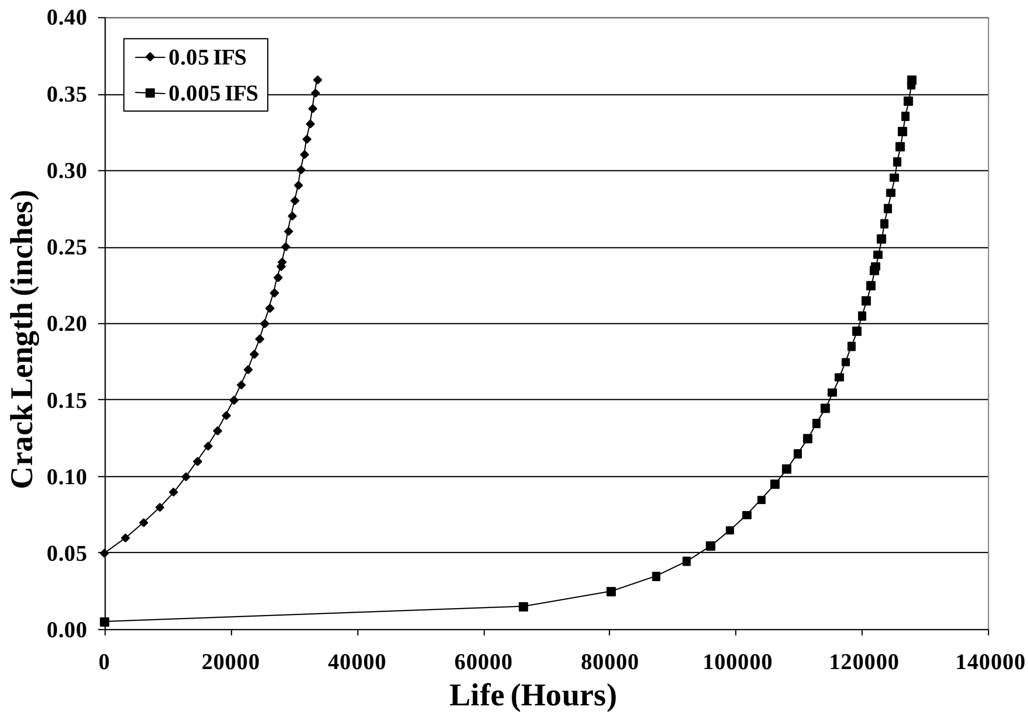

Figure 21 – Crack Growth Curves for 0.05in and 0.005in Initial Flaw Size

FTI[46] compared actual test data taken from Ozelton[47] to the analytical prediction based upon the reduced IFS approach. An assumed IFS of 0.005-inch corner flaw predicted a fatigue life less than one percent of the actual fatigue life observed. Warner[48] demonstrated situations where the reduced IFS approach is unconservative, specifically investigating peak spectrum influences on fatigue life at cold expanded holes.

Another issue that often arises with the reduced IFS philosophy is the determination of recurring inspection intervals, as illustrated in Figure 22. The damage tolerance analysis used to establish the recurring inspection interval of a component location is based upon an DFS which is determined by the detection threshold of the given inspection technique. Because of the limitation of the current detection thresholds with acceptable probabilities of detection, the fatigue life prediction benefits of the reduced IFS technique are often not perceived.

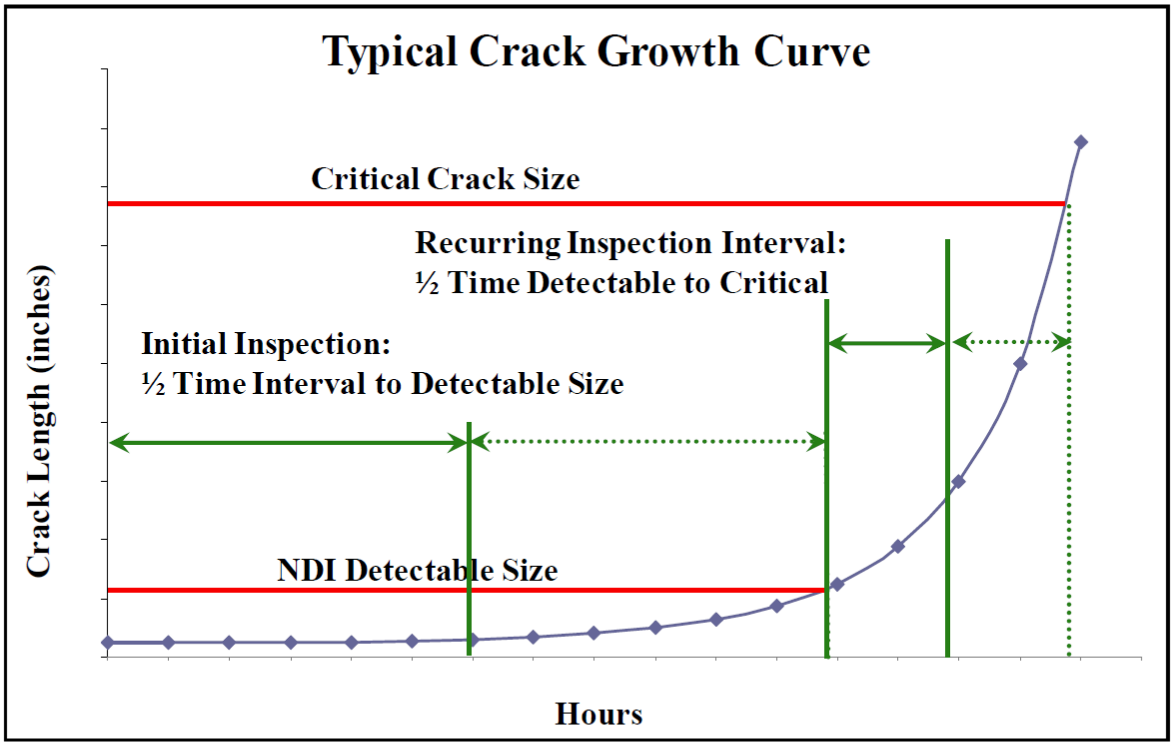

Figure 22 – Typical Crack Growth Curve Outlining the Methodology Used to Determine the Initial and Recurring Inspection Intervals for a Damage Tolerance Analysis[45].

6.3. *Linear superposition of residual stress intensities*

A common method developed and/or implemented to incorporate the effects of residual stress into the fatigue life analysis of components is linear superposition of stress intensities. This method involves calculating a two-dimensional (2-D) residual stress intensity profile which corresponds with the residual stress profile. To determine the residual stress intensity, K_{res}, the residual stress magnitude and profile without cracks present must be known, obtained, or assumed. Several methods that are used to obtain the residual stress magnitude and profile include weight functions, Green's function, measurement, eigenstrain, and finite element models. Once the residual stress profile is determined, K_{res} can be obtained by inserting a crack face at the desired location and loading it with the residual stress that exists normal to the plane of crack growth. As shown in Figure 23 developed by Stephens[13], the residual stress intensity is added to the applied stress component of the stress intensity, K, using linear superposition to determine the sum of the applied and residual stress intensities, K_T, under mode I conditions (see Equation 4). This effective stress intensity can be used with unmodified crack growth data to estimate the crack growth rate as a function of the total stress intensity.

$$K_T = K + K_{res} \tag{4}$$

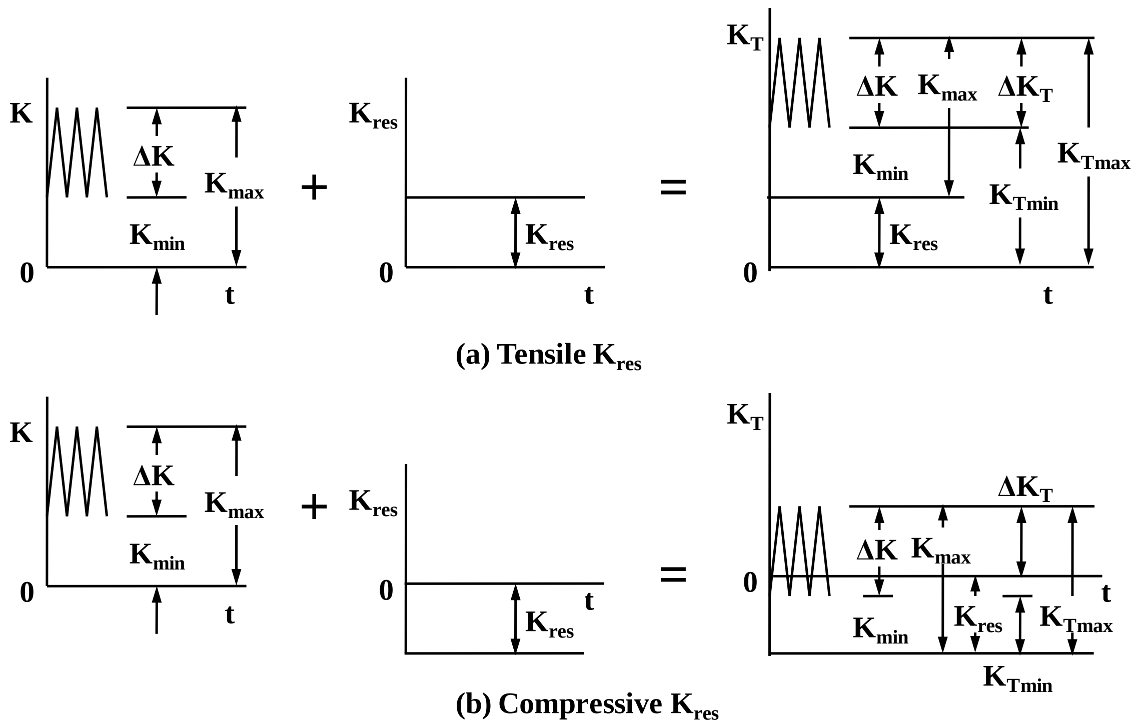

Figure 23 – Initial Stress Intensity Factors for Applied Loading, Residual Stress, and Superposition. (a) Tensile K_{res}, (b) Compressive K_{res}.[13]

Past research by various authors in predicting the fatigue life of cold expanded holes using the linear superposition approach have shown varying levels of success.[49,50,51,52] The linear superposition method is also highly dependent on the calculated or assumed residual stress profile.

As explained by Jones[59], the superposition approach for predicting fatigue through residual stress fields is not without criticism, with several researchers questioning the validity. Multiple references[53,54,55,56] question the accuracy of integration of the superposition model, da/dN, as a function of the initial calculated K_T, since the residual stress profile will change as a crack grows through the residual stress field, altering the original K_{res}. Parker [57] disagreed, stating this change doesn't specifically invalidate the superposition principle. Also, the crack tip contains its own residual stress field within the plastic zone that will interact with the original residual stress, which is not incorporated into the superposition methodology. Stephens[13] also mentions that the integration past the change in sign of the initial residual stress sign is not reasonable since the original residual stress field would have changed significantly. Residual stress relaxation due to cyclic plasticity can also be an issue.

6.4. *Inverse analysis methods*

Kokaly,[49] compared an inverse analysis approach to two-dimensional (2-D) and a three-dimensional (3-D) FEA. Unlike the typical linear superposition approach, the inverse analysis method performed by Kokaly assumed the residual stress profile and K_{res} was unknown. The baseline stress intensity, K, was obtained from a known solution and the total stress intensity, K_T, was calculated from the experimental crack growth data published by Saunder.[58] Given that the baseline and total stress intensities are known, the residual stress intensity, K_{res}, can then be calculated. Kokaly noted that the predicted fatigue life was found to be very sensitive to a +/- 1% variance in the inversely generated K solution. Kokaly compared the inverse analysis results to 2-D and 3-D FEA models to simulate the effects of the Split Sleeve Cold Expansion™ process on fatigue cracks at the hole. The 2-D FEA model predicted that a crack would remain closed over a range of crack lengths even though the crack growth was observed with the experimental testing (see Figure 24). Kokaly concluded based upon this study and the fact that significantly faster crack growth was observed on the mandrel entrance side of the hole that the 2-D FEA model was inadequate to accurately predict the residual stress profile induced by the Split Sleeve Cold Expansion™ process. The 3-D FEA model was able to model the residual stress profile through the thickness of the model and indicated a higher residual stress on the exit side of the hole. This model was a more accurate representation of the residual stress profile. Kokaly concluded that a better understanding of the crack front geometry was necessary to provide a more accurate understanding and prediction of the fatigue crack growth behavior at a cold expanded hole.

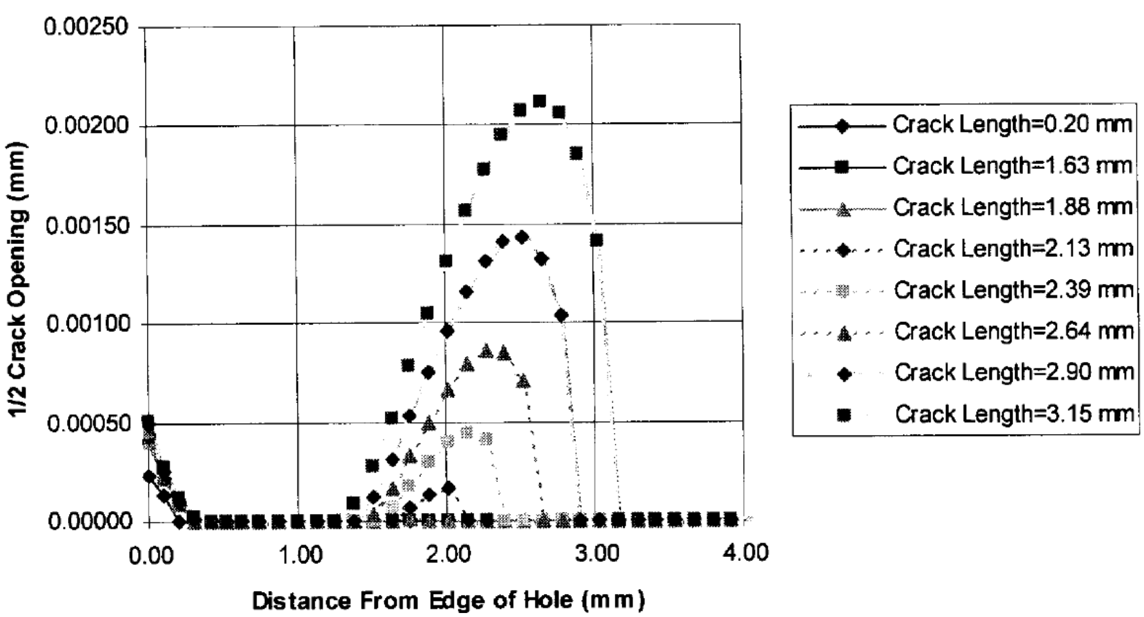

Figure 24 – Crack Opening Data from the FEA Model for Various Crack Length[49]

Carlson[44] and Pilarczyk[45], investigated a similar inverse analysis method, but characterized results in terms of a residual stress beta correction. This research included fatigue tests of baseline and cold expanded coupons. As shown in Figure 25, the principle of superposition was utilized to compare the baseline and cold expanded coupon behavior. To accurately characterize the stress intensities for the unique crack shapes observed, 3-D FEA models were developed. Figure 26 details the resulting beta corrections from this investigation. Similar to other programs, significant fatigue life improvements were identified for the cold expanded coupons. Also, marker-banding was implemented to characterize the unique crack shape evolution. The research, similar to the findings by Kokaly, also identified differences between FEA residual stress predictions and the test derived beta corrections. These differences were in both the magnitude of inferred residual stress as well as the location of the local minima.

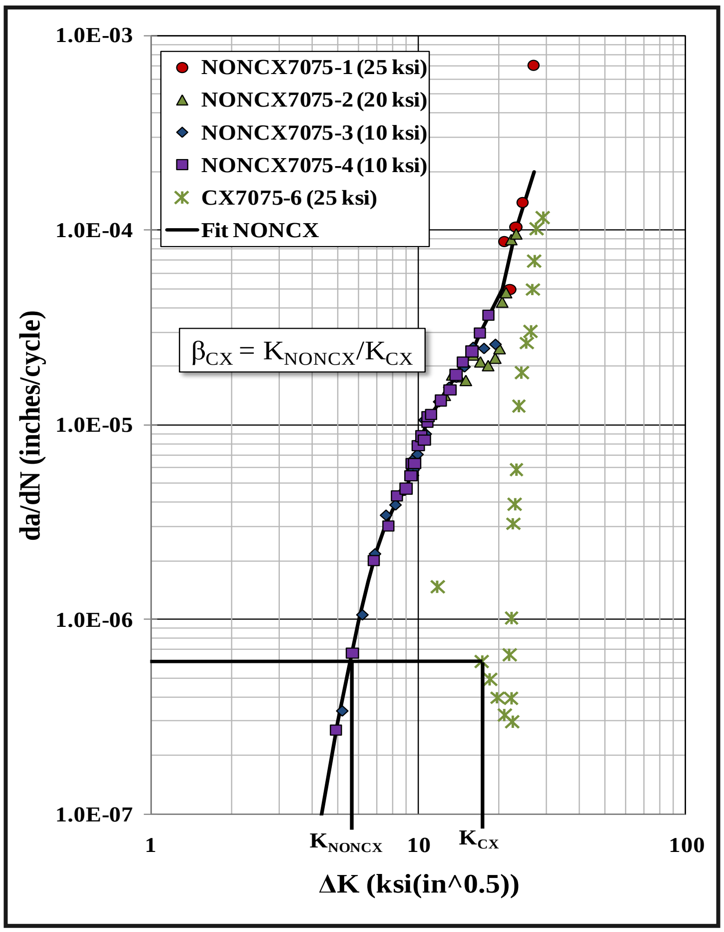

Figure 25 –Beta Correction Calculation Methods[45]

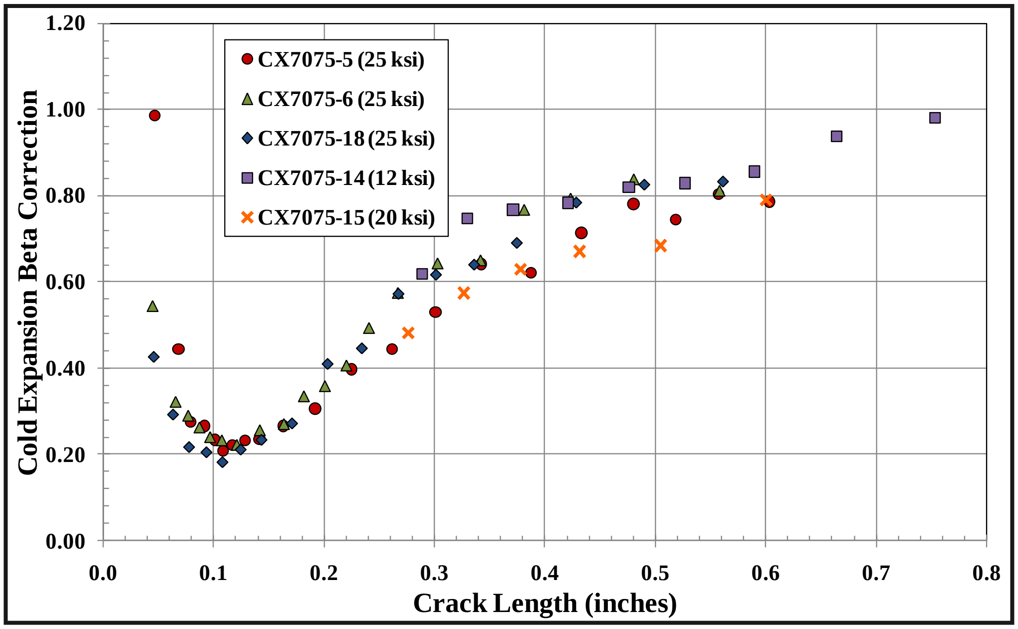

Figure 26 – Beta Correction as a Function of Crack Length[45]

7. *CONSIDERATIONS FOR MODELING APPROACHES*

Previous research and modeling approaches have resulted in several key analysis aspects that are necessary to accurately predict fatigue behavior when incorporating residual stress. Multiple references[49,59,60] highlight these key aspects:

- Linear superposition of residual stress appears to reasonably characterize the life benefits with residual stress, however, there are several factors that must be considered:
    - Residual stress redistribution as a result of the crack
    - Crack tip plasticity interaction with residual stress
    - Partial crack closure
- Quantifiable characterization of residual stress
- Accurate characterization of crack shape evolution

These key factors make crack growth scenarios with residual stress different than a classic crack growth analysis. These key factors, and the analytical processes and methods to account for them are discussed in subsequent sections.

CHAPTER II – ANALYTICAL PROCESSES

This best practice document is intended to be an initial step to define typical analytical processes, highlight best practices, identify pitfalls, and provide benchmarks and case studies to empower the community moving forward. The analytical processes discussed in the initial release are focused primarily on USAF methods and tools with specific emphasis on cold expanded fastener holes. Moving forward, as the maturity of the document grows, additional methods, tools, and data will be added from other sources and for other residual stress applications. This document is intended to be a living document that grows with time and not necessary all-inclusive of the possible methods used by other organizations and analysts.

8. *OVERVIEW OF ANALYTICAL PROCESSES*

As a result of the first Engineered Residual Stress Implementation workshop (Fall 2016), an overarching process flow, as shown in Figure 27, was developed to highlight the key aspects of incorporating residual stress into damage tolerance assessments. This process flow breaks each component down into four main categories: policy, input data, analysis process, and risk. As shown in the figure, validation testing is a key step between input data and the analytical process. Risk factors and the risk management approach influences the analysis process and ultimately drive the repair and inspection requirements for the component analyzed. This chapter will focus on the input data and analytical process. Details related to policy, validation testing, risk, and NDI will be discussed in subsequent chapters.

The combination of extended service life requirements and aging fleets have resulted in a renewed focus to sharpen the analytical pencil and improve fatigue analysis methods. One aspect that continues to be a primary focus is characterizing and incorporating the benefits of residual stress in justification analyses. This renewed focus has resulted in a concerted effort within the USAF and beyond to advance the state-of-the art in analysis methods and the understanding of residual stress. Multiple programs have established a fundamental framework to incorporate the residual stress into damage tolerance predictions, with several key factors for success. These factors include:

- Advancements in residual stress determination techniques leading to improved quality and resolution of data
- Direct incorporation of residual stress into fracture mechanics based predictions
- Improved understanding of key variables influencing residual stress
- Established sources for residual stress inputs
- Improved analysis tools to execute advanced fracture mechanics simulations
- Improved efficiency/methods for finite element based stress intensity solutions
- Multi-point crack front shape evolutions

- Coupled crack growth and finite element based stress intensity calculations including multi-point capability

Leveraging this established framework, multiple gaps still exists in the analysis process that are current focus items. These include:

- Established standards, benchmarks, and best practices
- Defined certification requirements that address:
    - Acceptable analysis methods
    - Conservatism/safety factors
    - Testing requirements
    - Measurements requirements
    - Inspection considerations
    - Application limitations and restrictions
    - Risk quantification
- Exercise existing analysis tools to identify and address limitations
- Benchmark with different analysis tools
- Compare/contrast different residual stress input sources
- Improve confidence and quantify uncertainty in residual stress input data
- Improve material models addressing “low” ΔK ranges, negative R, grain orientation influences, etc.
- Continue to refine understanding of factors that may affect residual stress
- Understand translation to “real world” applications, i.e. fatigue details
- Define approaches to ensure safety, i.e. risk mitigation through statistical quantification
- Define approaches to handle conservatism and safety factors

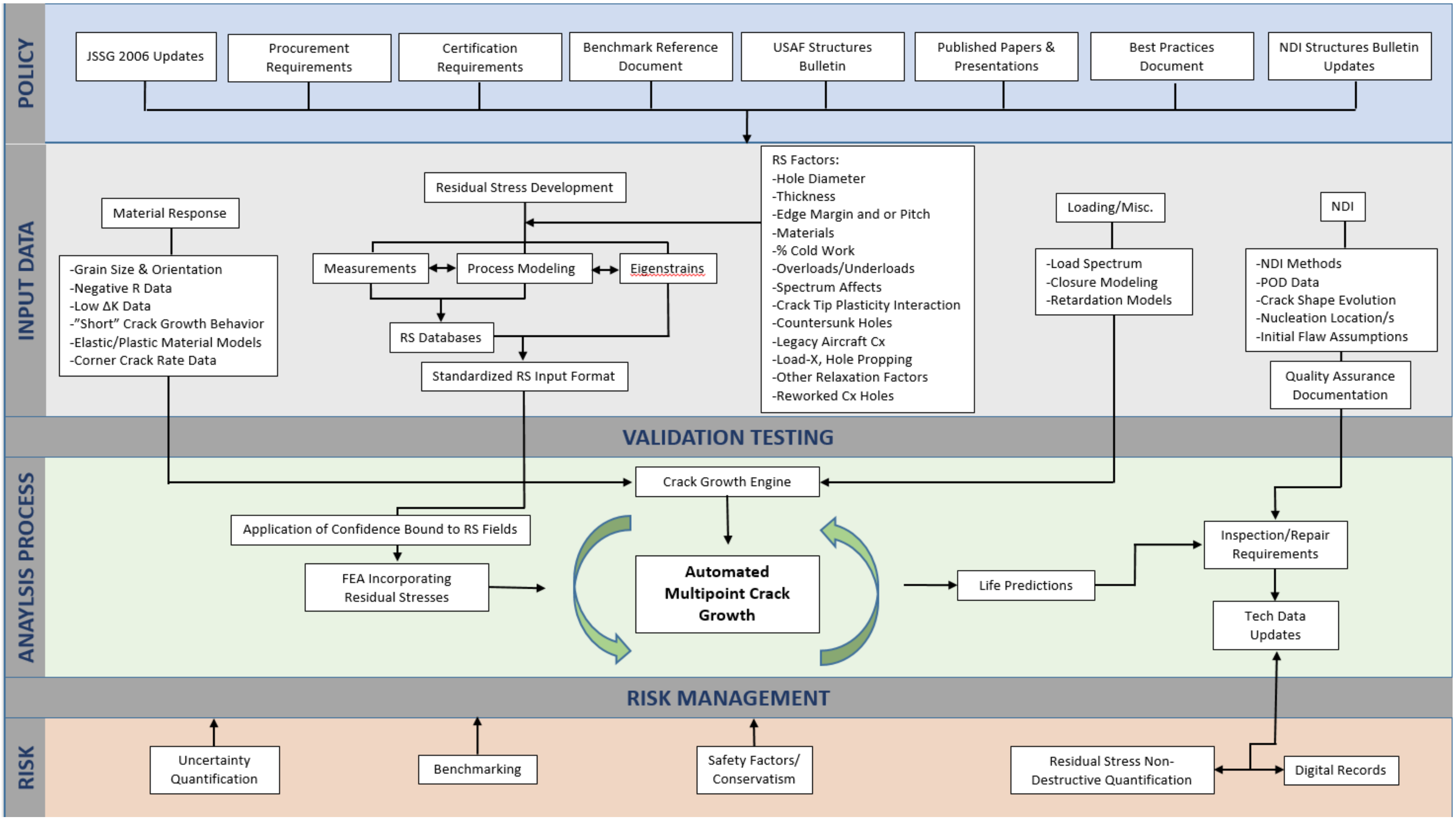

Figure 27 – Engineered Residual Stress Analysis Process Flow

9. *INPUT DATA*

A diagram of the general analysis inputs is shown in Figure 28. The basic input data considerations are discussed with additional details included in subsequent sections. The main inputs include: design information, material models, load spectrum, retardation models, and residual stress. Residual stress (residual K) are combined with the applied stress (applied K) using the principle of superposition discussed in a previous chapter. Automated 3D crack growth is coupled with a crack growth engine to iteratively growth cracks and predict the damage tolerance life.

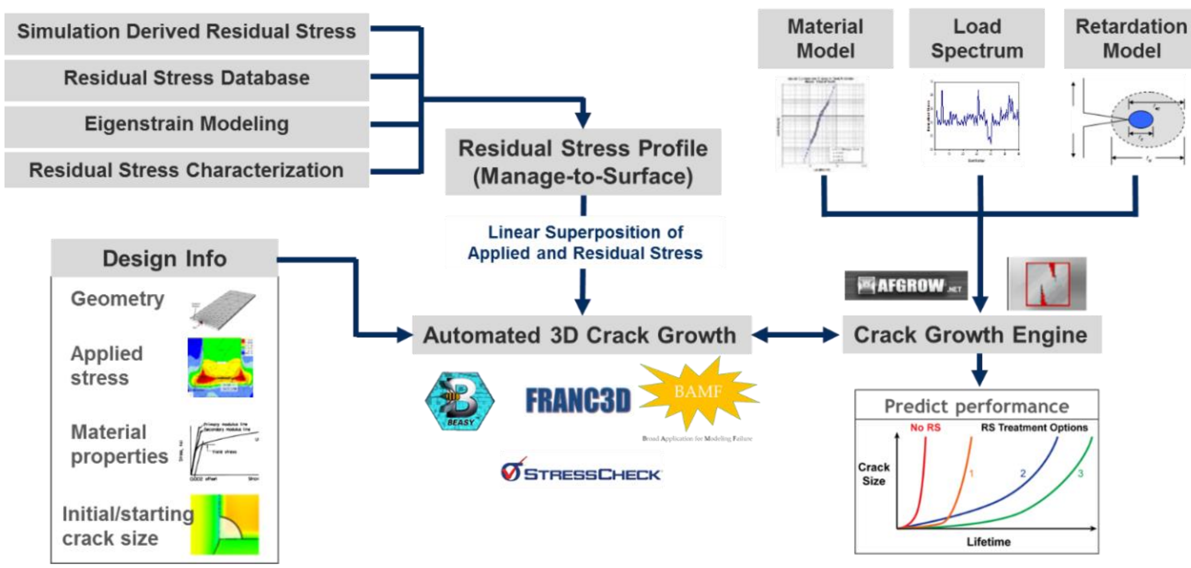

Figure 28 – Analysis Inputs Diagram

9.1. *Design information*

In general, the design information includes the part geometry, applied loads/stress, material properties and initial flaw sizes utilized in a standard analysis would be used for analysis predictions with residual stress. For the initial flaw size, the goal is to move away from a reduced flaw size approach. In general, the same initial or detectable flaw size (typically 0.05" for USAF applications at fastener holes with bolt-hole eddy current inspections) would be used for the analysis predictions. Other NDI considerations are discussed in Section 14.

9.2. *Material models*

An accurate characterization of the material crack growth rate behavior (da/dN vs. ΔK) is always an important factor for accurate damage tolerance predictions, but the sensitivity is amplified for analysis incorporating residual stress. Incorporating residual stress will typically drive analysis into atypical regimes, most notably "low" effective ΔK ranges with highly negative stress ratios. When residual and applied stress intensities are combined, for typical applied loads the resulting ΔK and R effective can exercise material models in areas of sparse or limited data. Figure 29 provides an example of crack growth rate data for R=-0.2, a typical R_{lo} cutoff for aluminum alloys. For this example, there is no data below a ΔK of 5 ksi-root-inch, resulting in estimating the behavior in this regime. Inaccurate characterization of the material behavior in this regime can have a significant influence on the damage tolerance prediction and can often result in the difference between a prediction running or not. Close consideration should be given to the data and material model in this regime when incorporating residual stress into analysis.

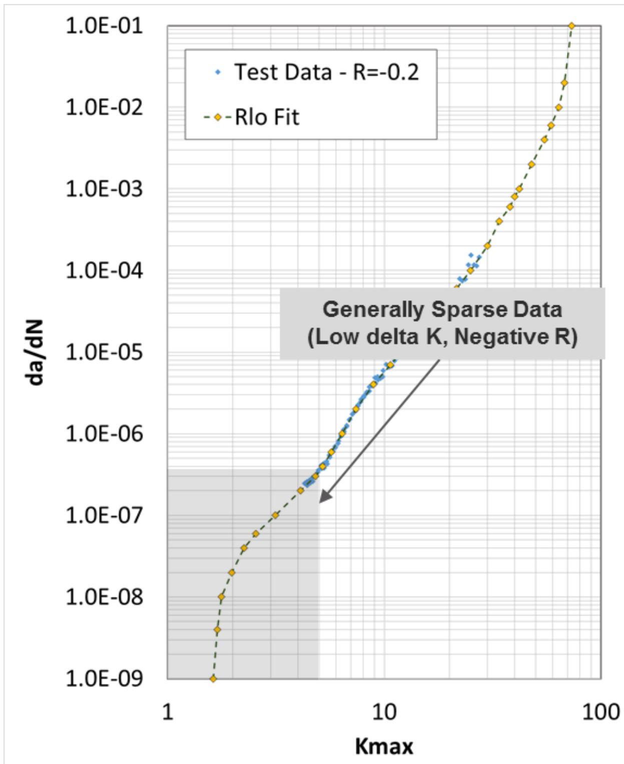

Figure 29 – Material Model Considerations – Low ΔK and Negative R Regime

9.3. *Load spectrum and retardation models*

The load spectrum utilized for baseline analyses with constant or variable amplitude loading can typically be utilized for analyses with residual stress (special conditions with restrictions may apply). The appropriateness of utilizing retardation models for analyses with residual stress is still unclear. In general, predictions including the retardation approach for baseline analyses have resulted in reasonable predictions relative to test data, however, these evaluations have been limited.[60,78] In general, the benefits of residual stress without the inclusion of residual stress far exceeds the baseline performance. A recommended initial approach would be to not consider retardation when completing predictions with residual stress.

9.4. *Residual stress determination*

The determination of residual stress is primarily accomplished by finite element based process modeling, determination techniques such as contour, or continuum mechanics based eigenstrain approaches. Ultimately, all three approaches would yield the same results providing complementary data to substantiate the residual stress in a part, however, the maturity and confidence in each of the techniques varies. Currently, the most widely used is determination techniques like contour. Eigenstrain approaches, such as those available with the ERS Toolbox®, have demonstrated similar results when compared to determination techniques. Process modeling has typically not yielded consistent results compared to other methods. Confounding the problem is the “lack of truth”, resulting in uncertainty in the different approaches and the need for additional cross-method comparisons.

9.4.1. *Process modeling*

The details of this section are currently in work or planned for future work.

9.4.1.1. *Discuss the various approaches for process modeling*

The details of this section are currently in work or planned for future work.

9.4.1.2. *Consideration for material properties used*

The details of this section are currently in work or planned for future work.

9.4.1.3. *Basic modeling approach and key factors that are important*

The details of this section are currently in work or planned for future work.

9.4.2. *Determination techniques and associated implementation methods*

There are several determination techniques commonly utilized to quantify residuals stress (see Section 4). Each approach has its strengths and weaknesses, however, the spatial resolution through the thickness of the part is of key importance for analysis purposes. Currently, the contour method is uniquely positioned to provide the necessary data. Other methods, as discussed in Section 4, can provide complementary data, however, are not commonly utilized for crack growth analyses.

9.4.2.1. *Contour method and input format*

The contour method provides data in a X, Y, Szz format, which for implementing into a crack growth analyses utilizing crack face traction is nearly ideal. Most crack growth analysis programs only allow for a point cloud to be implemented if the entire 6 tensor residual stress field is known. To use the data from the contour method a 2-D equation needs to be generated that best fits the data. After generating the equation, it is ideal to apply the equation to a grid spacing much smaller than the grid spacing of the contour data. This is necessary to ensure that the equation is smooth and does not have any large inflection points in-between the residual stress determination data points.

9.4.3. ***Eigenstrain***

The eigenstrain method can be used to predict residual stress fields from a variety of surface-based processes in arbitrarily shaped bodies. The term “eigenstrain” was created by Mura[61] to refer to incompatible strain fields in a body without any external forces. An eigenstrain (incompatible strain) field is one which cannot exist in a body without stress. They have been shown to model strain from plastic deformation particularly well. This makes it a good approach for residual stress modeling as plastic deformation is the root cause of residual stress. Currently, there is active work in modeling shot peening (SP), laser shock peening (LSP), and cold hole expansion (Cx) using the eigenstrain method. It may be possible to extend the method to other processes of interest in the future.

An important property of eigenstrain is geometry independence. For a given process the eigenstrain field depends only on the material and the process parameters. Eigenstrain does not depend on the geometry of the material in question. This geometry invariance in extremely beneficial since once the eigenstrain distribution is known for a given material and process, residual stress predictions can be made for the same process and material in any number of arbitrarily complex bodies. It’s important to note that the geometry independence of eigenstrain extends to the process region which is of particular importance to SP and LSP where the processed surface region may change during the design stage of a part.

When examining the equilibrating response of a body to the presence of eigenstrain it is useful to work with stress. Eigenstress is directly related to eigenstrain via Hooke’s law. When an object undergoes a residual stress-inducing process such as LSP, the resulting eigenstress field does not satisfy equilibrium by itself. The total stress state in the body (σ_{TOT}) will be made up of the eigenstress from laser peening (σ_{LP}) plus an equilibrating stress field $\left(\sigma_{\mathrm{EQ}}\right)$.

There are four main steps when using eigenstrain to solve an engineered residual stress in a specimen:

1. Apply the desired residual stress inducing process to a simplified specimen. The specimen must be designed so that the measurement location is free from geometric effects on the stress field or the calculated eigenstrain distribution will be incorrect[62.] Eigenstrain may be geometry independent but it’s measurement is not.
2. Determine the residual stress in the simplified specimen using a method consistent with data requirements, i.e. 1D, 2D, etc.
3. Determine the eigenstrain distribution from the residual stress determination data by decomposing the total stress field.
4. Use the eigenstrain distribution to predict residual stress in the actual part being designed.

Details on how to use eigenstrain to solve for residual stress in complex parts can be found in work by DeWald A.T.[63] and Afazov S.M.[64].

A library of eigenstrain distributions can be developed to eliminate the need for the first three steps in a majority of cases. Such a library is only possible due to the properties of eigenstrain. This is the main benefit for working with eigenstrain instead of residual stress where measurements must be made for each unique geometry.

9.4.4. *Sources of "canned" residual stress data*

9.4.4.1. *Residual stress database*

The residual stress database is a .NET assembly that contains a database of residual stress and a standalone visualizer. The software was created by APES, Inc. and ESRD, Inc. under a USAF rapid innovation fund program and is designed to provide 2-dimensional residual stress fields for a wide array of Cx holes[60].

The database contains 47 different residual stress profiles based on experimental data which is used to provide the user with a residual stress that best suits their application. The user has the option to select from the list of residual stress or can provide geometric parameters and let the software find the closest approximation in the database. If the input parameters do not directly correlate to an entry in the database a 4D (ED, D, t, and %Cx) Delaunay simplex finder is used to interpolate a residual stress field. The visualizer outputs the data to a user-defined grid spacing which the analyst can manipulate for their specific analysis.

9.4.4.2. *ERS-Toolbox®*

The ERS-toolbox® is a computational design tool, developed by Hill Engineering, that predicts, via the eigenstrain method, the full field residual stress field and distortion caused by residuals stress inducing processes.

The user will input a process specification and a finite element mesh. The program then uses a library of eigenstrain data to obtain the appropriate distribution. The distribution may exist directly in the database or it can be obtained by interpolating between relevant data. The eigenstrain distribution is then mapped onto the finite element mesh, based on the process surface region. Finally, the mesh based residual stress information is written out to a file which can be used in a FE analyses.

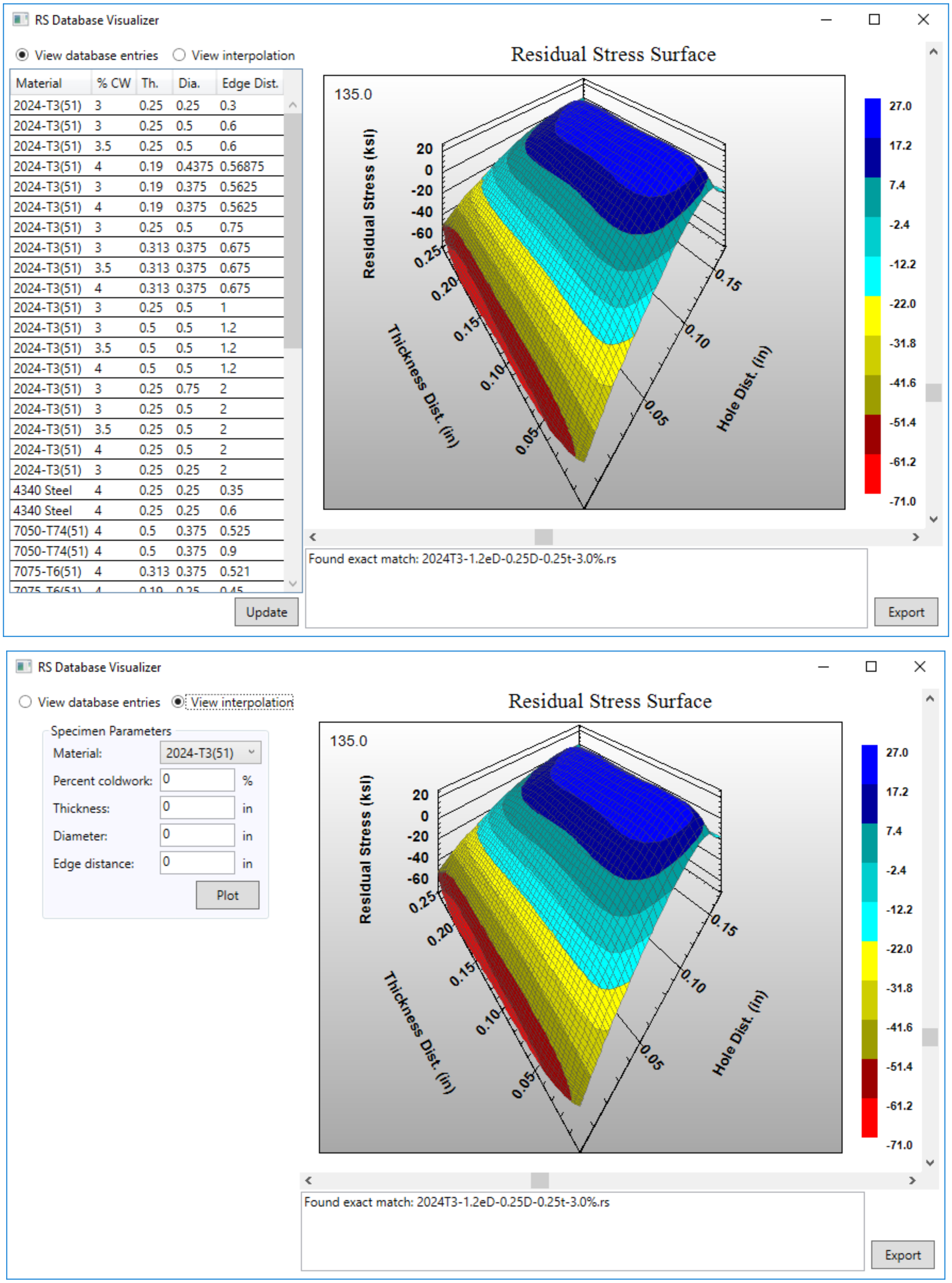

Figure 30 – Residual stress database (Top) database entry selection (Bottom) input parameter selection.

10. THE ANALYSIS PROCESS

10.1. *Multi-point fracture mechanics*

10.1.1. *Importance of multipoint crack growth analysis*

Marker banded specimens have shown that, even without secondary cracking, unique crack shapes can form due to residual stress. The crack will seek out the path of least resistance in the residual stress field causing unique shapes. Traditional elliptical shape crack fronts cannot capture the shapes observed in coupons with residual stress. The use of two-point (one point representing surface, one point representing bore) crack predictions often result in errors in life predictions. In addition to erroneous life predictions, details of crack growth and crack shape are important when it comes to defining inspection methods, detectable flaw sizes, and recurring inspection intervals. For example, the crack observed in Figure 31 (bottom) would not be inspectable using typical FPI and Surface scan eddy current measurements, even though the crack is approximately 0.40-inch on the entrance surface and at 99.8% of the total damage tolerant life. This drives the importance of accurately predicting both residual stress as well as crack shape evolution for both the analyst and the NDI technician. A multi-point analysis, characterizing the crack at multiple points along the crack front, allows the analysis to seek out the path of least resistance more closely modeling the behavior observed in tests.

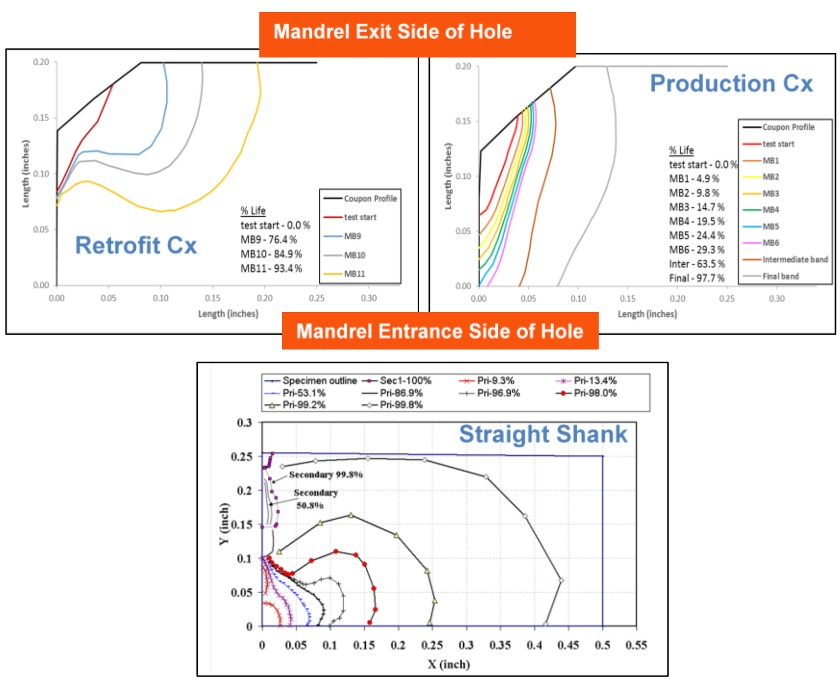

Figure 31 – Marker banded specimen of Cx Hole; (top) countersunk holes, retrofit and production Cx processing; (bottom) straight shank hole[78].

10.2. *Coupled FEA-crack growth*

Due to the uniqueness of the crack growth when incorporating residual stress, coupling multi-point stress intensity calculations with a crack growth lifing code is critical to capture accurate crack shape evolution and fatigue predictions. Several options are available, including but not limited to BEASY, FRANC3D, and BAMF.

The basic steps these analysis codes use are outlined by:

1. Create model with the initial boundary conditions
2. Add/update cracks into the model
3. Apply residual stress field to the cracked model (crack face traction or full-field)
4. Compute stress intensities of cracked and un-cracked models and combine via superposition
5. Calculate incremental crack growth at multiple points along crack front based on preferred crack growth model (NASGRO equation, Paris, Walker, tabular, etc.)
6. Update crack front based on incremental growth
7. Repeat steps 2-6 until the part is considered failed

Each tool has its unique implementation approach, utilizing different Finite Element Model (FEM) or Boundary Element Model (BEM) frameworks for stress intensity calculations as well as different crack growth engines with associated capabilities and limitations. Also, the key details regarding interaction between FEM/BEM and the lifing code differ between each tool and are important to understand as they influence the resulting predictions.

10.2.1. *Broad Application for Modeling Failure (BAMF)*

10.2.1.1. *Overview*

The Broad Application for Modeling Failure (BAMF) was originally developed by the USAF and is currently being maintained by Hill Engineering, LLC. It is a AFGROW Plugin that couples StressCheck™ FEA stress intensity calculations with AFGROW's powerful crack growth engine. The current release is v5.0 was released in February 2018. Its key features include having access to the full suite of AFGROW capabilities including material models, spectra, retardation models and more, as well as the full suite of StressCheck™ modeling capability. It has multi-crack and multi-point crack front support including capabilities to include residual stress via crack face traction and a bulk residual stress field. StressCheck™ is a P-element finite element code which allows for a reduced mesh density during solutions. This is beneficial for solution time in solving detailed crack growth analyses. BAMF is currently limited to planar cracks in 3-d models.

10.2.1.2. *Crack face modeling*

BAMF defines the direction of crack propagation perpendicular to the crack front on a point by point basis. Each point uses its adjacent points to define perpendicular. Each point is grown based on magnitude of the stress intensities at that point. The user has the ability to manipulate the range which the stress intensities are averaged to smooth out any anomalies. The new crack front is then re-splined essentially smoothing out any artificial stress risers. Certain aspects of the finite element model of the crack can be manipulated. The crack front can be more precisely defined by adding more analysis points to the geometry. For corner cracks general guidance is to use 11 points for non-residual stress and 21 points for cracks that are expected to form unique shapes due to residual stress. 21 points seems to be able to capture unique features in the crack front without making solutions unstable.

BAMF has a built-in mesh creator. It is based on guidance from the StressCheck™ user's manual[66] on the development of mesh density. The mesh refinement consists of a default of two layers of refinement with a common factor of 0.15. The user can modify number of elements along the crack front. The default is set to 1.25 the number of points, but the user is encouraged to interrogate the mesh refinement prior to running the model. In unique crack shape scenarios, a higher mesh density will provide a more detailed and stable solution[65]. The radius of integration path is computed so that it runs just outside the inner most layer. Its recommended the user follow the guidelines outlined below from the StressCheck™ user's manual when evaluating the mesh quality.

The following guidelines should be followed when designing a coarse mesh near crack tips for planar and axisymmetric analyses:

- *Avoid very distorted elements near the crack tip.*
- *Keep the size of the elements near the crack tip about the same.*
- *When computing SIF or J-integral, select the radius of the integration path such that it runs roughly through the middle of the second layer of elements around the crack tip. The first layer of elements is considered "sacrificial" due to the singularity at the crack, and extraction through this layer of elements will result in inaccurate SIF calculations.*
- *Consider incorporating the comparison of different number of layers and the K results*

10.2.1.3. ***Residual stress implementation***

Two different methods are available in StressCheck™ for calculating stress intensities due to residual stress. The J-integral method requires the full tensor and the bulk residual stress module in StressCheck™. The contour integral method for loaded cracks, CIM-LC, method typically only needs the component of the residual stress normal to the crack face, which is ideal for contour method measurements. Each of these methods provides benefits and disadvantages. In comparison to SIF extractions via the J-Integral, the CIM-LC has three advantages[66]:

• Faster solution times when tractions are defined on crack faces instead of volumetric residual stress over the cracked component.

• For most practical applications only one RS component is needed (normal to the crack face) to compute SIFs with the CIM-LC.

- The extraction of CIM-LC is faster than the J-integral.

The advantage that the J-integral method has over the CIM-LC method is that it can be applied to non-planar cracks. It also allows for different constraints to be placed on cracks such as contact elements. This allows the user to investigate the effects of crack closure due to residual stress.

To induce a residual stress in a model using CIM-LC a traction must be applied normal to the surface. This traction must be applied as an equation utilizing the stress check formula box. Current best practice is to build a multi-order polynomial equation that reduces the error between contour data and the fitted surfaces. Typical residuals are targeted to be less than 2 ksi in magnitude. After the user has established a best fit equation to the data it is recommended that they apply the equation to reduced grid spacing to insure no oscillations are occurring due to Runge's phenomenon. Currently StressCheck™ limits the length of an equation to ~4000 characters, which corresponds to a 15th order polynomial using the MATLAB code polyvalRS2array.m.

10.2.2. *BEASY*

10.2.2.1. *Overview*

BEASY is a boundary element method (BEM) software suite for predicting fatigue crack growth behavior. Unlike other software solutions, BEASY doesn't integrate with existing FEA codes. Instead, it uses its own meshing code and solver. BEASY supports 2D and 3D crack growth simulations with complex loading such as multiple independent spectra and residual stress. Users can select from several crack growth models such as the NASGRO equation or tabular $\frac{da}{dN}$ vs R data. Each crack face is represented by a mesh of triangular or quadrilateral elements. The crack front is a series of edges on the crack face mesh. BEASY uses rings of internal points centered around specific locations on the crack front to extract SIF values using the J-integral method.

10.2.2.2. *Crack face modeling*

BEASY provides several methods for determining the crack growth angle in a 3D analysis. The default method is the strain energy density method with the other options being maximum principal stress direction, planar (K_I only), and the multiaxiality Q-plane method. BEASY computes separate stress intensity factors for all three modes of fracture (K_I, K_{II}, and K_{III}) and provides different models for combining them into a single K_{eqv} such as (but not limited to) mode I only, the Yaoming Mi model, or sum of squares. The resulting K_{max}^{eqv} and K_{min}^{eqv} are used in calculating ΔK across the crack front where negative ΔK values are allowed by default. The resulting ΔK distribution is smoothed using a tension spline with natural boundary conditions at the crack breakout points. This smoothed ΔK distribution is then used to find the total crack growth on a point by point basis for the current growth increment.

10.2.2.3. ***Residual stress implementation***

BEASY can make use of both the Crack Opening Displacement (COD) Method and the J-Integral Method for calculating the stress intensity factor (SIF) due an applied residual stress. By default, BEASY completes both COD and J-Integral calculations, but it does not make use of the COD calculations unless specified by the user. To calculate SIF values using the J-integral, BEASY requires a full stress tensor as an input called the neutral file. The neutral file is generated by using an ABAQUS ODB with a high spatial refinement in the crack growth region to avoid interpolation error. To increase detail in the J-Integral variation, the number of J-Integral points in the radius of integration is increased from the default of 3 points every 90 degrees to 6 points every 90 degrees.

10.2.3. ***FRANC3D***

10.2.3.1. ***Overview***

FRANC3D is a fatigue crack growth software package that works with existing H-element FEA suites such as ANSYS and ABAQUS. FRANC3D supports 2D and 3D crack growth with complex loading involving both dynamic and static loads as well as residual stress. Users can select from several crack growth models such as the NASGRO equation or tabular $\frac{\mathrm{da}}{\mathrm{dN}}$ vs R data. Each crack front is represented by a series of discrete points and the crack face is made up of triangular facets. FRANC3D uses a special meshing algorithm for the region directly around the crack tip to ensure validity of the SIF results extracted using the J-integral method.

10.2.3.2. ***Crack face modeling***

FRANC3D defines the local direction of crack propagation by the "kink" angle, which is defined as the amount that the crack will deviate from the self-similar direction measured in a plane perpendicular to the crack front. There are five options for determining the kink angle. FRANC3D computes separate stress intensity factors for all three modes of fracture (K_I, K_{II}, and K_{III}). However, conventional crack growth rate models consider only one stress intensity factor range. FRANC3D provides the option to use an equivalent stress intensity factor that is a function of all three modes of fracture. The resulting K_{max}^{eqv} and K_{min}^{eqv} are used in calculating ΔK across the crack front where negative ΔK values are allowed by default. FRANC3D uses the calculated ΔK crack front distribution to find the total crack growth on a point by point basis for the current growth increment. The grown crack front shape is then smoothed using a variety of user selectable options such as polynomial least squares, tension splines, or a moving average.

10.2.3.3. ***Residual stress implementation***

Residual stress in FRANC3d can be defined by crack face tractions or pressures. FRANC3d allows for many different types of crack face loading, but for purposes of residual stress and data from the contour method only the user defined 2-D radial residual stress distribution will be discussed. The 2-D radial residual stress option allows for a variation of stress in 2-directions (axial and radial). The user has the option to define the distribution as an equally spaced point cloud containing the results from the contour measurements.

10.2.4. *General recommendations*

Several general recommendations are provided for specific aspects of coupled stress intensity and crack growth analysis predictions:

10.2.4.1. *Crack growth increment*

In general, a recommended crack growth increment between 1-5% is ideal. Previous analyses have demonstrated with higher growth increments there can be inaccuracies in characterizing the crack shapes and resulting life predictions. Smaller growth increments, however, require more solutions and drastically increase the time of the analysis. Comparisons between solution time and lives for various growth increments have been presented by Pilarczyk[67].

10.2.4.2. *Crack front points*

When unique crack shape evolution is expected, which is typically the case for analyses with residual stress, the number of points defining the crack front can influence the crack shape evolution and resulting predictions. As a general rule of thumb, if unique crack shapes are expected a minimum of 20 points should be utilized to define the crack front. For situations with 180-degree cracks with residual stress, consideration should be given to increasing the number of points beyond 20.

10.2.4.3. *Stress intensity and/or crack front geometry smoothing*

The various coupled FE-crack growth tools allow for smoothing the stress intensities and/or geometry along the crack front. The amount of smoothing can impact the accuracy of the crack front characterization. Over-smoothing can washout local behavior along the crack front. Under-smoothing can result in a jagged crack front, especially in analyses with higher crack growth increments. An example of over-smoothing is detailed in Chapter IV, Benchmark Case #2, Case #2, Submission 8. The plots detailing the stress intensity along the crack front demonstrate an appreciable difference for the applied and residual stress intensities relative to the other predictions with similar crack front smoothing. In general, averaging stress intensities over a range of +/- 4 degrees produces reasonable results, however, in situations with steep changes in stress intensity or geometry smaller ranges to capture the local behavior may be required. Ultimately, it’s important to understand the impact of smoothing along the crack front, completing sensitivity studies where necessary, to determine the appropriate parameters for the analysis.

10.2.4.4. *Crack front meshing*

Crack front meshing, utilizing a gradated mesh, is critical to optimize the meshing and run times while maintaining convergence of the solution. For p-element finite element methods a minimum, two layers of refinement is necessary. Convergence studies, investigating the impact from different local meshing techniques should be accomplished prior to running predictions. Also, meshing will change as the crack front progresses through the model and the analyst should review the meshing at different stages of crack growth to ensure convergence is maintained. In general, stress intensities should be converged with less than 1% error.

10.3. *Weight functions*

Weight functions methods have been traditionally utilized in fracture mechanics calculations to characterize a range of unique geometric and loading scenarios that result in complex stress profiles on the crack face. The incorporation of residual stress is one such example of complex stress profiles. Multiple weight function options to incorporate residual stress exist in common fracture mechanics toolsets (i.e. AFGROW, NASGRO). Historically, these predictions have resulted in mixed results relative to test data. Due to the unique two-dimensional state of stress on the crack plane, bivariant weight functions are more appropriate than univariant functions when characterizing residual stress. In recent round robin exercises (see Section 19) the bivariant weight function approach resulted in good predictions relative to test data. Additional comparisons relative to test data is necessary to understand the appropriateness of weight functions, specifically when utilizing assumed elliptical crack front shapes.

10.4. *Other approaches*

Details of other analytical approaches will be included in this document upon requests/receipt of analysis approaches from the residual stress analysis community.

11. *WAY FORWARD & RECOMMENDATIONS*

The analytical process for direct incorporation of residual stress continues to go through stages of refinement as the community exercises new capabilities. As a community, the process of multi-point fracture mechanics, coupling FE based stress intensity calculations with traditional crack growth engines, appears to be the most common and reliable method to predict crack growth with direct incorporation of residual stress. The ERSI Analytical Methods subcommittee has a focused effort to dissect analytical methods, understanding the influence of key factors, and ultimately recommend best practices. The first ERSI round robin focused on Cx holes (see Section 19) and resulted in specific findings and action items. Overall, the predictions relative to test were quite good for the coupled-FEA (various approaches) and weight function predictions (NASGRO). Several key findings were noted and are under investigation:

1. Crack aspect ratio
    a. Across each condition investigated, including the baseline conditions, all predictions resulted in poor correlation with the observed crack shape evolution (a/c) evident in the test coupons. This finding is consistent with the results of the recent AFGROW round robin[68] where residual stress was not included. Recent investigations by A-10 ASIP and LexTech[69] have demonstrated accurate characterization of crack shape evolution when considering crack growth rate differences for different material orientations. Additional test data and investigations are necessary to understand the best approach to accurately predict crack aspect ratio behavior. Moving forward, considerations should be given to incorporating the capability to characterize data in various material orientations in the crack growth predictions. This will necessitate additional data to understand the changes in material behavior and how to account for different growth rates in a multipoint analysis.
2. Sensitivity to stress intensity calculations
    a. Of key importance with predictions incorporating residual stress is understanding the typical operating range of the applied and residual stress intensities for the given spectrum, the fatigue crack growth rate data is being exercised, and the influence of inaccuracies in the K solutions. Notably, the results for submission #3, which utilized classic Newman-Raju k solutions for the applied stress, and Gaussian integration for the residual stress, were significantly impacted by inaccuracies in the Newman-Raju solutions. Errors in the K solutions are often amplified for predictions incorporating residual stress, giving additional credence to utilizing a coupled FEA-crack growth approach.
3. Characterization of FCGR data, to include negative R behavior
    a. It was evident in the ERSI round robin that lack of certainty in the

negative R data, and an appropriate Rlo, could be influencing the predictions. Additional testing is underway to characterize the negative R behavior and update the predictions.

4. Weight function predictions
    a. The initial ERSI round robin resulted in good predictions for NASGRO weight function methods. Additional investigations, to include situations with more complex crack shape evolution, are necessary to understand the accuracy of the weight function method. It should be noted that the NASGRO predictions had two key factors that should be investigated: 1) the assumed elliptical crack front shape and 2) the utilization of bivariant weight functions.
5. Crack front and K-solution smoothing
    a. Different smoothing/averaging approaches were used in the ERSI round robin, specifically for Submission #8. The resulting K-solutions for this submission were quite different than the other submissions. Ultimately, for the specific case studies the influence was "washed-out" by under- and over-predictions along the crack front for the applied and residual stress intensities; however, this will likely not hold true for other situations. As a result, additional guidelines should be developed for crack front and K-solution smoothing.

As a result of the ERSI round robin and other efforts, the following recommendations are proposed for the analytical methods for residual stress analyses:

1. Investigate material properties in various orientations and their influence on crack shape evolution and crack aspect ratios.
2. Investigate and resolve the analytical approach for crack aspect ratio behavior. Considerations should be given to the methods to characterize the behavior between two orientations (i.e. multi-point crack fronts).
3. When practical, utilize FE based solutions of actual geometries and loading to mitigate errors in the K-solutions.
4. Continue to develop FCGR data with specific focus on the negative R regime.
5. Investigate the behavior and appropriate method to characterize the Rlo threshold in the presence of residual stress
6. Investigate the utilization of weight functions and elliptical crack fronts for residual stress prediction applications.

CHAPTER III - OTHER CONSIDERATIONS

12. FACTORS THAT INFLUENCE RESIDUAL STRESS AND THE ASSOCIATED UNCERTAINTY

Many factors can influence the residual stress induced in a component, including processing parameters, geometry and material response, and degradation factors once in service. There's also the uncertainty that exists in the processes used to determine the residual stress in the component. All of these factors are important when completing crack growth predictions with residual stress. It's incumbent on the analyst to ensure they understand the key factors for their given situation and the resulting residual stress that is representative, including the uncertainty as well as in-service degradation risks. The following sections detail some of the key factors to consider.

12.1. *Variability in residual stress data*

When residual stress measurements are performed on a set of nominally identical specimens, measurement variability will occur. This measurement variability can be influenced by both specimen-to-specimen variability and measurement uncertainty.

Specimen-to-specimen variability is caused by differences in the manufacturing process creating the samples and generally cannot be determined. Often measurement uncertainty is further divided into two categories, one is random uncertainty and the other is bias errors. The root cause for random uncertainty is derived from random fluctuation in the source measurement data (e.g., noise in strain gage reading for incremental hole drilling) and bias errors are errors that are caused by differences between the experimental practice and the theoretical principle used to determine residual stress (e.g., assuming incorrect strain gage location in an incremental hole drilling measurement). In general, bias error can and is corrected for during data analysis. Therefore, random uncertainties are of primary importance in practice application.

12.1.1. ***Recommended criteria to specify when acquiring residual stress data***

When acquiring residual stress measurement data, it is important to ensure that the measurement data will be able to satisfy its end use. In general, it is important to ensure that the measurements determine the needed stress components, at the needed locations, with the needed measurement spatial resolution, and with an acceptable measurement uncertainty.

12.1.2. ***Determination uncertainty***

Each determination technique has difference sources of measurement uncertainty and general levels of measurement precision. The stress calculation procedure for both incremental hole drilling and incremental slitting uses an elastic inverse to fit the measured strains and these "fitted strains" are different than the measured strains (usually to a very small degree). The difference between the fitted and measured strains is called the strain misfit and this difference is the primary source of uncertainty reported for incremental hole drilling and incremental slitting. To determine the level of uncertainty that is caused by strain misfit, the strain misfit is propagated through the stress calculation procedure. To ensure this uncertainty source is conservatively estimated, a minimum value for the strain misfit is applied (i.e., if the strain misfit is below a given minimum value the strain misfit will then be taken as the chosen minimum value).

The uncertainty in the contour method has been found to be primarily driven by the analytic model used in the analysis[70]. This uncertainty is estimated by determining the residual stress using a range of analytic models (and subsequently calculating residual stress). The uncertainty is then determined by taking the standard deviation of the calculated residual stress from each of the analytic models at each spatial location.

12.2. *Key factors influencing residual stress*

Many factors can influence the initial residual stress imparted into a component, including the processing parameters, the component geometry, and the materials. Also, once placed in service, there are factors that can degrade residual stress over time. These key factors are reviewed in this section, with specific focus on laser shock peening and Cx of holes.

12.2.1. *Key factors that influence residual stress at LSP locations*

A significant amount of research has been directed towards understanding the effects of various laser peening processing parameters on the resulting residual stress and material performance. In general, the effects of the laser peening process are a function of the shock wave (shape and time history) and the specimen (geometry and material). The shock wave is primarily a function of the pressure pulse on the surface of the component, which is controlled by many of the different laser peening processing parameters including (but not limited to): the properties of the laser pulse (mainly the irradiance and pulse duration), the ablative layer material, and the inertial tamping layer material.

Three basic methods have been used to understand the effects of various laser peening processing parameters. First, measurements of the shock wave produced by laser peening have been performed for a range of parameter variations. Residual stress measurements have also been used to understand the effects of various laser peening processing parameters. There are several residual stress measurement techniques that have been used to measure the residual stress resulting from laser peening treatment including: x-ray diffraction with layer removal, hole drilling, the slitting method, and the contour method. Laser peening process models have also been developed to understand the effects of various processing parameters.

It is important to note that the residual stress resulting from laser peening depends on other factors besides just the laser peening processing parameters. For instance, the residual stress that develops in a given material treated with a given set of laser peening parameters depends on the constraint provided by the geometry of the specimen as well as the amount of area covered with laser peening.

The irradiance of the laser pulse is one of the primary laser peening processing parameters. It is generally accepted that a square root relationship exists between the irradiance of the laser pulse and the magnitude of the shock wave with an increase in the irradiance leading to an increase in the magnitude of the shock wave (diminishing returns). There is a level above which no further gains in shock magnitude will result. This limit is due to the dielectric breakdown of the inertial tamping layer (water) above certain irradiance levels (typically around 10 GW/cm^2 for 1.06 μm wavelength lasers).

Residual stress measurements have also been used to understand the effects of laser irradiance. The general consensus is that an increase in the laser irradiance leads to an increase in the magnitude of the compressive surface residual stress as well as an increase in the depth of compressive residual stress (with diminishing returns at high irradiance).

The number of laser peening layers is another primary laser peening processing parameter. The benefits of multiple layers result from the combined effects of repeated impacts. The general consensus is that multiple layers of laser peening will increase the depth of compressive residual stress (diminishing returns with subsequent layers) by as much as a factor of 2.

Other process parameters can have a less significant impact on the resulting residual stress including the pulse duration, type of ablative layer material, and the spot size/shape.

12.2.2. *Key factors that influence residual stress at Cx holes*

Over the past 5+ years, significant focus and investment has been leveraged to understand and quantify the influence of key factors on the residual stress at Cx fastener holes[71,72,60]. These efforts focused on utilizing the contour method to quantify residual stress over a range of different hole sizes, applied expansion levels, edge margins, and materials. The contour method offers a unique utility of the data, providing the necessary data density on a plane of interest, and is relatively easy to obtain. These benefits make it a unique method to support predictions at Cx holes.

12.2.2.1. *Hole diameter influence on residual stress*

The scalability, or nondimensional behavior, of residual stress at Cx holes based on hole diameter (or radius) was initially demonstrated with replicated coupons investigating hole diameters of 0.25-inch, 0.50-inch, and 0.75-inch in 2024 and 7075 aluminum coupons. These investigations indicated a strong correlation between residual stress at Cx holes and the hole diameter[71] (see Figure 32).

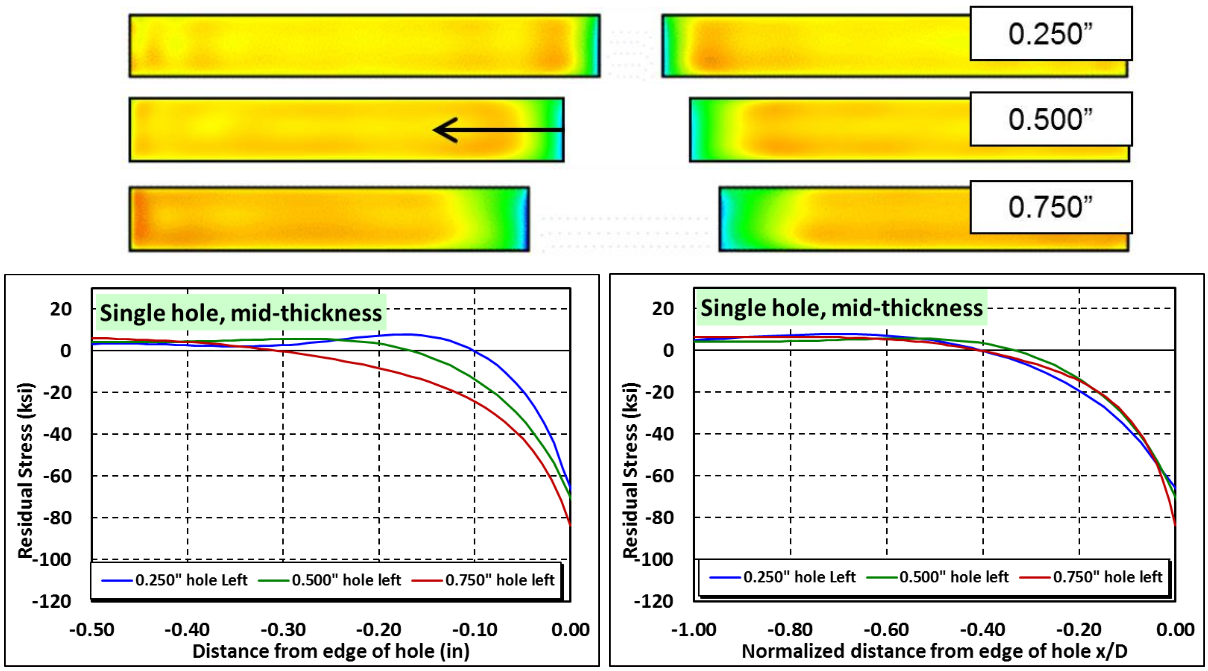

Figure 32 – Contour and mid-thickness plots for 2024 coupons with 0.25-inch, 0.50-inch, and 0.75-inch diameters. Left side – dimensional data; right side – nondimensional data based on hole diameter.

12.2.2.2. *Applied expansion influences on residual stress*

Applied expansion has also been investigated to understand residual stress behavior at Cx holes[71]. Utilizing 2024 aluminum coupons with a 0.50-inch centered hole, the applied expansion was varied within the FTI specification limits (controlling pre-Cx hole and mandrel diameters) to characterize the change in residual stress. The applied expansions included 2.3%, 3.7%, and 4.2%, representing minimum, mean, and maximum applied expansions within the allowed specification, respectively. Replicate coupons are detailed in Figure 33 with 7.2 ksi error bars (10% of maximum stress). The resulting average of the replicates for each applied expansion population indicate a trend, albeit minor, of deeper residual stress away from the hole with increased applied expansion (see Figure 34). More recent investigations have exhibited a similar trend related to applied expansion with high applied expansions resulting in slight reverse yielding at the surface of the hole. On a separate program[60] out of plane deformation was characterized and demonstrated a clear correlation to applied expansion (see Figure 35).

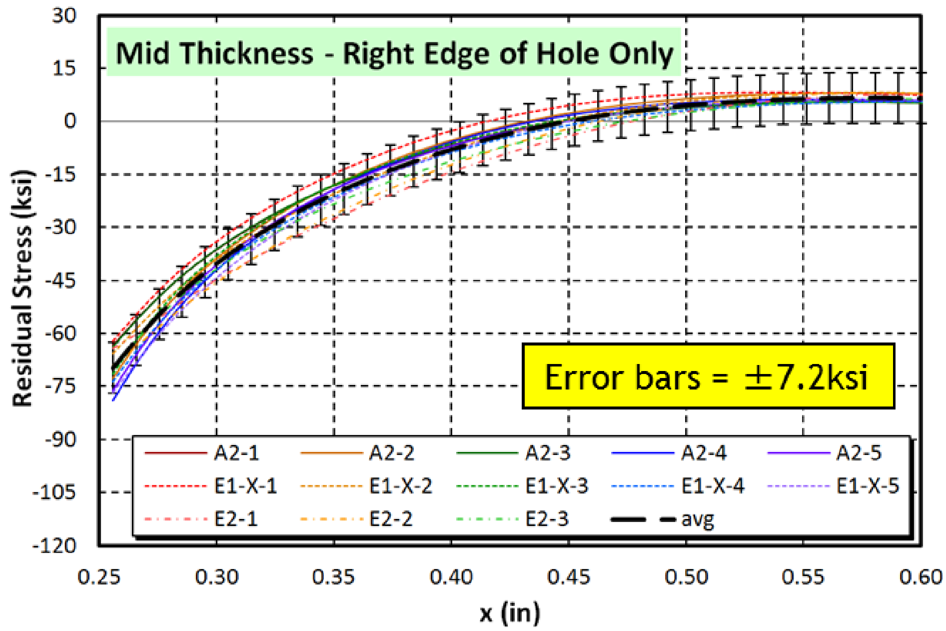

Figure 33 – Variation in residual stress for different applied expansions– mid-thickness plots for replicate coupons (A2-X – minimum Cx, E1-X – mean Cx, E2-X – maximum Cx).

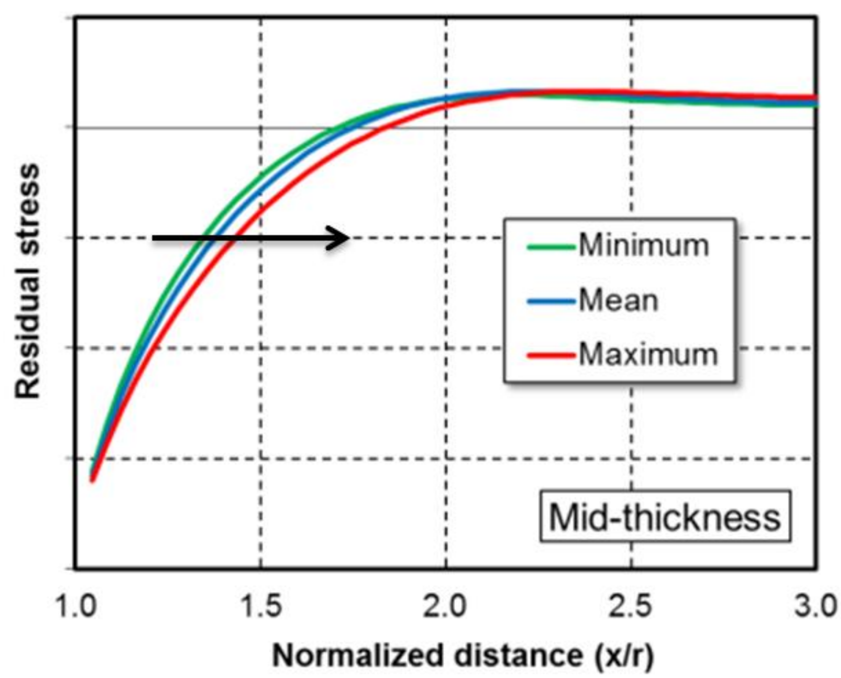

Figure 34 – Variation in residual stress for different applied expansions– mid-thickness plots for 2024 coupons with 0.50-inch diameter hole.

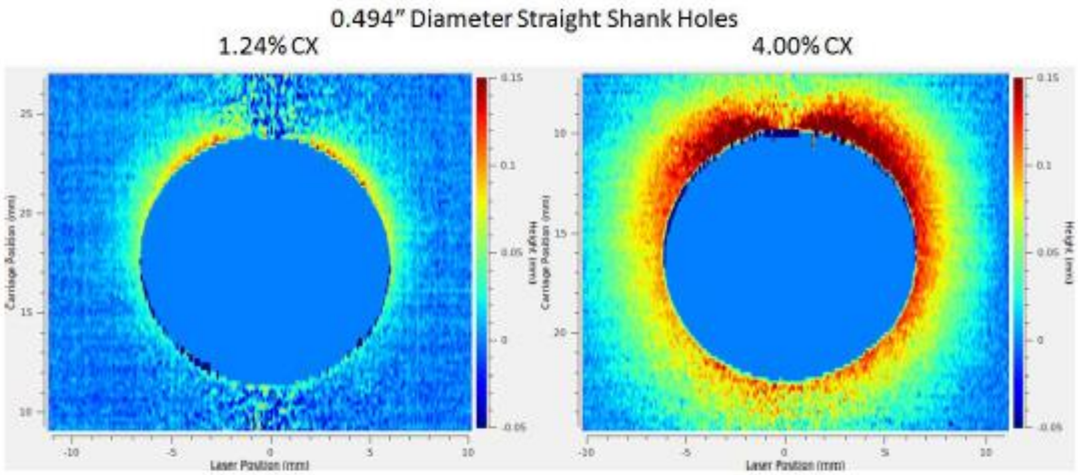

Figure 35 – Deformation around a Cx straight shank hole with different amount of applied expansion. The left image is out of specification; the right image is in specification. Location of the slit sleeve "pip" can clearly be seen at the top of each image[60].

12.2.2.3. ***Edge margin influences on residual stress***

Repair scenarios often require oversizing of holes to remove damage, reducing the edge margin below original production levels. Short edge margins are often a key driver for short inspection intervals and Cx is often utilized to mitigate the impact. As a result, understanding and quantifying the changes in residual stress as a function of edge margin is critical for analyses. To address the key factors, a previous program investigated the change in residual stress as a result of reduced edge margin[71]. Coupons with edge margins ranging from e/D of 4.0 to 1.2 were evaluated to understand the key behavior. Ultimately, the residual stress directly at the edge of the hole was similar for all the replicates and edge margin conditions, however, there was a distinct difference in the behavior moving away from the hole. Most notably, there was a direct relationship between the edge margin and the tensile residual stress at the edge of the part adjacent to the hole. Tensile residual stresses were greatest for the e/D=1.5 condition with slightly less tensile residuals in the e/D=1.2 condition. For this short edge margin condition (e/D=1.2), there was a noticeable "bulge" in the edge of the part and a reduction in overall residual stress relative to the other conditions (see Figure 36 and Figure 37).

To complement the residual stress characterization above, fatigue tests were accomplished to characterize the relative damage tolerance life between baseline non-Cx holes (NO CX), precracked, then Cx holes (PC then CX), and Cx and precracked holed (CX then PC) for edge margins (e/D) of 1.39, 1.89, and 2.4[60]. These results indicate a reduction in the life improvement factor relative to a non-Cx hole with decreasing edge margin (see Figure 38).

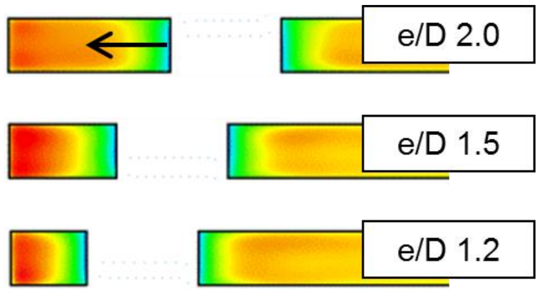

Figure 36 – Contour plots for various edge margins (e/D)[71].

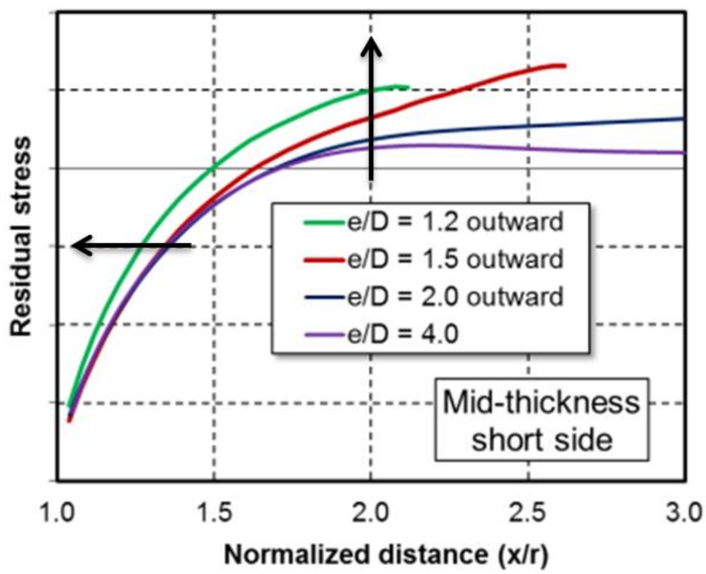

Figure 37 – Mid-thickness line plots for various edge margins (e/D)[71].

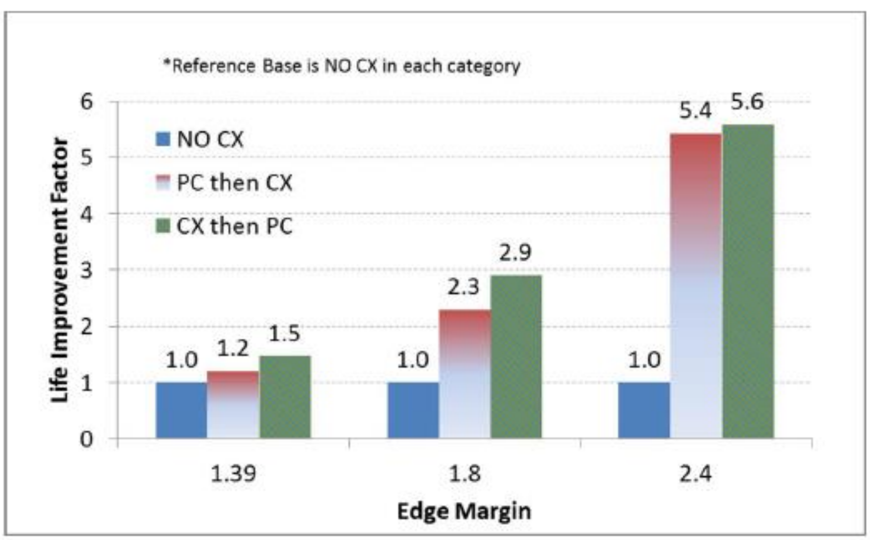

Figure 38 – Life improvement factors for various edge margins referenced to "no CX" in each category[60].

12.2.2.4. ***Material influences on residual stress***

Investigations into the effects material parameters have demonstrated a correlation between the residual stress at Cx Holes and the bearing yield strength, F_{bry}. This relationship is defined by Equation 5.

$$S_{zz\_nondimensionalized} = \frac{S_{zz}}{A*F_{bry}{}^{\alpha}\left[-\left(B^{-x/r}\right)+1\right]+F_{bry}\left(B^{-x/r}\right)} \qquad (5)$$

Where A=300, α=0.75, and B=1.1 for all materials. Data indicates that when the residual stress data is non-dimensionalized based on Equation 5 the resulting residual stress profiles are comparable and consistent (Figure 39). Currently the physical meaning behind the Parameters A, B and α are unknown but have resulted in the greatest reduction in residuals when transforming from one material to another. Four materials (7075-T651, 7075-T7351, 2024-T351, and 4340) and three diameters (0.250-inch, 0.500-inch, and 0.750-inch) were non-dimensionalized based on Equation 2 for comparison (Figure 39). The results provide insight into the impact of non-dimensionalized residual stress profiles based on hole diameter and material and their influences on the stress intensity. The residuals were as much as 5 ksi different, but the overall effect that those differences had on stress intensities were reasonably close to the replicate variation ~5%. If residual stress data is not available for the actual condition of interest, transformations based on hole diameter are a reasonable approach to develop the residual stress for analyses, given other variables are representative between conditions. Further investigation with different materials would be provide additional insight into the non-dimensional behavior of residual stress at Cx holes.

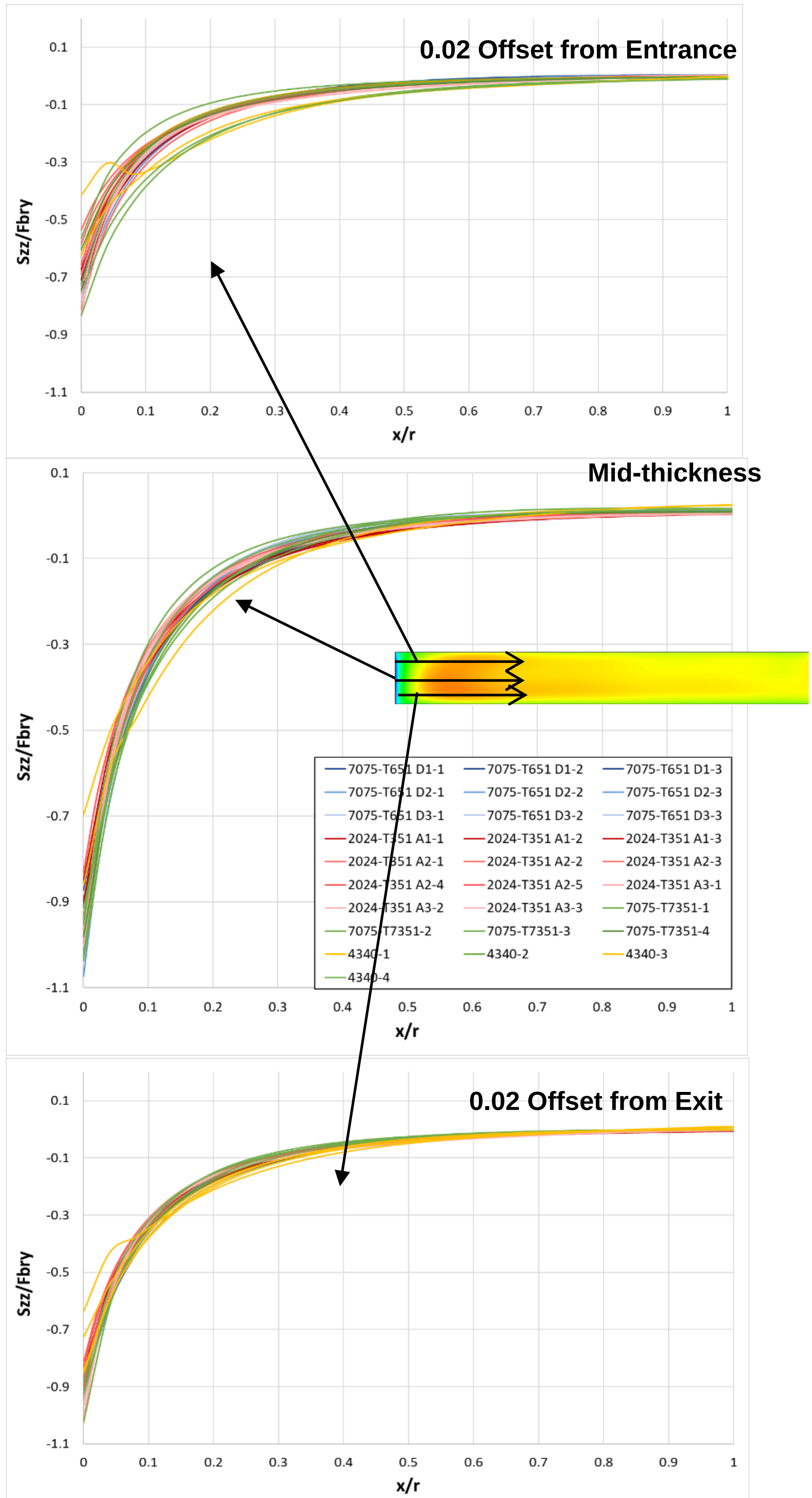

Figure 39 – Non-dimensional line plot comparisons between similar samples, transforming based on hole diameter and Fbry using appropriate edge margin values

12.2.2.5. ***Thickness Influences on residual stress***

Recent investigations have focused on quantifying the change in residual stress as a function of thickness and thickness/diameter (t/D) ratio[73]. The results of these investigations have demonstrated a distinct change in residual stress with increased thickness, with a decrease in stress at the bore surface but greater residual stress away from the hole (see Figure 40). Reverse yielding is observed in the 1-inch thick coupons. Considering the increased constraint in the part with increased thickness, the localized stress at the edge of the hole would increase as well, resulting in a threshold where reverse yielding is observed.

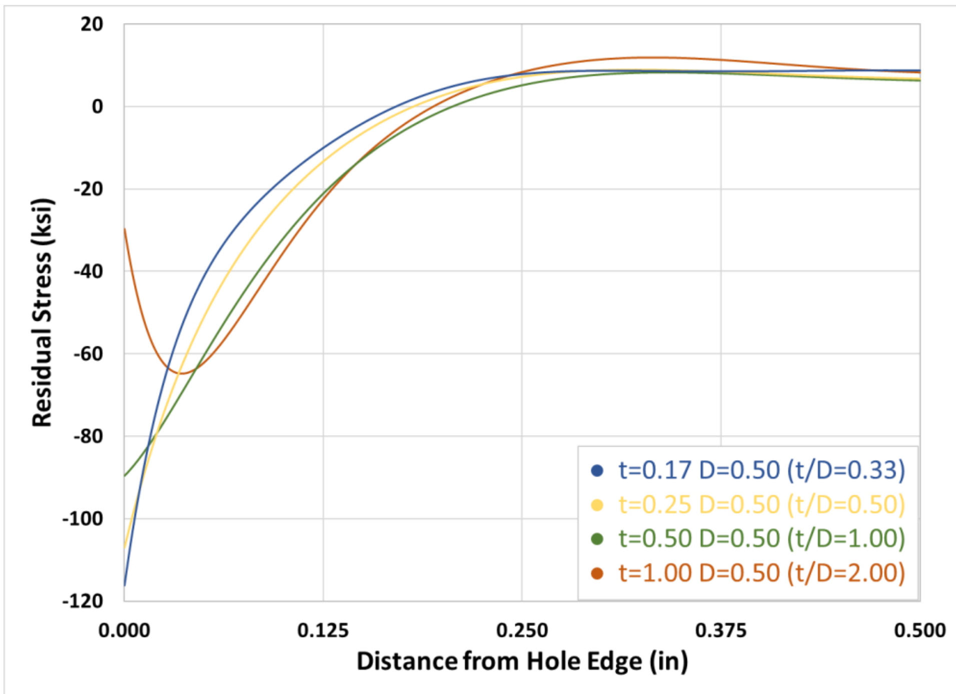

Figure 40 – Mid-thickness residual stress for various thickness/Diameter (t/D) ratios.

12.2.2.6. ***Hole geometry/processing influences on residual stress***

The influence of hole geometry and processing parameters can have a significant influence on the resulting residual stress at Cx holes. Figure 31 details the crack shape evolution differences between straight shank, retrofit countersink Cx, and production Cx conditions. For each of these cases, the crack shape evolution and damage tolerance life were significantly influenced by the processing steps and resultant residual stress. Ultimately, it's critical to understand the processing steps followed for the condition of interest and ensure the utilized residual stress is representative of that condition.

12.2.3. ***Factors that may relax residual stress***

Environmental, aging, and/or service factors can degrade residual stress over time. Some of these key factors. Also, general guidance is provided for situations where analytical benefit should not be taken for residual stress.

12.2.3.1. *Elevated temperatures*

Stress relaxation of residual stress can be an issue for components exposed to “elevated temperatures”. The rate of relaxation is greatest when the finishing process produces the steepest residual stress gradient normal to the surface[74]. The residual stress relaxation rate is also a function of the true plastic strain induced in the material during plastic deformation, sometimes referred to as the percent cold work. When a material is plastically deformed energy is stored in the material in the form of elongated grains, dislocation density, dislocation entanglement, and reorientation of grains. At “elevated temperatures” this stored internal energy acts as a driving force for stress relaxation; therefore, the greater the amount of cold work and stored energy in a material the greater the likelihood of stress relaxation at “elevated temperatures”.

Figure 41 illustrates a comparison of residual stress profiles and percent cold work distributions for an Inconel 718 steel surface processed using shot peening, gravity peening, laser shock peening, and low plasticity burnishing methods. The residual stress profile for shot and gravity peening compared to laser shock peening and low plasticity burnishing has similar maximum residual stress but their residual stress profile depths are much shallower. The percent cold work was determined using x-ray diffraction line broadening. The percent cold work plot indicates a greater percent cold work at the surface for shot peening relative to the other processes. As a result, residual stress inducing processes such as shot peening are comparably more susceptible to residual stress relaxation at “elevated temperatures” versus processes that produce relatively deeper residual stress profiles and less cold work at the surface of the material.

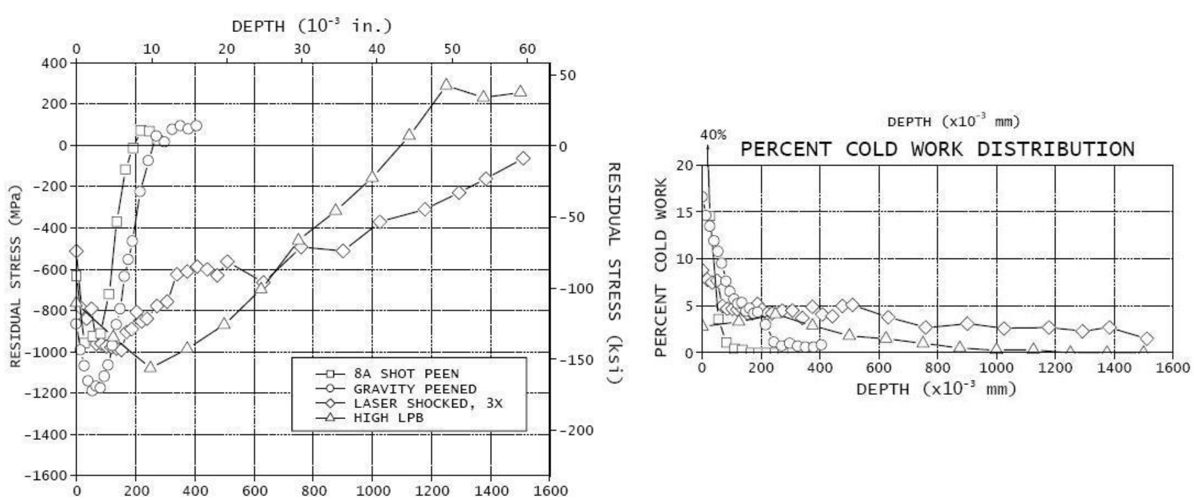

Figure 41 – Subsurface residual stress and percent cold work distributions produced by shot peening (8A, 200%), gravity peening, LSP (3X), and LPB in IN718.[34]

12.2.3.2. ***Overloads/Underloads***

Recent investigations (analytical and testing) by AP/ES have focused on quantifying the impacts of tension and compression loads at open and filled Cx holes[75]. These experiments demonstrated limited redistribution resulting from applied tension loads (27.9 ksi), for both the open and filled hole conditions, with damage tolerant lives and residual stress measurements within expected population variance. For the compression loaded coupons (-12.6 ksi), however, there was a discernable difference from the baseline coupons, with differences in fatigue life and residual stress measurements. As expected, greater redistribution of residual stress was observed for the open vs. filled holes, with the propping effect minimizing the compressive yielding at the hole. Additional details are contained in reference 75, however, the damage tolerant life differences between the various conditions is detailed in Figure 42.

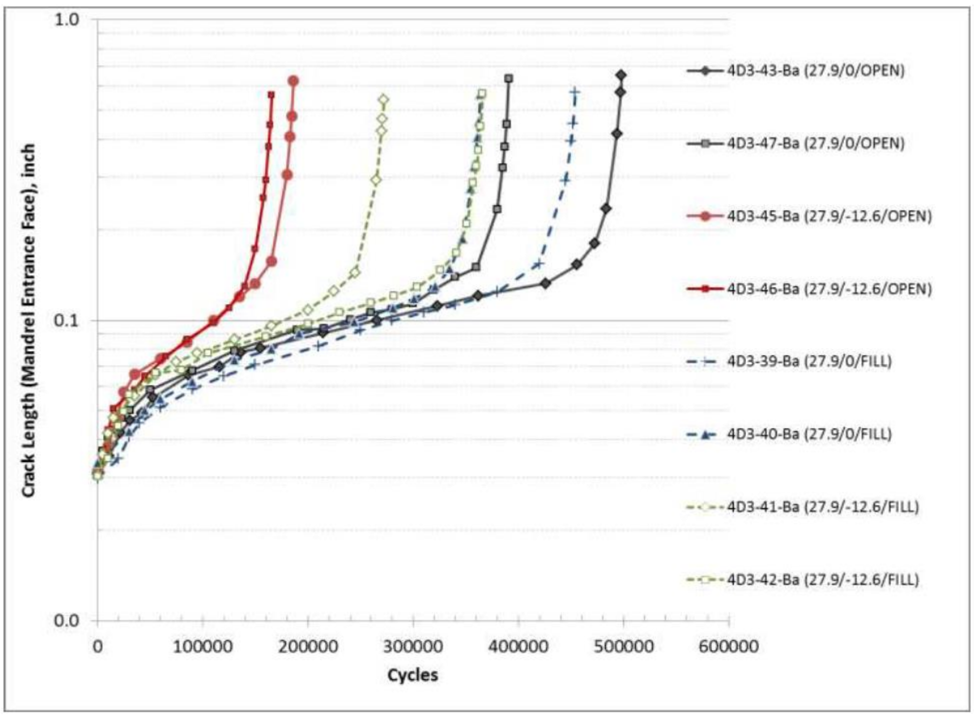

Figure 42 – Residual stress redistribution with applied tensile and compressive loads, open and filled Cx holes[75].

12.2.3.3. ***Initial cyclic redistribution***

Recent observations with residual stress measurements have indicated in some situations an initial redistribution of residual stress. These changes have been observed in situations with relatively high stress concentrations at the hole (open countersunk hole). The change in residual stress appears to stabilize rapidly, however, there is an initial "set" of residual stress. Figure 43 details the results of a recent investigation which included comparisons of baseline non-cycled coupons and cycled coupons, comparing the residual between the two conditions (cycled / non-cycled). In these coupons, a reduction of approximately 10-20 ksi is observed near the hole surface with increased residual compressive stress (0-10 ksi) away from the hole. This behavior is not observed universally and it's unclear, at this point, in what conditions it may occur. When developing a residual stress determination effort, consideration should be given to applying initial cycles to the coupons prior to accomplishing the measurements.

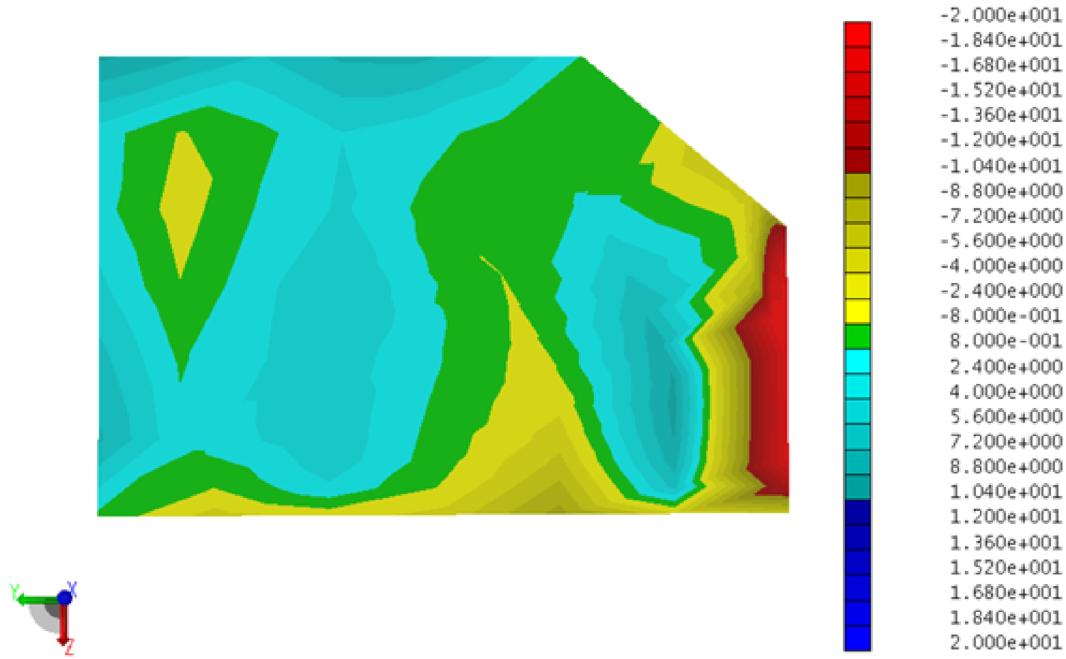

Figure 43 – Residual stress residual (cycled coupon – non-cycled coupon) for countersunk open hole coupons.

12.2.3.4. ***Crack tip plasticity interaction***

Carlson[76] recently investigated the interaction of a fatigue crack and the residual stress induced from the Cx process, focusing on the FTI Split Sleeve Cold Expansion process applied to 2024-T351 and 7075-T651 aluminum alloy coupons. Baseline coupons as well as coupons with fatigue cracks grown to specific surface lengths ranging from 0.08-0.50 inch were processed with the contour method to determine the residual stress. Spatial comparisons between each condition were completed to determine if there was a quantifiable change in the residual stress field as a result of the fatigue crack.

For the 2024-T351 coupons, there was a measurable difference in residual stress near the surface of the bore of the hole (0.01-inch) for crack sizes greater than 0.125-inch in surface length (see Figure 44). For the 7075-T651 coupons, there's a distinct difference between the baseline residual stress, shown in red in Figure 45, and the coupons with various crack sizes. It's unclear if this difference is attributed to differences between the baseline and cracked populations, initial changes in residual stress due to cycling (the baseline coupons weren't cycled), or an artifact of the interaction of the fatigue crack. Additional testing and analysis are necessary to quantify the results observed by Carlson.

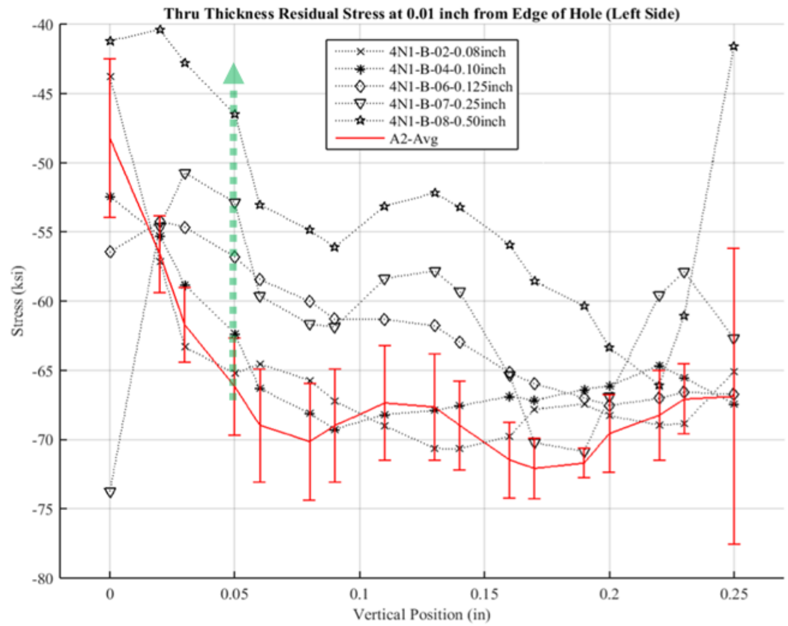

Figure 44 – Thru thickness line plot of residual stress at 0.01-inch from edge of hole; 2024-T351 coupons, various crack lengths.

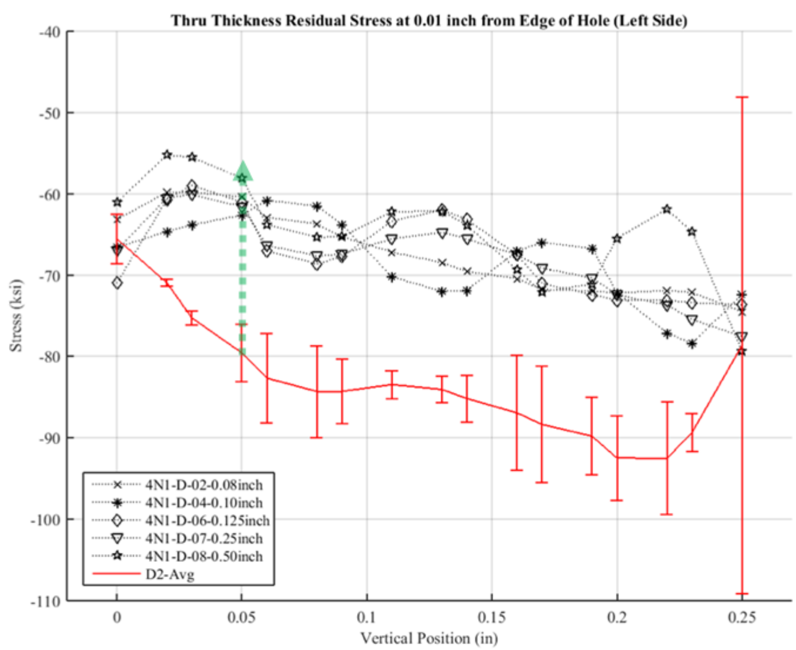

Figure 45 – Thru thickness line plot of residual stress at 0.01-inch from edge of hole; 7075-T651 coupons, various crack lengths.

12.2.3.5. ***Local stress from fastener loads***

As mentioned in Section, 12.2.3.2, AP/ES has sought to examine residual stress redistribution (from initial cold work) due to externally applied spectrum stresses, focusing on the maximum tensile stress present in a spectrum as well as the most compressive stress. Those results showed varying degrees of tensile stresses (up to 42 ksi peak spectrum stress) had minimal impact on the overall residual stress distribution. However, compression (down to -12.6 ksi) showed measurable influence on the residual stress field and attendant fatigue response. These experiments included filled holes but no load transfer (NLT). Thus, additional specimens were examined, both with contour method residual stress data and with fatigue crack growth, that contained low levels of load transfer (LLT, 10%) and high levels of load transfer (HLT, 50%).

Note that the specimens were not fatigued in the fully assembled condition. The goal was not to determine fatigue behavior under load transfer scenarios. Rather, the goal was to examine residual stresses and fatigue crack growth compared to the open hole and filled hole cases. Thus, the specimens were cold worked, assembled into joints, precycled two times at the levels seen for the no-load transfer cases, and then disassembled. The primary coupon was then subjected to residual stress mapping or fatigue testing.

Testing budget was limited, so these load transfer cases were limited to the -12.6 ksi compression cycles (as opposed to no compression), since the compression cases for the open and filled holes were the only case that showed measurable difference in fatigue response.

Figure 46 shows crack growth data from the low-load transfer conditions compared open hole and filled hole specimens with no load transfer. Note that crack growth rates, if anything, are slightly slower than the filled hole case without load transfer. In no way does the data suggest that the 10% load transfer is detrimental to the residual stress state.

The HLT case (50%) showed that, when the crack was less than 0.1-inch, crack growth rates were not unlike that of the LLT (10%) case. As the crack grew larger, however, rates increased much more rapidly than all other cases. This is likely due to the change in crack shapes associated with the HLT specimen. All specimens contained corner saw cuts (0.01-inch x 0.01-inch), and for NLT and LLT cases, the cracks generally formed and propagated as corner cracks. In the HLT cases, however, despite the saw cuts, the cracks formed all along the bore of the hole and exhibited very early transition to a full through crack. Thus, the likely explanation of the faster growth rate at longer crack sizes is the difference in K for a 0.1-inch corner crack versus a 0.1 inch through crack.

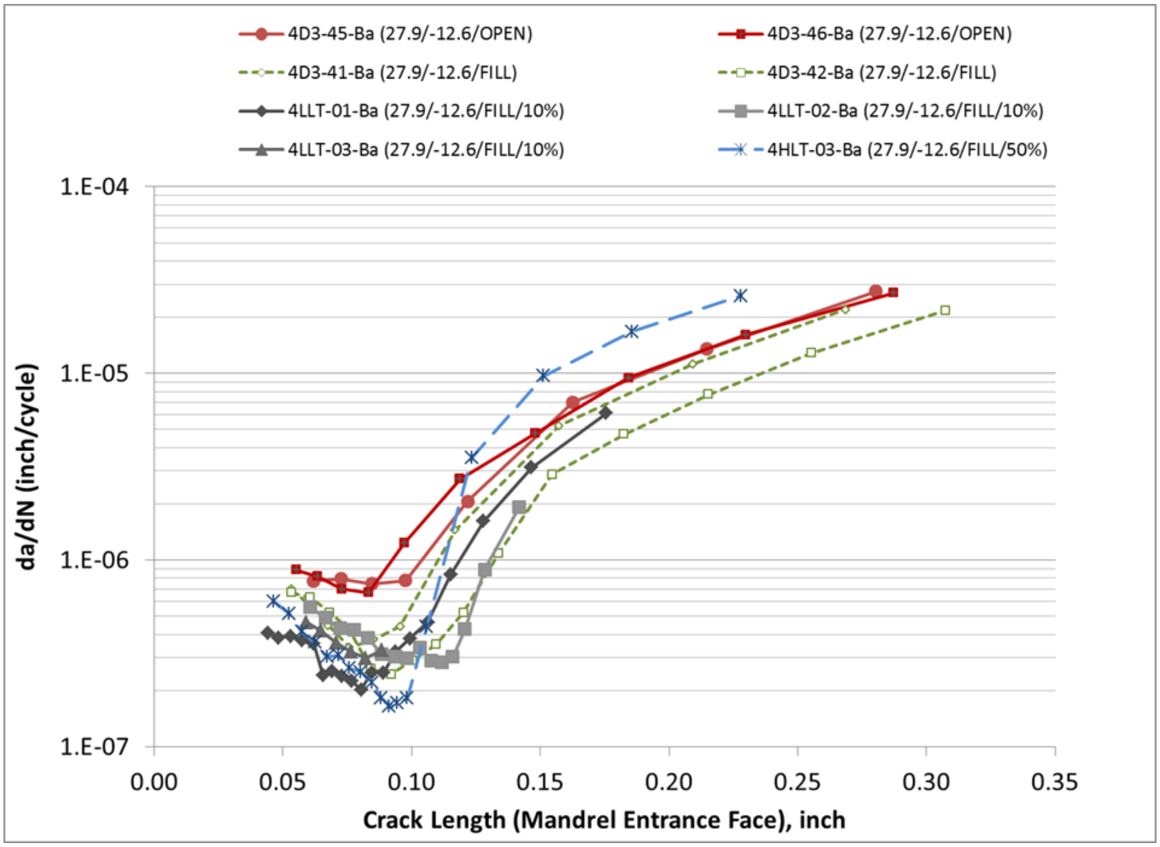

Figure 46 – da/dN vs. crack length for a variety of hole fill (open, filled) and load transfer conditions (none, 10%, 50%) for 2024-T351 containing a 0.25-inch Cx hole (nominal 4% expansion).

12.2.3.6. ***Operational usage***

The stability and presence of residual stress over the service life of an aircraft is important in terms of aircraft sustainment. To understand this key aspect of aircraft sustainment, the USAF and Hill Engineering LLC developed a program focused on quantifying the level of residual stress remaining in post-service aircraft structure[77,78]. As part of this effort lower wing skins from A-10 and T-38 aircraft were disassembled and 205 residual stress measurements were performed using the contour method. The service life of these aircraft reflects some or all of the effects that could reduce residual stress discussed in sections 12.2.3.1-12.2.3.5. The measurements from the fleet assets were compared with 105 specimens representing specific structural details that were manufactured and measured to establish a baseline for the original (pre-service) residual stress from cold expansion.

Overall, the comparison program was successful in interrogating and comparing residual stress from post-service aircraft structure. In this investigation, no “missed Cx” locations were identified. A comparison strategy was developed and the level I comparisons (high level initial look) were completed, resulting in comparable stress between the teardown and new manufacture coupons. Given the wealth of data developed, additional comparisons and analyses should bear benefits, however, initial comparisons indicate substantial residual stress remains in assets with many years of operational usage. A few comparisons between the original and remaining residual stress are presented herein with additional details of the analysis and results can be found in references 77 and 78.

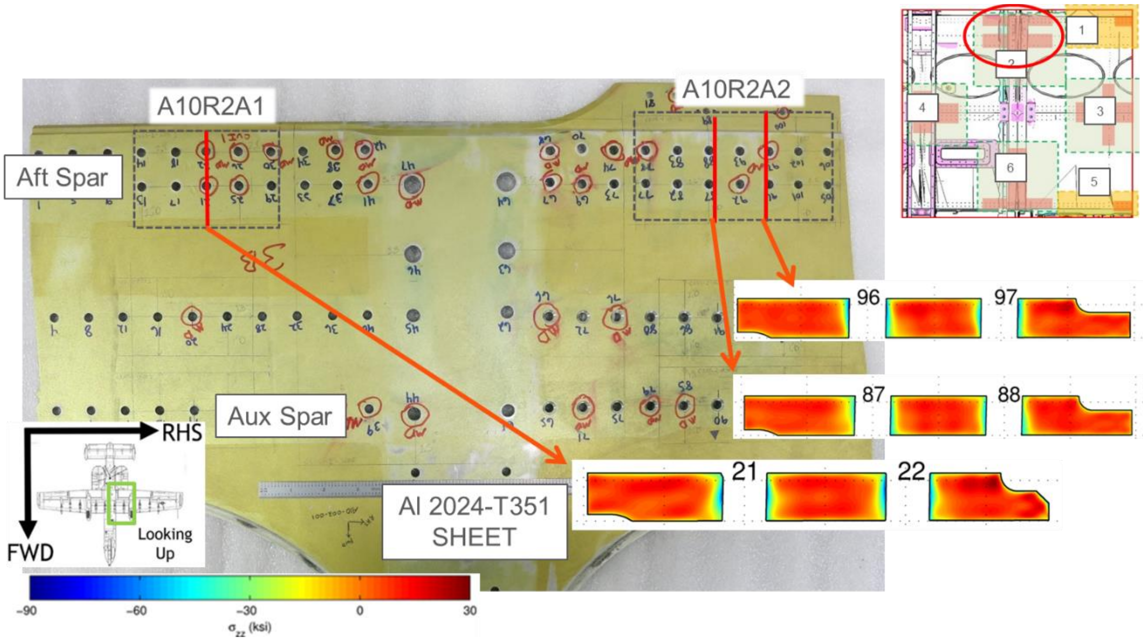

Figure 47 – Residual stress teardown measurements, A-10 section A10R2A.

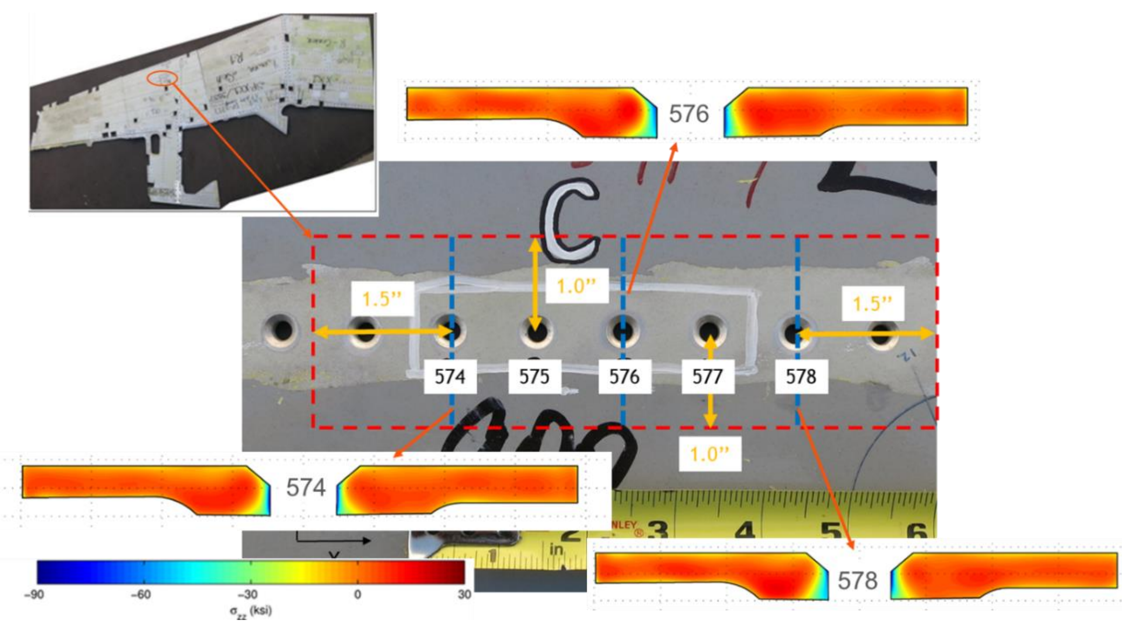

Figure 48 – Residual stress teardown measurements, T-38 section C.

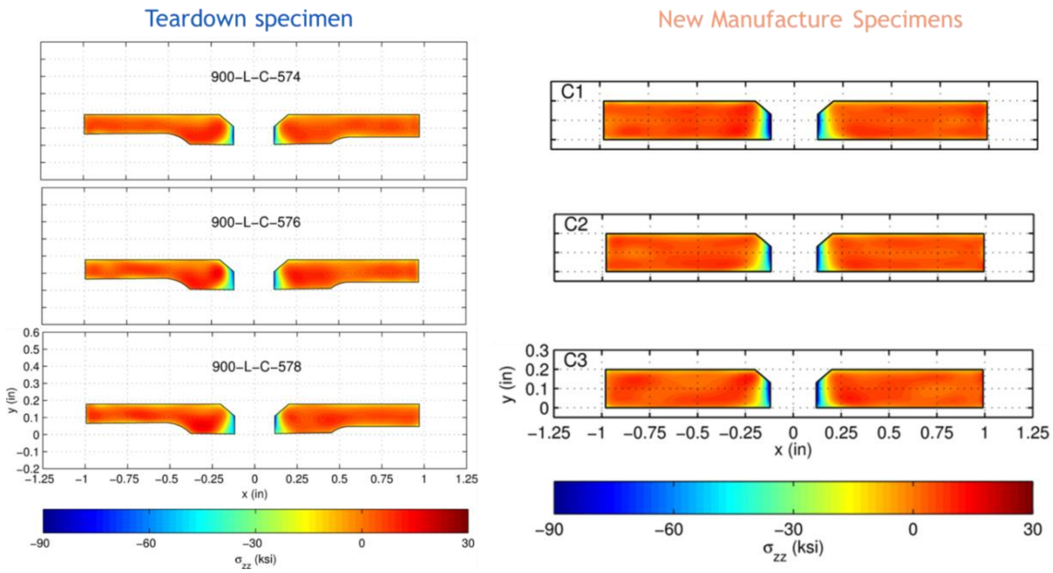

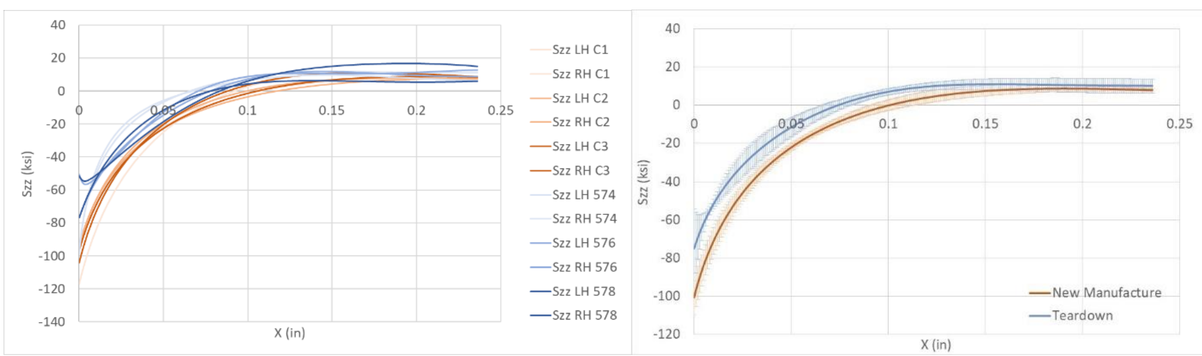

Sample ID	Midthickness 0.125*rad	Midthickness 0.25*rad	Midthickness 0.5*rad	Midthickness 0.75*rad	Depth at crossover (midthickness)	Point Value of Entrance	Avg RS in 0.05" Radius Entrance	Standard Deviation of Avg RS in 0.05" Radius CSK Entrance	Point Value CSK Knee	Avg RS in 0.05" Radius CSK knee	Standard Deviation of Avg RS in 0.05" Radius CSK Knee
L-574	-38.43	-19.75	-2.03	6.75	0.07	-53.16	-40.28	16.15	-63.92	-27.65	21.75
R-574	-35.04	-16.91	-2.02	4.98	0.07	-42.27	-37.02	15.61	-85.85	-27.03	25.09
L-576	-46.61	-30.49	-5.84	6.59	0.07	-40.76	-41.01	6.95	-60.31	-37.44	16.65
R-576	-45.99	-29.64	-8.43	4.48	0.08	-59.14	-42.29	14.00	-77.47	-33.03	19.90
L-578	-46.17	-33.41	-12.04	2.43	0.08	-44.08	-43.69	6.42	-83.04	-33.72	17.61
R-578	-43.63	-26.04	-6.29	2.77	0.08	-6.57	-36.56	11.06	-86.97	-32.75	23.03
L-C1-A-1	-70.33	-45.47	-16.31	-0.53	0.09	-76.77	-55.63	20.02	-120.86	-58.23	27.32
R-C1-A-2	-56.72	-37.29	-15.60	-4.02	0.11	-43.28	-46.30	12.49	-90.34	-47.26	23.50
L-C2-A-1	-55.40	-37.00	-16.62	-5.72	0.12	-58.33	-44.72	11.89	-98.20	-47.81	23.96
R-C2-A-2	-54.73	-35.17	-13.42	-2.13	0.10	-59.49	-49.26	13.93	-87.51	-44.52	22.29
L-C3-A-1	-57.99	-38.39	-16.07	-3.89	0.11	-28.51	-45.27	14.78	-106.08	-49.72	25.38
R-C3-A-2	-60.71	-38.44	-12.67	1.09	0.09	-26.75	-52.90	15.59	-104.08	-49.88	24.71
Mean	**-42.64**	**-26.04**	**-6.11**	**4.67**	**0.07**	**-41.00**	**-40.14**	**11.70**	**-76.26**	**-31.94**	**20.67**
Stdev	**4.81**	**6.48**	**3.85**	**1.83**	**0.01**	**18.30**	**2.85**	**4.27**	**11.50**	**3.94**	**3.24**
Mean	**-59.31**	**-38.63**	**-15.11**	**-2.53**	**0.10**	**-48.86**	**-49.02**	**14.78**	**-101.18**	**-49.57**	**24.53**
Stdev	**5.80**	**3.56**	**1.65**	**2.51**	**0.01**	**19.58**	**4.44**	**2.91**	**12.11**	**4.67**	**1.73**
Residuals (Td-NM)	16.67	12.59	9.01	7.20	-0.03	7.86	8.87	-3.09	24.92	17.63	-3.86
P Value	0.00	0.00	0.00	0.00	0.00	0.24	0.00	0.09	0.00	0.00	0.02
Significant	Yes	Yes	Yes	Yes	Yes	No	Yes	No	Yes	Yes	Yes

Figure 49 – Residual stress comparison results, T-38 section C.

13. VALIDATION TESTING

13.1. *Testing considerations with residual stress*

Residual stress often brings additional complication for validation tests. The purpose of this section of the document is to highlight some considerations, lessons learned, and best practices to consider when designing and executing fatigue testing of coupons with residual stress. Nuances of each test will ultimately drive the final details of the test plan; however, the following should be considered:

13.1.1. *Coupon geometry considerations*

In traditional fatigue tests without the inclusion of residual stress, considerations for coupon geometries to mitigate cracking away from the test location are always important. When residual stress is introduced, fatigue lives often increase exponentially, making design considerations away from the test section even more critical. For cold expanded fastener hole tests, dogbone coupons are a preferred approach to mitigate the risk of coupon failure at the grips. The grip width to test section should typically be greater than 1.5x with a gradual transition radius (~radius=5-10 inch). The grip width, test section width, and transition geometry can be optimized to minimize stress concentration, K_t, effects while efficiently managing the size of the coupon. Figure 50 is an example of a dogbone coupon design. An alternative approach is to bond tabs onto the coupons at the grip location, however, special care must be taken during surface preparation for bonding to minimize the risk of coupon and bond-line failures. Surface preparation, if completed with incrementally finer sand paper, should orient the sanding direction parallel to the loading axis to mitigate cracking. Grit blasting is a proven approach to prep the coupon for bonding. Also, if bolted grips or additional fastener holes are included in the coupon, consideration should be given to cold expand these holes to mitigate undesired secondary cracking.

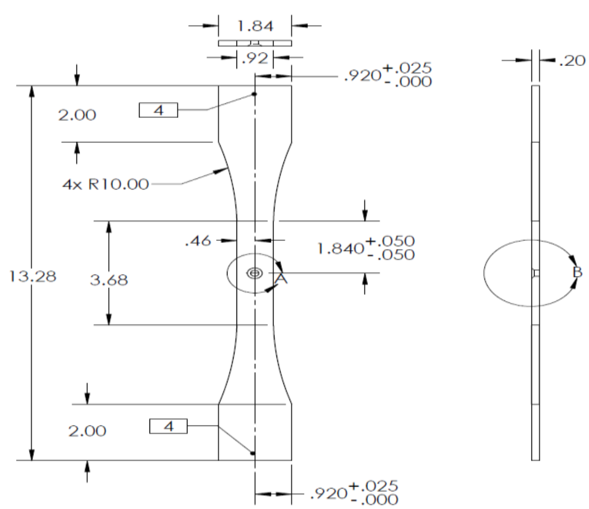

Figure 50 – Example dogbone coupon design

13.1.2. *Notched versus naturally nucleating cracks*

When developing coupons with residual stress, the tradeoffs between notched (EDM, jeweler's saw, etc.) and naturally occurring cracks should be considered. Notching coupons has benefits and drawbacks, and the goals of the test program will drive the best option.

13.1.2.1. *Notch benefits:*

- Greater likelihood for one dominant crack – better for validation tests where secondary cracking can convolute analysis vs. test comparisons.
- Crack measurements and tracking are more effective if the crack origin is known. Naturally occurring cracks can be problematic to identify in their "smaller" stages, increasing the risk of missed data and unexpected failures

13.1.2.2. *Notch drawbacks:*

- Natural crack shape evolution (coalescence of multiple cracks) may be different than a notched coupon with one dominant crack
- Natural crack nucleation locations are suppressed, which could mask competing failure locations or other complications
- Depending on the depth of the residual stress, notch effects on the crack may be difficult to mitigate

When considering notching coupons, the benefits and drawback should be reviewed to tailor to the goals of the test program. If notching is accomplished, the notch size, location, and shape should be reviewed carefully. Typically, the notch is placed at the expected nucleation location. In some instances, the notch is located at or near the location that correlates with DTA assumptions. Processes like Laser Shock Peening will change the peak stress profile and the resulting preferential nucleation location. Careful planning, supported by FEA, should be considered to correctly identify the appropriate notch location. For cold expanded fastener holes, the typical notch location is the mandrel entrance corner of the hole. For countersunk holes, the preferential nucleation and growth location is typically from the countersunk knee. Previous programs[45,78] have demonstrated difficulties notching coupons with cold expanded holes at other locations. Also, the notch size should be minimized (<0.025-inch) to mitigate the notch effects on the crack. Notch shapes can be tailored to represent the semi-circular shape of a corner crack using a circular shaped EDM plunge geometry. If possible, removal of the notch after precracking is preferred (without reaming the hole beyond the size limit recommended for the cold expansion tooling).

13.1.3. *Secondary cracking considerations*

Because of the extended fatigue lives often observed when engineered residual stress are induced at critical locations, secondary cracking is often prevalent. In the case of cold expanded fastener holes, secondary cracking often occurs at multiple locations along the bore of the hole and on the opposite side of the hole. This is more prevalent when a starter notch is not introduced into the coupon. Careful monitoring of the coupon at these locations should be accomplished during testing to identify when secondary cracks nucleate. Secondary cracking growth should be documented and, when stress intensity calculations are completed, evaluated to determine their impact on the primary crack. It is important to note that these secondary cracks, particularly those along the bore, often mask the growth of the primary crack. One must be careful, when measuring these secondary cracks, to not associate their growth with that of the primary crack, as they are often unrelated.

13.1.4. ***Documentation considerations***

When completing testing of coupons with residual stress, it is important to measure and record processing parameters during the manufacturing of coupons. For cold expanded fastener holes, the pre- and post-cold expanded hole sizes, mandrel major diameter, and sleeve thickness should be measured to facilitate applied and residual expansion calculations. These measurements can be useful to support evaluations of variation in post-test fatigue results. Typical precision of measurements should be to X.XXXX inch. Process controls and documentation requirements should be detailed in the test plan to ensure the appropriate data is documented during the program. Additional details are included in the quality control chapter of this document.

13.1.5. ***Crack measurement consideration***

The unique crack shape evolution often associated with residual stress brings unique considerations for crack measurements during testing. To capture the crack growth during testing, a combination of visual, Direct Current Potential Drop (DCPD), and markerbanding typically results in sufficient data to characterize the crack growth and shape evolution. Visual measurements tracking each crack tip during testing (surface and bore for cold expanded holes), coupled with DCPD and post-test fractography can characterize the crack shape evolution as a function of surface crack length. Marker banding is a complex process that differs directly based on material system, stress level, and loading (constant versus variable amplitude). Iterations are typically required, especially if it as new application, stress environment, or alloy. Markerbanding is a very useful tool for validating automated DCPD data and crack front shape.

13.1.6. ***Stress level considerations***

The sensitivity of durability and damage tolerance fatigue lives for coupons with residual stress cannot be overlooked. Multiple programs have identified this sensitivity[60,78], with changes in remote stress of 5-10ksi resulting in the difference between coupon runout and extremely short fatigue lives. Careful consideration should be given in establishing stress levels when developing a test program. For cold expanded holes and constant amplitude testing in common airframe aluminum alloys, gross stress levels in the range of 25-30ksi have proven to result in successful tests, i.e. test that fail in the test section on the order of 1,000,000 cycles or less. Specific test conditions will impact the appropriate stress level and should be considered when defining the test program.

13.1.7. *Coupon quantities*

Inherent variability exists in the fatigue behavior of metals, and the additional of residual stress amplifies this variability. When defining the replicates for each condition in the test plan, this expected variability should be considered. As a minimum, (5) replicates should be considered for each test condition that includes residual stress. This is consistent with the guidance in the recent USAF structures bulletin for utilizing the equivalent initial damage size for cold expanded holes[36]. Often, a statistical Design of Experiments (DoE) is helpful to optimize testing efficiency and quantify the influence of key variables. Also, the sensitivity to stress levels and markerbanding discussed above often drives some amount of iteration at the start of the test program to finalize the appropriate test conditions. Additional coupon spares should be considered in the test plan to support this effort.

13.1.8. *Load transfer coupon considerations*

Testing that includes multiple components and load transfer is quite complicated, and careful planning is necessary to ensure the desired coupon behavior is accomplished. Factors such as fastener fit, single versus double shear loading, fastener racking, fastener and collar type, fastener torque/preload, faying surface sealant, fastener loads, crack monitoring, and starter notch location (if applicable) are critical to ensure the desired behavior of the test. In the specific case of cold expanded fastener holes, the faying surface materials (sealant, primer, paint, bare) should be considered. Previous studies (ref X) have identified fretting-induced crack nucleation at the faying surface of load transfer coupons with no coatings on the faying surface (bare coupons). In that study, minimal coating thicknesses (x inches) completely mitigated the fretting issues. Parts are almost always coated with primer prior to assembly and faying surface sealant is often utilized in airframe assembly. These processes should be considered when developing a test plan. To mitigate load transfer through the faying surface sealant and focus loads through the fasteners, a release agent or Teflon film is often used during assembly of the coupons. Also, double cold expansion of non-target holes has been utilized successfully to mitigate cracking away from the test section. Markerbanding can be very helpful particularly in load transfer conditions where cracks are hidden at faying surfaces and under fastener heads. This minimizes the need for periodic disassembly.

13.2. *Recommendations for additional validation testing*

The details of this section are currently in work or planned for future work.

14. NON-DESTRUCTIVE INSPECTIONS & QUALITY ASSURANCE

There are several studies[79,80,60] that describe the impact of crack face clamping (caused by residual stress or other sources) on NDI detection capability. Detailed studies on USAF weapon systems have identified several challenges related with some standard NDI techniques in the presences of a residual stress[81].

14.1. *Inspection methods*

14.1.1. *Shear wave ultrasonic inspections*

Shear wave ultrasonic Inspection uses high frequency sound energy to detect flaws in a parent material. The sound energy propagates through the material in the form of waves. When there is a discontinuity in the material, part of the wave will be reflected back from the discontinuity surface, this response is what the inspection technique requires to highlight a crack indication. Issues arise when residual stress causes crack face clamping in the parent material because the discontinuity becomes smaller than the ultrasonic wave length. This makes the probability of detection nearly impossible until either the crack grows out of the compressive residual stress field or there is a large enough applied load to overcome the clamping force due to the compressive residual stress field.

14.1.2. *Eddy current inspections*

Eddy current inspections use a process called electromagnetic induction as the basis for conducting examinations. A dynamic magnetic field is developed as an alternating current is passed through the probe. This expanding and collapsing magnetic field induces an "eddy" current in the conductive material being inspected. These currents generate their own secondary magnetic fields which can be measured. When a discontinuity is present in the material the eddy current is disrupted and the secondary magnetic field is reduced. The discontinuity surface, regardless if it is closed due to clamping effect of the residual stress field, can be enough to disrupt the eddy currents which makes it beneficial for inspecting residual stressed materials[82].

14.1.3. *Fluorescent penetrant inspection*

Fluorescent penetrant is based on the process of capillary action. Liquid penetrant applied to the surface will penetrate into discontinuities open to the surface in the material. When the penetrant is removed from the surface, a developer is applied that helps draw the liquid from the discontinuity. Using a fluorescent light, the inspector can visualize discontinuities on the part. Detectability is related to the amount of penetrant absorbed. Compressive residual stress that result in excessive clamping forces reduces the amount of penetrant entering the discontinuity and the, reducing the effectiveness of the inspection.

14.2. *NDI on Cx holes*

The following sections describe the pros and cons of some common inspection methods as they relate to Cx holes. These conclusions suggest, when possible, to utilize bolt hole eddy current when inspecting Cx fastener holes. If bolt removal is not a viable option, surface scan eddy current can produce acceptable results depending on geometry and inspection locations. Discontinuity size, shape, and location should all be considered when developing the NDI procedures.

14.2.1. *Shear wave ultrasonic inspections*

Due to the nature of the ultrasonic inspection, it is not recommended to use on Cx holes. The crack is not reliably detectable until it grows out of the compression dominated field. Results from Mills *et. al*. provides measurements that show the $a_{90/95}$ for a Cx hole is 0.242", well beyond the compressive zone for the specimen geometry (see Figure 51).

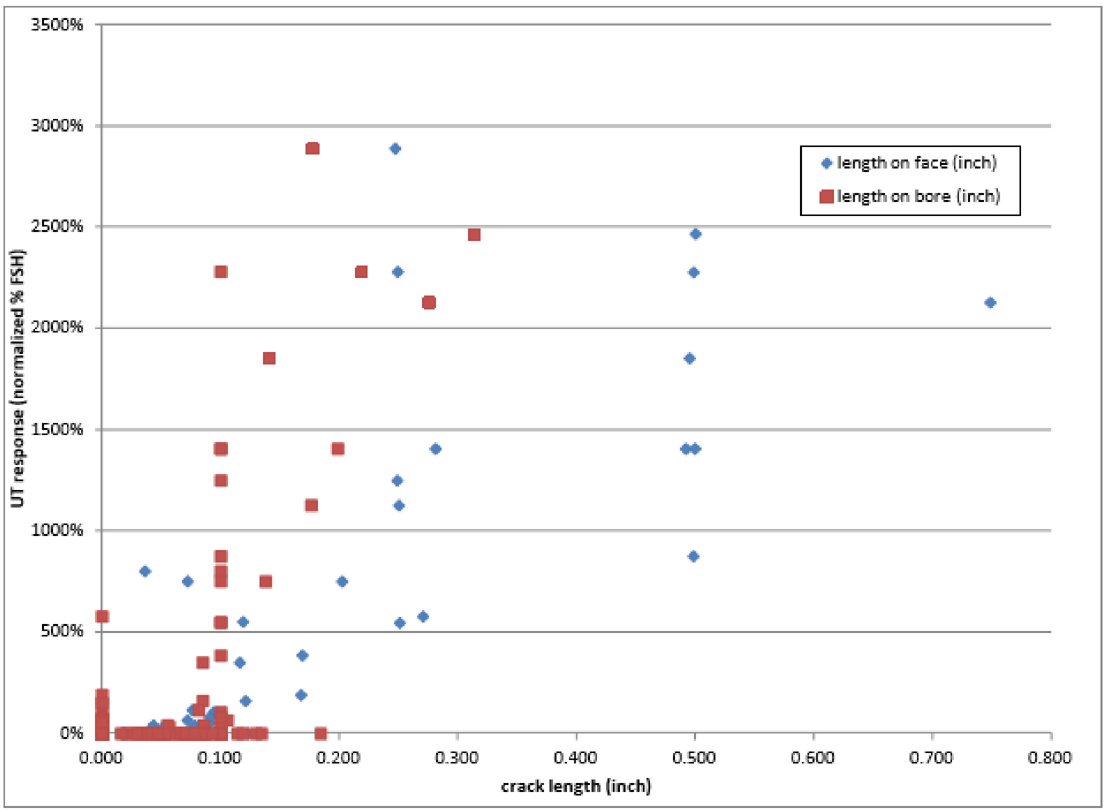

Figure 51 – UT Response as a function of crack length for a Cx hole[81].

14.2.2. *Rotary bolt hole eddy current inspections*

Rotary Bolt Hole Eddy Current (BHEC) inspections provide the best probability of detection for Cx holes. The discontinuities typically nucleate along the bore which correlates to the inspection surface. The crack face boundary provides enough disruption in the eddy current signal that the change in $a_{90/95}$ Is not significant.

One issue with BHEC is that it necessitates the removal of the fastener. This can lead to maintenance induced mechanical damage and the need for costly repairs that can remove the compressive residual stress in the material.

14.2.3. *Surface eddy current inspections*

Even though eddy current inspections provide good results when detecting flaws in residual stress fields, certain geometric features can provide mixed results with a surface eddy current inspection. Typically, access is only available to perform inspections on the mandrel exit side of the specimen. The unique crack shapes discussed in section 10.1.1 shows that occasionally a crack can get pinned and will not break through to the exit surface until the opposite surface crack length is sufficiently long to create a stress intensity that overcomes the clamping action of the compressive residual stress. This reduces the eddy current disturbance thus making it difficult to detect cracks.

Another limitation in a surface eddy current inspection is countersink fastener holes. In countersink fasteners, the discontinuity must grow past the countersink before it is detectable. Under certain geometric conditions, the detectable crack size would be greater than the critical crack size.

14.3. *NDI on surface treatments*

The following sections describe the pros and cons of some common inspection methods as they relate to residual stress surface treatments. These conclusions suggest that a combination level 4 FPI and a surface ECI be used in combination when possible. Discontinuity size, shape, and location should all be considered when developing the NDI procedures.

14.3.1. *Ultrasonic inspections*

Similar to results seen in studies with ultrasonic inspections on Cx holes, a significant reduction in detectability was seen on a laser peened surface (see Figure 52). The residual stress on these samples were large enough to cause crack face clamping which made the cracks undetectable. Both surface wave and shear wave ultrasonic proved to be incapable of detecting cracks as large as 0.300” in the LSP specimens.

14.3.2. *Fluorescent penetrant inspections*

Two different processes were used to investigate the effects residual stress have on Fluorescent Penetrant Inspections (FPI). Both the level 3 and 4 FPI processes showed a decrease in detectability over non-residual stressed cracks of equivalent lengths. Images show the difference in fluorescence of the Top row (non-LSP) and the bottom row (LSP) for the level 3 process (see Figure 53). The level 4 process provides slightly better results as seen in Figure 54.

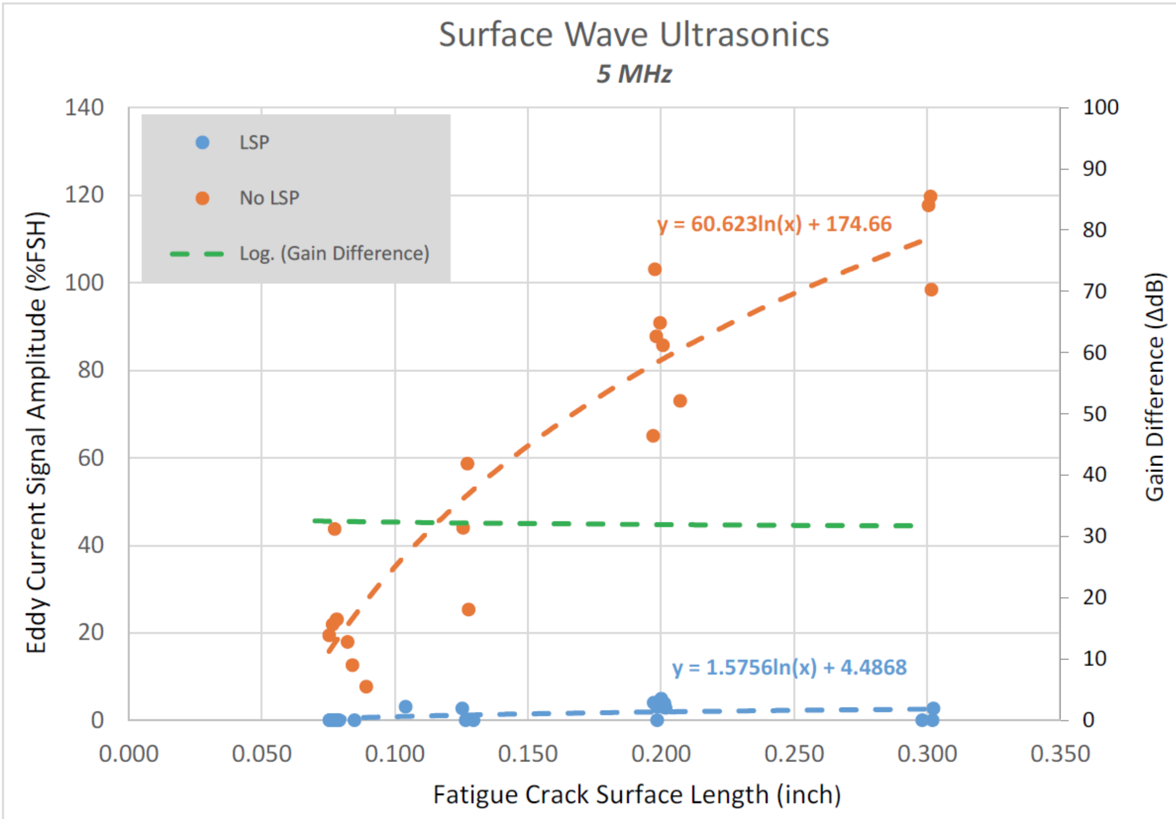

Figure 52 – UT Response as a function of crack length for a LSP specimen[81].

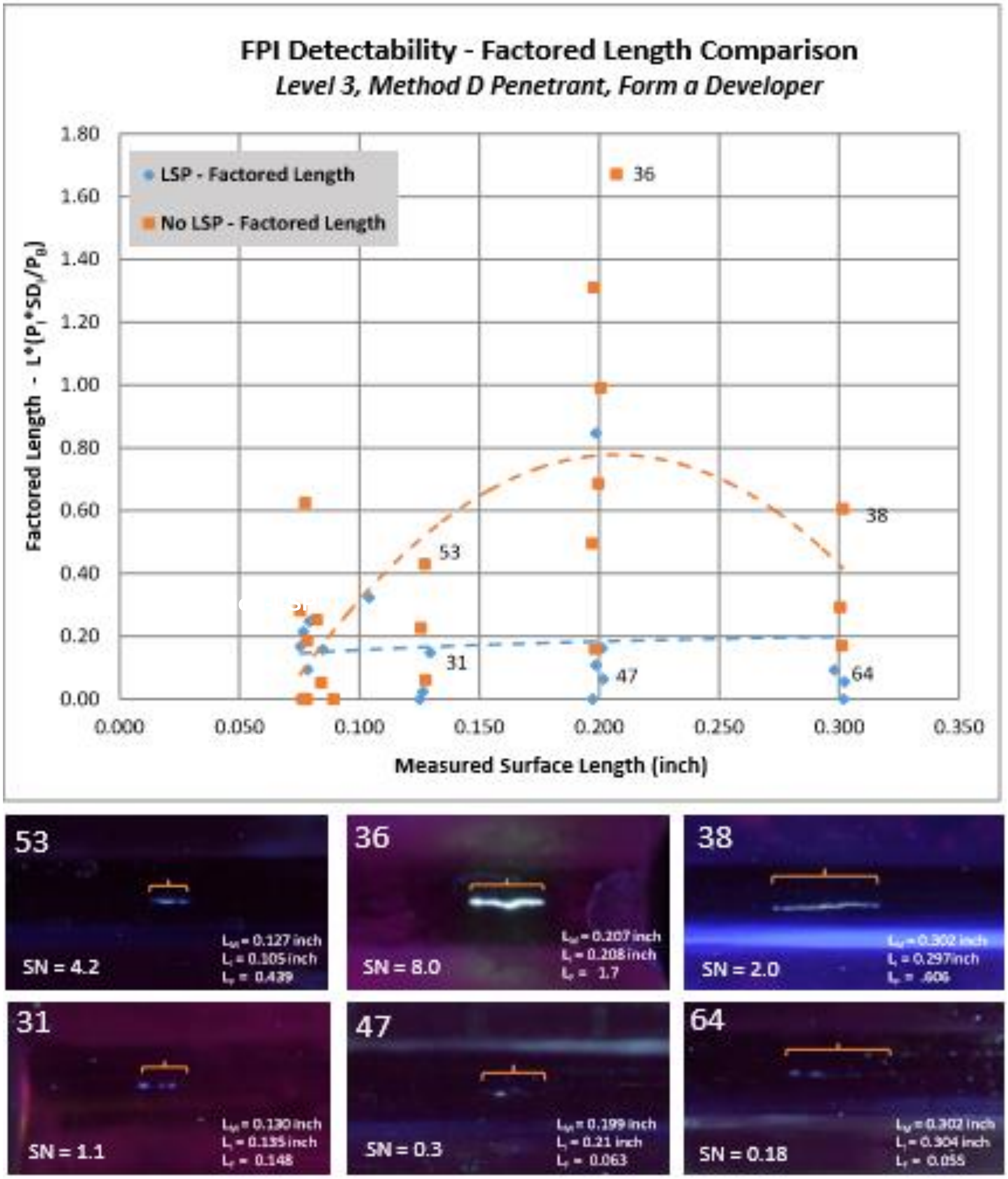

Figure 53 –Level 3 FPI Response as a function of crack length for a LSP specimen[81].

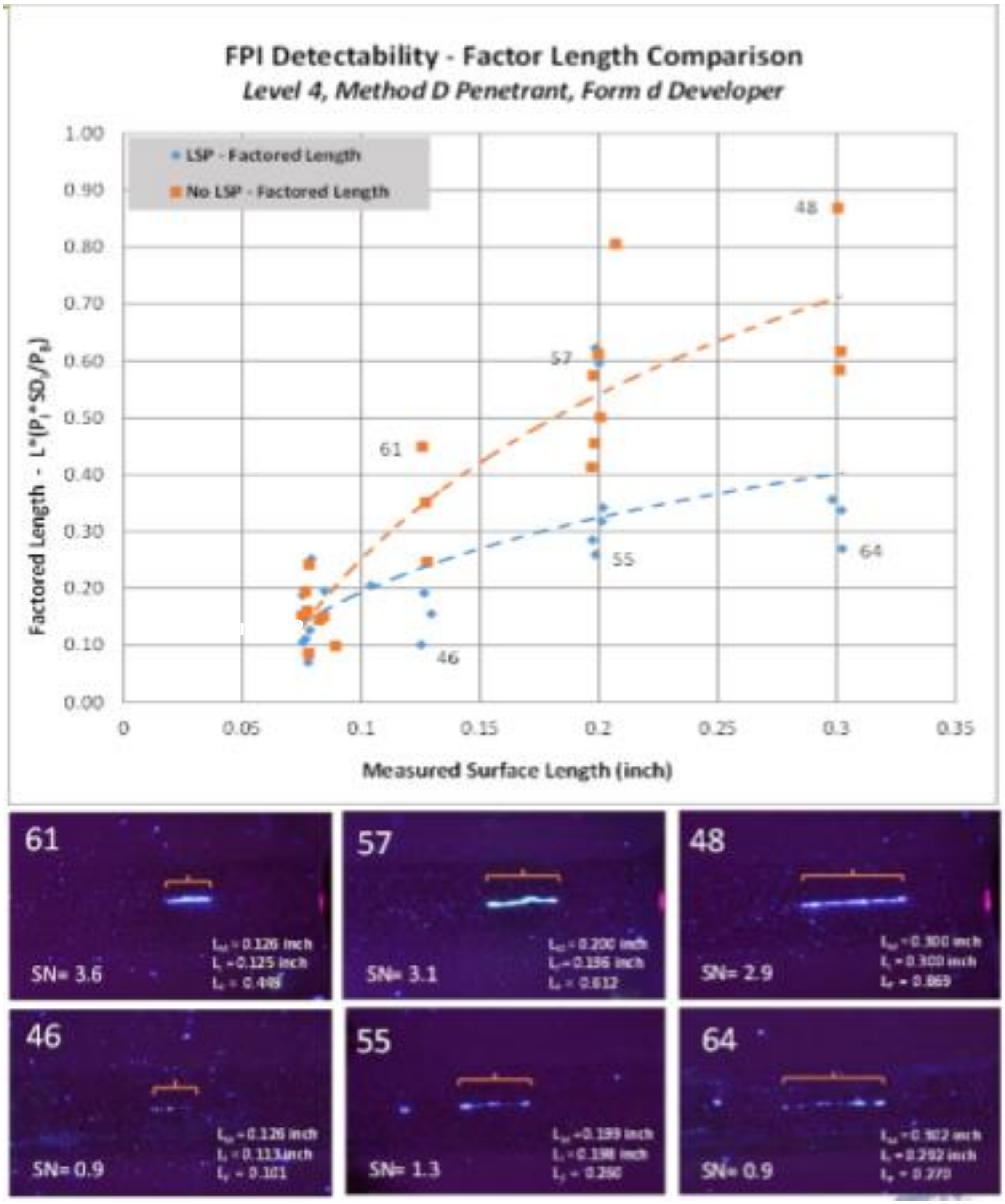

Figure 54 –Level 4 FPI Response as a function of crack length for a LSP specimen[81].

14.3.3. ***Surface eddy current inspections***

Surface eddy current provided the best inspection method for LSP surfaces. The reduction in response was minimal as seen in Figure 55. For this case, the inspection was performed on the nucleation surface, where there is the greatest probability of crack detection. Similar to surface eddy current inspections on Cx holes, consideration needs to be given to crack shape and nucleation site when determining the inspection threshold and intervals.

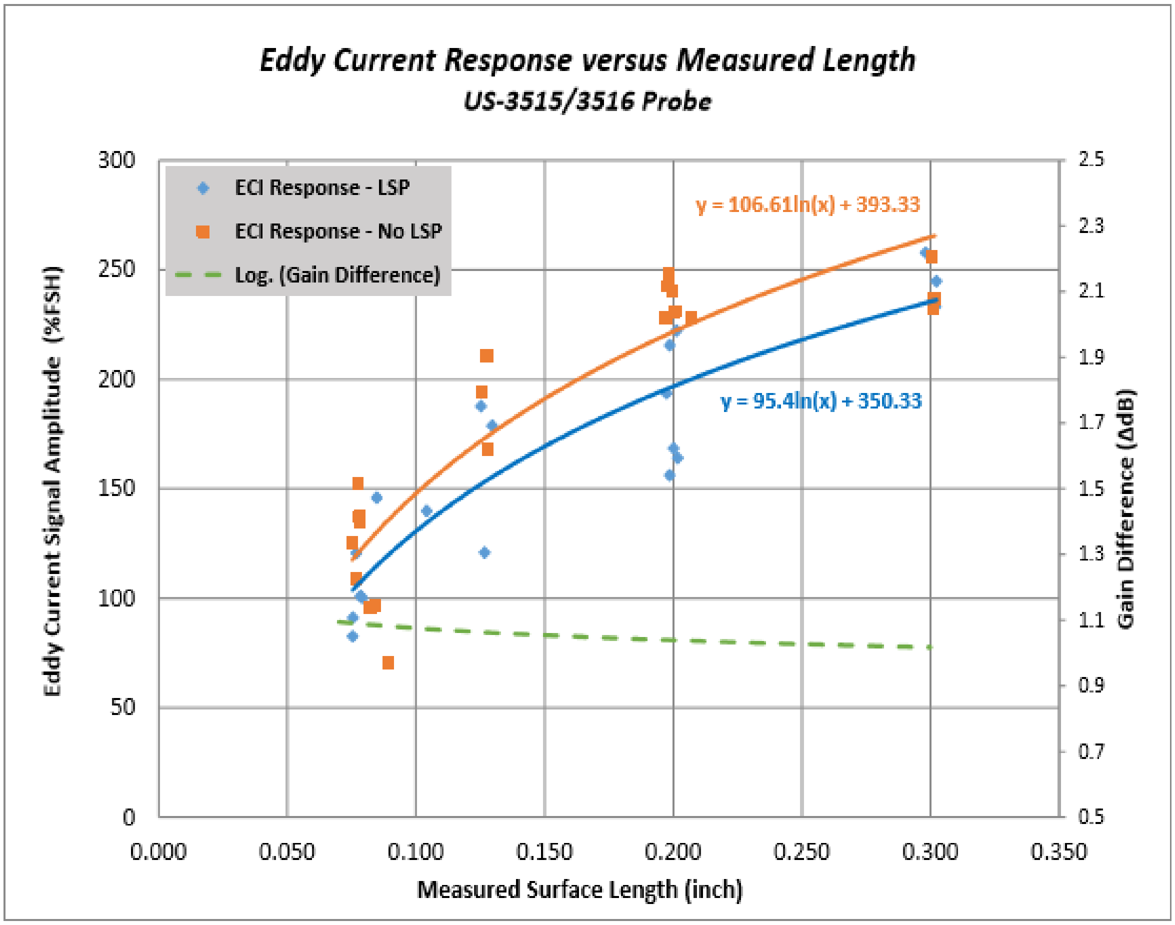

Figure 55 –Surface Scan EC Response as a function of crack length for a LSP specimen[81].

14.4. *Future considerations*

Significant progress has been made related to understand the applicability and limitations of NDI techniques in the presence of "deep" residual stress. Additional research is necessary to understand key factors, including the following considerations:

- Notches vs. Naturally Occurring Cracks
    - Many of the preliminary investigations of NDI techniques focused on utilizing notches instead of naturally occurring cracks to facilitate ease of coupon manufacturing. In most instances the translations

from notches to cracks is fairly straightforward, however, in application with residual stress where significant crack face contact can occur the response can be significantly different for some NDI techniques, notably penetrant and ultrasonics. In these applications the crack faces contact has a significant impact on signal response. Additional investigations with naturally occurring cracks are necessary to provide a better understanding of the signal response.

- NDI and Teardown Evaluations of Post-Service Structure
    - Much of the NDI development in residual stress applications has utilized laboratory coupons. Additional programs should focus on utilizing post-service teardown assets with naturally nucleated and propagated cracks. The unique nuances of cracks with residual stress require an extra level of focused attention and post-service teardown assets will provide valuable data to bolster the communities understanding of crack shape evolution and crack detectability.
- Ultrasonic Dead Zone
    - The crack face contact resulting from compressive residual stress have demonstrated significant signal response degradation for ultrasonic techniques[60,81]. This degraded response has been coined the “ultrasonic dead zone”. Initial quantification of the dead zone is defined in reference 38, however additional investigations are necessary to quantify the impacts of residual stress on ultrasonic inspections. Additionally, investigations to date have focused primarily on “standard” ultrasonic methods, however, many USAF weapon systems employ sophisticated ultrasonic techniques for inspections at Cx fastener holes. Probability of detection studies should be accomplished with naturally occurring cracks in the presence of the expected residual stress in service utilizing these specialty ultrasonic techniques to understand and quantify their signal response.
- Applicability to Various Materials
    - The applicability of various NDI techniques should be investigated for various materials to understand any unique influences.
- Interference Fastener Applications
    - The interaction between residual stress at Cx holes and interference fasteners has not been investigation for NDI impacts. These scenarios should be evaluated to quantify any beneficial effects from hole propping.

14.5. *Various QA efforts*

14.5.1. *FastenerCam overview*

TRI’s FastenerCam™ is designed to support the “third leg” of the ERSI “stool”: quality assurance. Currently at MRL 7, the FastenerCam™ is a hand-held tool which uses a laser profilometer to measure the holes’ characteristics to verify and digitally document that newly cold expanded aircraft fastener holes have been processed within specifications. Currently implemented cold expansion quality assessment (QA) techniques rely on process controls and feeler gauges, which do not generate a quantitative, auditable digital record and must be performed during the expansion process. Because no auditable record or post-process evaluation techniques are available to ASIP managers, full credit cannot be given in design calculations to the benefits and effectiveness associated with cold expansion process.

Developed for the US air force under contracts FA9453-12-C-0218 and FA8100-16-C-0011, it is designed to operate in depot environments. In addition to percent applied expansion, it can measure and document hole diameter, roundness, and countersink depth, alignment, and angle. In its current form, FastenerCam™ provides an effective method for establishing a pass/fail for the cold expansion process on straight shank holes. It is currently capable of measuring the amount of cold expansion of fastener holes to within 0.5% for fasteners greater than 0.246 inches and plate thicknesses greater than 0.19 inches, recording the data for future use.

14.5.2. *Quality assurance processes for LSP*

Quality assurance is an important aspect of the production process, especially when critical structure is involved. As such, a quality assurance program is an important part of the development of the LSP treatment specification. A key aspect of a quality assurance program is the development of a quality control approach and associated coupon, to monitor and ensure the LSP process stays within acceptable bounds. An effective quality control coupon will achieve the following goals:

- Capture the magnitude of the LSP treatment at the point of impact
- Represent the geometry of the location of interest in terms of process access, line of sight, etc.
- Represent the geometry of the location of interest in terms of section size, shape, and thickness
- Minimize setup time and difficulty
- Minimize specimen cost
- Optimize ease of residual stress measurements

15. *RISK MANAGEMENT*

15.1. *Overview of risk management aspects*

The details of this section are currently in work or planned for future work.

15.2. *Uncertainty quantification*

The details of this section are currently in work or planned for future work.

15.3. *Benchmark problems and analysis consistency*

The details of this section are currently in work or planned for future work.

15.4. *Safety factor and conservatism considerations*

The details of this section are currently in work or planned for future work.

15.5. *Risk management processes and residual stress considerations*

The details of this section are currently in work or planned for future work.

16. *CERTIFICATION CONSIDERATIONS*

16.1. *Overview of certification considerations*

Certification considerations for “partial credit” is fairly well established with guidance provided in JSSG 2006[35] as well as the recently published AFLCMC structure bulletin[36], however, certification considerations for “full credit” is still nebulous. Recent presentations by the structural integrity technical advisors for the USAF and FAA have indicated common expectations to get to “full credit”. From a USAF perspective, the primary factors necessary to implement a new material, process, joining method, and/or structural concept detailed in MIL-STD-1530D[83] are used as a guide. These factors focus on proving the change 1) is stable, 2) is producible, 3) has characterized properties, 4) has predictable performance, and 5) is supportable. Utilizing these key factors as a guide, each one can be tailored for the unique characteristics of engineered residual stress. These factors are discussed in more detail below as well as other certification considerations that should be addressed.

16.2. *Stable*

The initial factor associated with implementing new processes, etc. is to ensure the process is stable. In general, processes such as Cx of holes and laser shock peening have established processes to ensure a stable result. Some of the key aspects of a stable engineered residual stress process should have:

- Defined process limitations (e.g. particular material, specific geometries)
- Specifications for tooling, equipment, etc.
- Process specifications
- Manufacturing instructions
- Qualified personnel

A stable engineered residual stress should result in:

- Consistent and repeatable quality
- Predictable costs for implementation

16.3. *Producible*

Once a stable process is established, validated Quality Assurance (QA) or Non-Destructive Evaluation (NDE) methods are necessary to verify the engineered residual stress was attained as intended, ultimately to confirm the DTA with engineered residual stress applies for the particular application. Considerations are given to:

- Tooling, equipment, etc. variability
- Engineered residual stress variability
- QA/NDE accuracy

Effective QA/NDE results should be:

- Quantitative
- Retained as a permanent record
- Auditable

16.4. *Characterized properties and predictable performance*

To support a validated fatigue analysis, the engineered residual stress field and associated damage growth rates through the engineered residual stress field must be quantified for the particular application. Whatever the source of residual stress (destructive on nondestructive determination methods, process modeling, etc.), the analysis must accurately quantify the crack growth rate through the full field residual stress fields considering factors such as:

- Material application
- Specification range of applied work/energy
- Various geometries (e.g. edge margin)
- Various loading spectra (e.g. stress ratio effects)
- Occasional overloads/underloads
- Effects of the crack on the engineered residual stress changes
- Effects of multiple cracks
- Detrimental tensile residual stress

The analysis methods will depend on the specific industry and application (e.g. durability, damage tolerance, low cycle fatigue, fatigue crack growth), however, all methods require an understanding of the impact the engineered residual stress has on all the analysis inputs and methods. Also, the analyses should address the evolution or degradation of residual stress in-service. Ultimately, the goal is to quantify, with confidence, the engineered residual stress effect on structural integrity.

16.5. *Supportable*

Once the key properties are characterized and the performance of the application with engineered residual stress is predictable, validated QA/NDE and NDI methods as necessary to support the sustainment phase. In the context of the USAF and damage tolerance, there are distinct certification differences for initial and recurring inspection requirements. For initial inspections, based on the ½ life from the damage tolerance initial crack size to critical crack size, there must be a validated QA/NDE method to verify the engineered residual stress is attained as intended to confirm the DTA with engineered residual stress applies. For recurring inspections, based on ½ life from detectable crack size to critical crack size, the following requirements apply:

- Validated NDE method to ensure the same engineered residual stress is still present (or quantify change in analysis)

- Quantified NDI probability of detection (PoD) for applicable NDI methods
    - Impact of engineered residual stress on crack detectability
    - Characterization of preferential crack path and impacts on NDI access and associated detectability

16.6. *Other certification considerations*

In addition to the primary certification considerations detailed above, the following aspects should also be addressed in certification documents:

- Procurement vs. Sustainment
    - Certification guidance should explicitly discuss the application/limitations for procurement vs. sustainment scenarios. This guidance should address the ability to take "full credit" during the procurement phase of a program or if this benefit should be reserved for the sustainment phase. This guidance will likely vary between industries.
- Quantification of risk
    - Even though engineered residual stress often result in significant fatigue life increases, they also have demonstrated an increased sensitivity to input data (e.g. material properties, residual stress, etc.). Certification requirements should address the expectations for quantification of risk and incorporate the statistical variation of analysis inputs.
- Testing/measurement requirements
    - The details of this section are currently in work or planned for future work.
- Conservatism/safety factors
    - The details of this section are currently in work or planned for future work.

17. *WAY FORWARD & RECOMMENDATIONS*

The details of this section are currently in work or planned for future work.

CHAPTER IV - BENCHMARK CASES FOR COMPARISON

Benchmark cases, ranging from handbook solutions to complex cases, are essential to provide references to measure performance of analytical predictions. Several benchmark cases were selected, and are included in this chapter, to provided common references for analysts to compare against.

18. *BENCHMARK CASE 1*

18.1. *Overview*

The first benchmark case focuses on a standard condition with a defined handbook solution, the center crack in a plate geometry. Handbook solutions for this crack condition/geometry are readily available in NASGRO (TC01) and AFGROW. This benchmark problem was broken down into two parts: 1) stress intensity comparisons relative to handbook solutions and 2) fatigue life prediction comparisons utilizing the Paris relationship. Multiple Finite Element (FE) or Boundary Element (BE) software suites (StressCheck, BEASY, and FRANC3D) were utilized to demonstrate consistency. Both plane stress and strain conditions were modeled (note that the handbook solution is for plane strain).

18.2. *Part 1*

Figure 56 details the geometry and loading for the part 1 analyses.

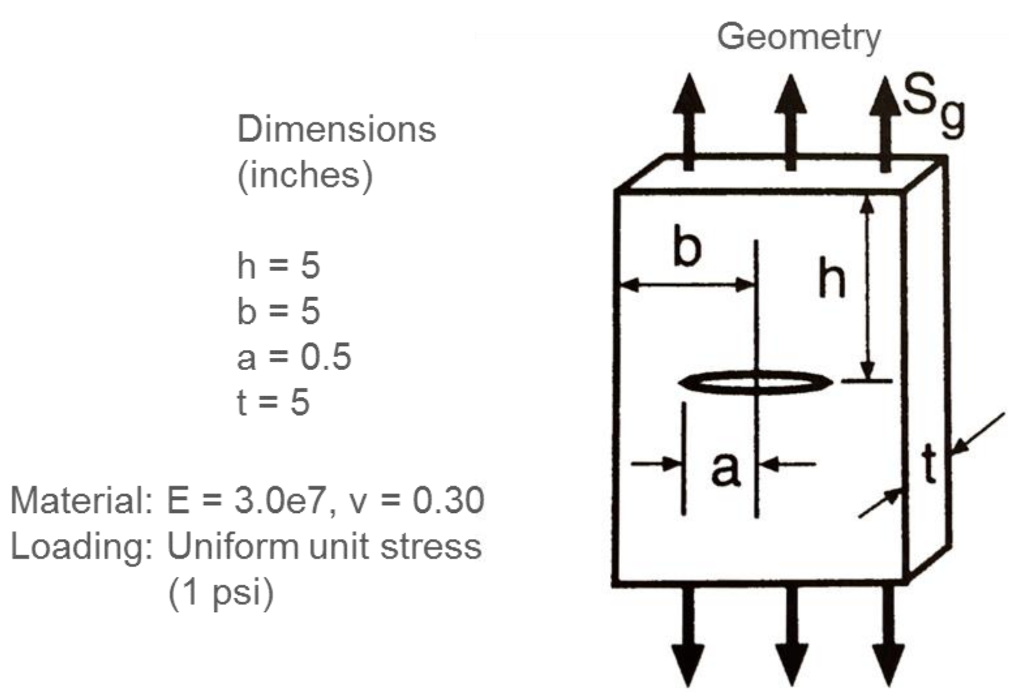

Figure 56 – Benchmark case 1 – geometry, material, and loading

The part 1 results, focused on stress intensity comparisons, are shown in Figure 57, detailing the mode I stress intensity factor for a half crack length of a = 0.5 inch. Differences are evident between the plane stress and strain conditions, with the maximum error relative to the handbook solution of 0.61% for the plane strain condition.

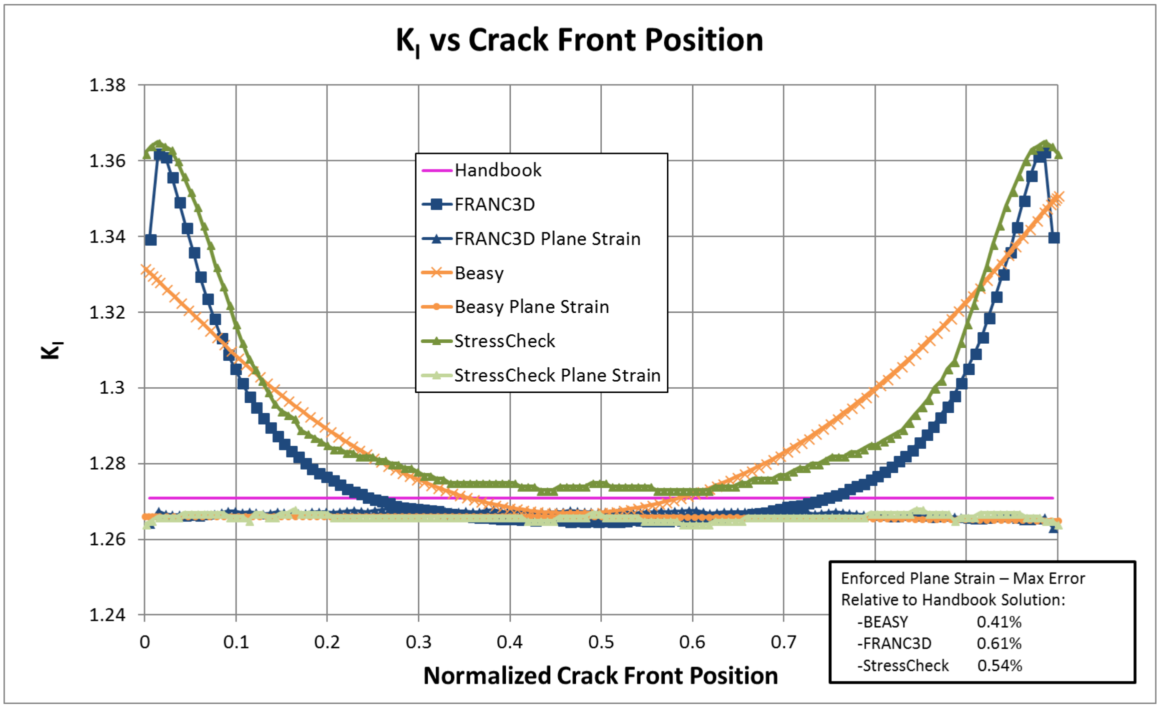

Figure 57 – Benchmark case 1, part 1 – mode I stress intensity comparisons

18.3. *Part 2*

The second part of benchmark case 1 focused on crack growth and stress intensity comparisons utilizing the Paris relationship. For these predictions plane strain was enforced. The geometry, material, loading, boundary conditions, and meshing are shown in Figure 58 and Figure 59. To reduce the model size and associated processing time, half the geometry was model and a symmetry boundary condition was applied as shown in Figure 59. The resulting crack growth life and stress intensities are shown in Figure 60 and Figure 61.

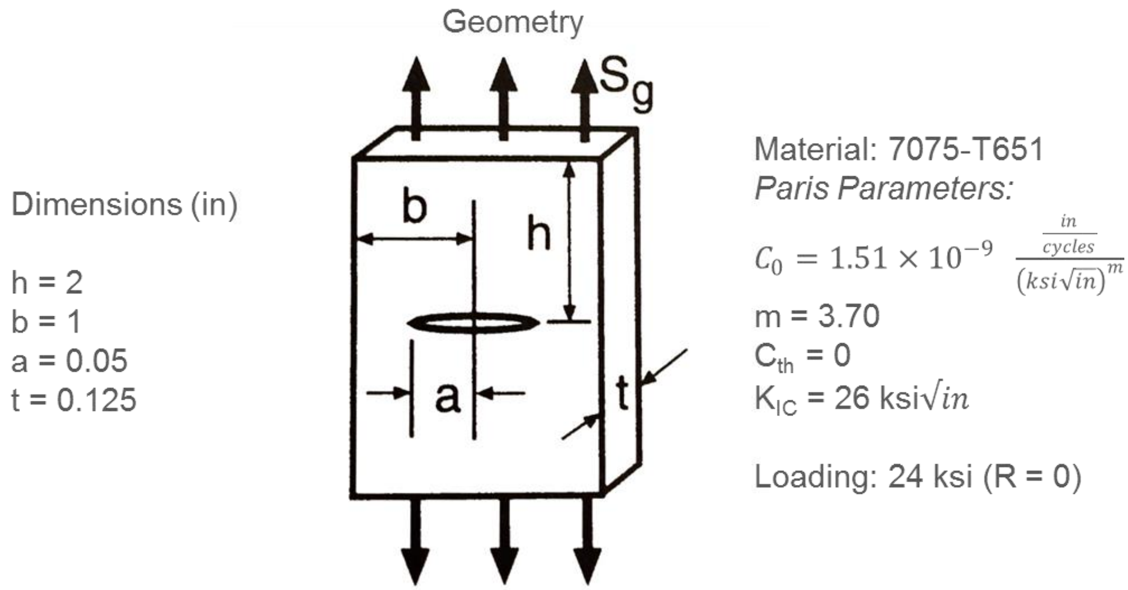

Figure 58 – Benchmark case 1, part 2 – geometry, material, and loading

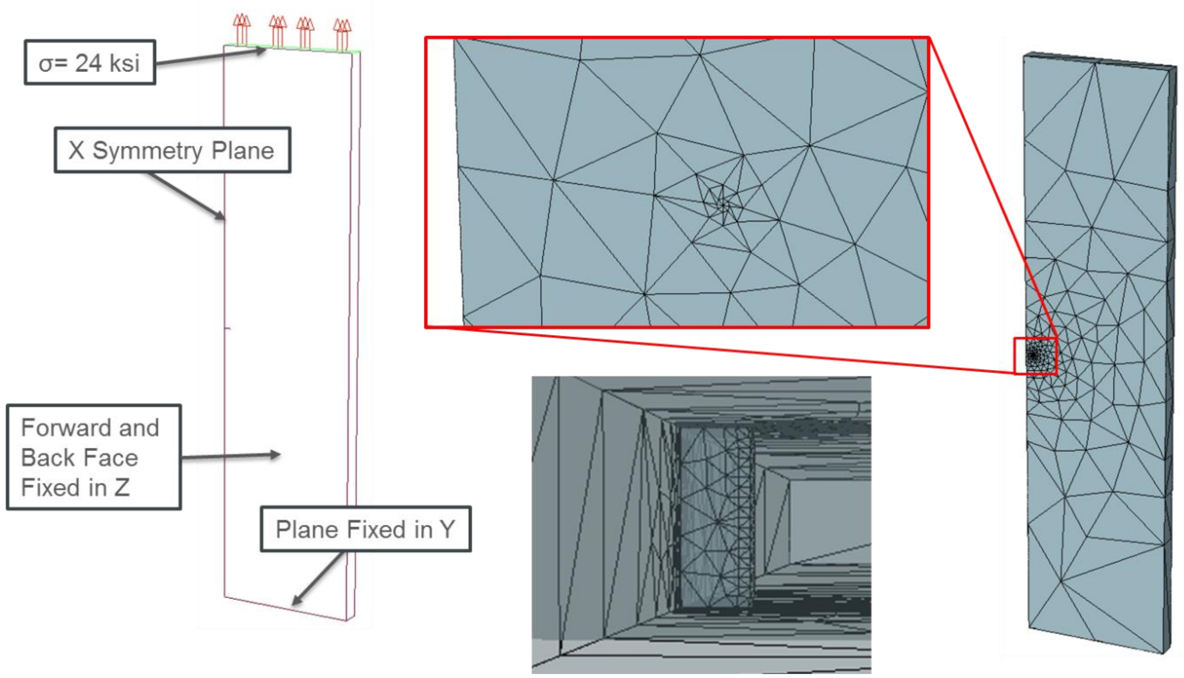

Figure 59 – Benchmark case 1, part 2 – boundary conditions and meshing

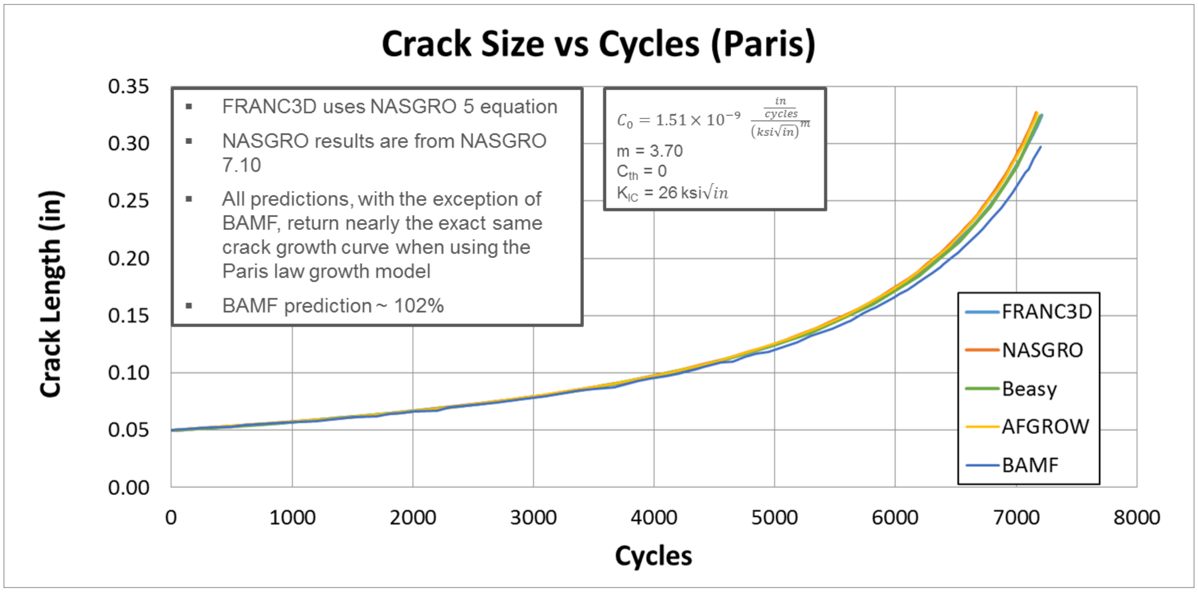

Figure 60 – Benchmark case 1, part 2 – crack growth life comparisons

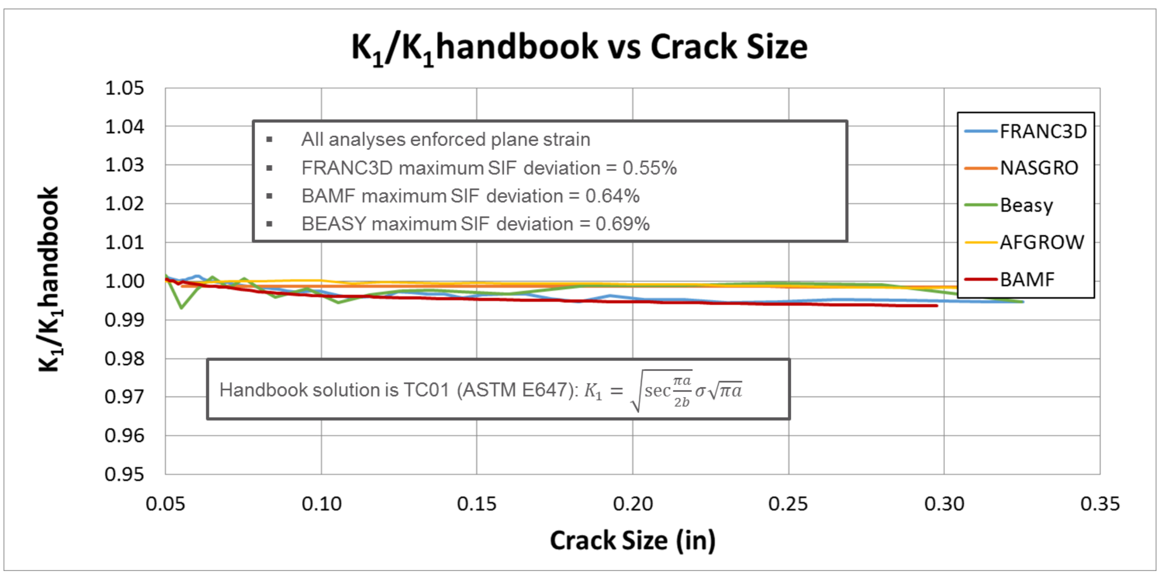

Figure 61 – Benchmark case 1, part 2 – stress intensity comparisons

19. *BENCHMARK CASE 2*

19.1. *Overview*

The second benchmark case focuses on a round-robin effort developed for the Engineering Residual Stress Implementation (ERSI) workshop, Analysis Methods Subcommittee. For this round-robin exercise, the particular focus was to identify the random and systematic uncertainties associated with Damage Tolerance Analyses (DTA) that incorporate residual stress produced by Cold Expansion (Cx) of fastener holes. Many factors influencing the total uncertainty have been discussed and are currently under investigation by various members of the ERSI team. For this round-robin exercise, the focus was on systematic uncertainties, or the uncertainty associated with the system or process used by the analyst (also known as epistemic uncertainties or model-form uncertainties). Specific input data was provided to each analyst participating in the exercise to minimize the random uncertainties associated with these types of analyses. The analyst was free to use any means to incorporate the residual stress into the DTA, any software suite, etc., however it was important that the analyst adhered closely to the guidance in this document so that the variability in the predictions would be limited to the aspects left to analyst's discretion.

19.2. *Input data*

Table 3 and Figure 62 detail the round robin analysis conditions and geometry. The specific details provided to the round robin participants is as follows:

- Initial crack size, shape, location, and orientation
    - Coupons were manufactured with undersized hole diameters and Electro Discharge Machining (EDM) notches were placed at the cold expanded entrance surface of the hole.
    - Precracking was accomplished for all coupons followed by reaming to a final diameter of 0.50" to remove any remnant of the EDM notch.
    - Note: For analysis purposes, the initial surface (x dimension) and bore (y-dimension) crack lengths are provided in Table 4 for each benchmark case, which represent the average test data lengths for each condition. Based on post-test fractography, all analyses should assume an elliptical shaped starting flaw.
- Material Properties
    - Tabulated crack growth rate data, fracture toughness, and other pertinent material properties are contained in Appendix C.
- Loading spectrum
    - All loading is constant amplitude with a stress ratio (R) of 0.1
    - Far field applied stresses are listed in Table 1.
- Constraints

- All coupons were tested in a servo-hydraulic test frame with hydraulic wedge grips. The grips engaged 4-inches of each end of the coupon.

- Residual stress resulting from the contour method
  - A tabulated list of x, y, and Szz on the crack plane (z=0) will be provided upon request.
  - For reference, the (0,0,0) location coincides with the cold expansion entrance surface corner of the hole, with the x-dimension oriented radially away from the hole, the y-dimension oriented through the thickness, and the z-direction perpendicular to the crack plane.
  - Note: All dimensions are in English units (inch, ksi)

Table 3 – Round Robin Analysis Conditions

Benchmark Condition #	Material	Specimen Type	Thickness (in)	Width (in)	Hole Diameter (in)	Hole Edge Margin	Loading	Max Stress (ksi)
1	2024-T351	Non-CX Baseline	0.25	4.00	0.50	4.0	CA (R=0.1)	10
2	2024-T351	CX	0.25	4.00	0.50	4.0	CA (R=0.1)	25
3	2024-T351	Non-CX Baseline	0.25	4.00	0.50	1.2	CA (R=0.1)	10
4	2024-T351	CX	0.25	4.00	0.50	1.2	CA (R=0.1)	25

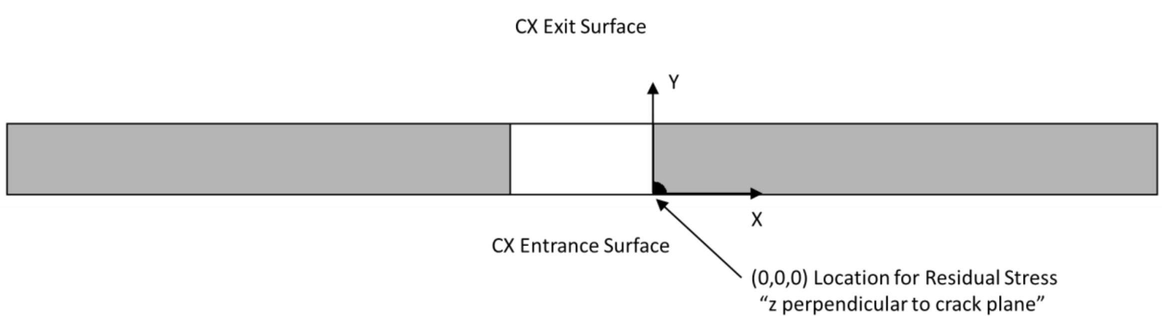

Figure 62 – Test specimen geometry

Table 4 – Starting Flaw Sizes

Benchmark Condition #	Starting Surface Crack Length (in)	Starting Bore Crack Length (in)
1	0.05	0.07
2	0.05	0.05
3	0.05	0.075
4	0.05	0.06

19.3. *Results*

As the round robin moved forward, it evolved into an evaluation of alternative methods and their impact on predictions. The overall objective shifted, to some extent, with participants exercising methods they might not typically utilize for engineered residual stress applications but added value when trying to understand the strengths and weaknesses of each. For example, the analyst that utilized the Gaussian integration method in AFGROW had prior experiences with unconservative predictions; however, this analyst utilized this method to compare and contrast the results with others to identify the key factors driving predictions differences. As a result, the submitted results from participants of the round robin were focused on covering the scope of possible methods, with the ultimate goal of determining best practices.

The results discussed herein will primarily focus on conclusions from Condition/Case #1 and #2. Additional details and comparisons of the results are contained in Reference 84.

19.3.1. *Case #1 results*

Table 5 – Case #1 Key Modeling Factors

Case #1 Key Modeling Factors										
	Software		Crack Definition			Material Model				
Submission #	Lifing Software	FE Software	Crack Front Shape	# of Points Defining Crack Front	Stress Intensity Calculation	Material Model	R shift	Negative R Behavior	Growth Increment	Other
1	CPAT	StressCheck	Multi-Point	30	Contour Integral Method	Tabular	linear log-log	Rlo, Kmax	2%	
2	CPAT	StressCheck	Multi-Point	20	Contour Integral Method	Tabular	linear log-log	Rlo, Kmax	0.5-2.0%	
3	AFGROW	N/A	Elliptical	2	Standard, Classic Newman/Raju	Tabular	Harter-T	Rlo, Kmax	cycle by cycle	
4a	NASGRO	N/A	Elliptical Straight Thru	2	NASGRO CC08/TC13 univariant WF	Tabular			10 cycles	Beta R
4b	NASGRO	N/A	Elliptical Straight Thru	2	NASGRO CC16/TC03 Fawaz/Anderson	Tabular			10 cycles	Beta R
4c	NASGRO	N/A	Elliptical Straight Thru	2	NASGRO CC10/TC13 bivariant WF	Tabular			10 cycles	Beta R
4d	NASGRO	N/A	Elliptical Straight Thru	2	NASGRO CC08/TC13 univariant WF	NASGRO Equation			10 cycles	Beta R
4e	NASGRO	N/A	Elliptical Straight Thru	2	NASGRO CC16/TC03 Fawaz/Anderson	NASGRO Equation			10 cycles	Beta R
4f	NASGRO	N/A	Elliptical Straight Thru	2	NASGRO CC10/TC13 bivariant WF	NASGRO Equation			10 cycles	Beta R
5	AFGROW-BAMF	StressCheck	Multi-Point	11	Contour Integral Method	Tabular	Harter-T	Rlo, Kmax	3%	
6	AFGROW	N/A	Elliptical Straight Thru	2	Standard, Classic Newman/Raju	Tabular	Harter-T	Rlo, Kmax	5%	
7	CPAT	StressCheck	Multi-Point	15	Contour Integral Method	Tabular	Harter-T	Rlo, Kmax	5%	
8	AFGROW	N/A	Elliptical Straight Thru	2	Standard, Classic Newman/Raju	Tabular	Harter-T	Rlo, Kmax	cycle by cycle	

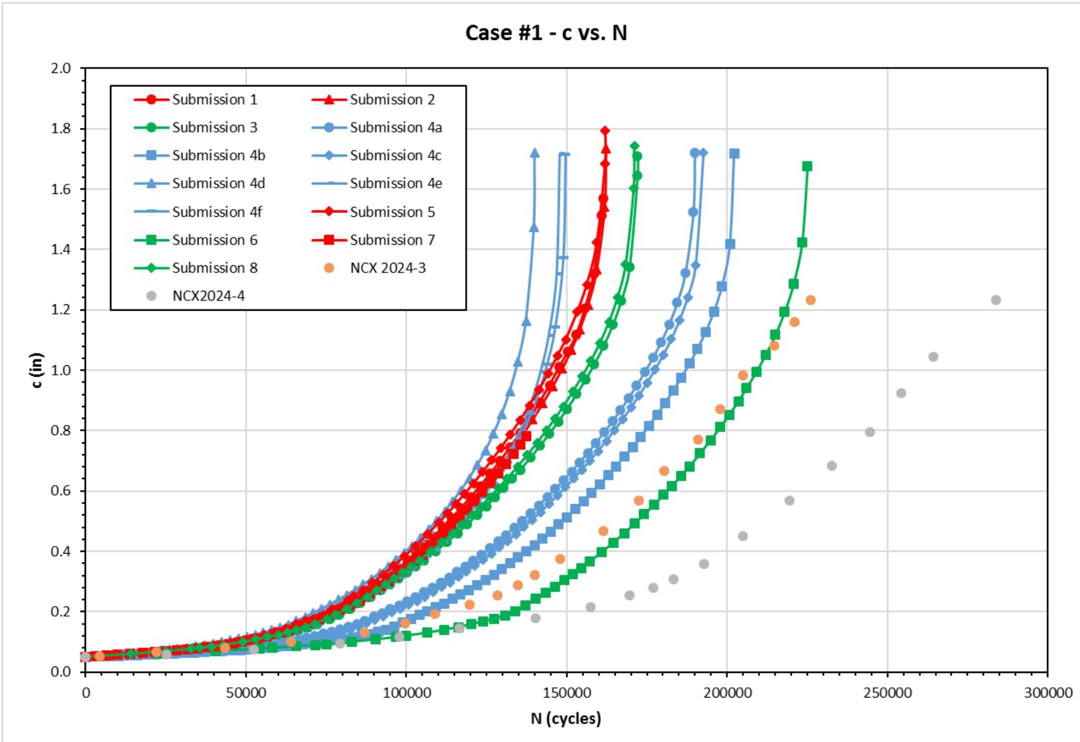

Figure 63 – Case #1 – Surface Crack Growth (c vs. n); Predictions vs. Test Data

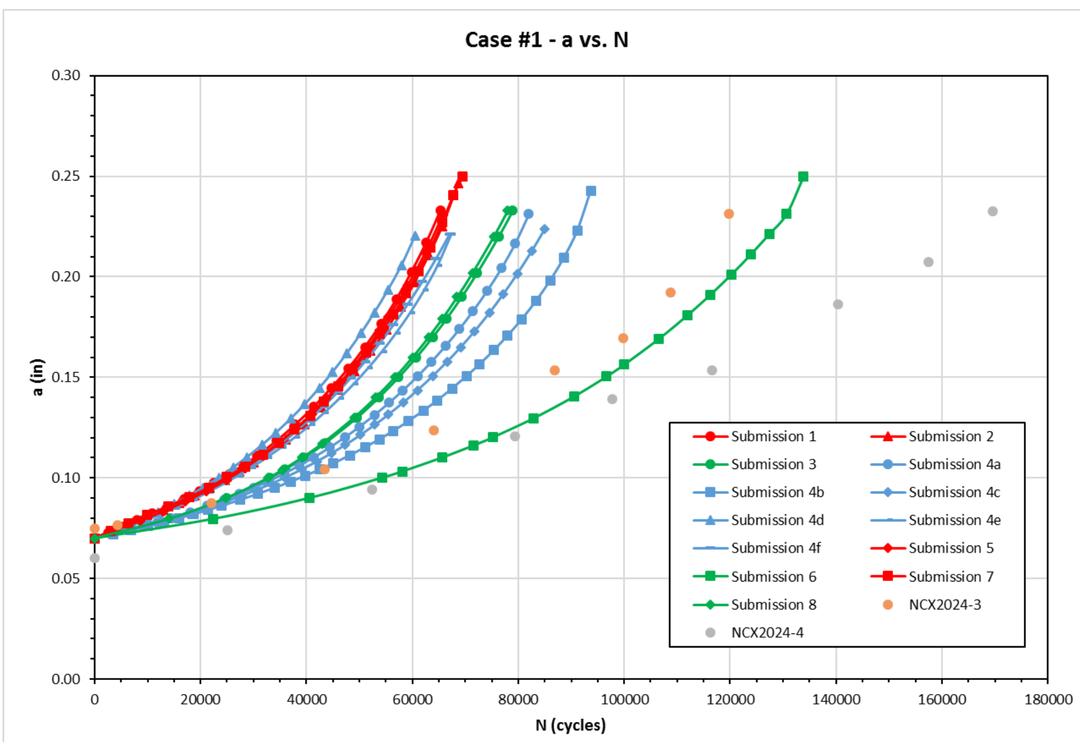

Figure 64 – Case #1 – Bore Crack Growth (a vs. n); Predictions vs. Test Data

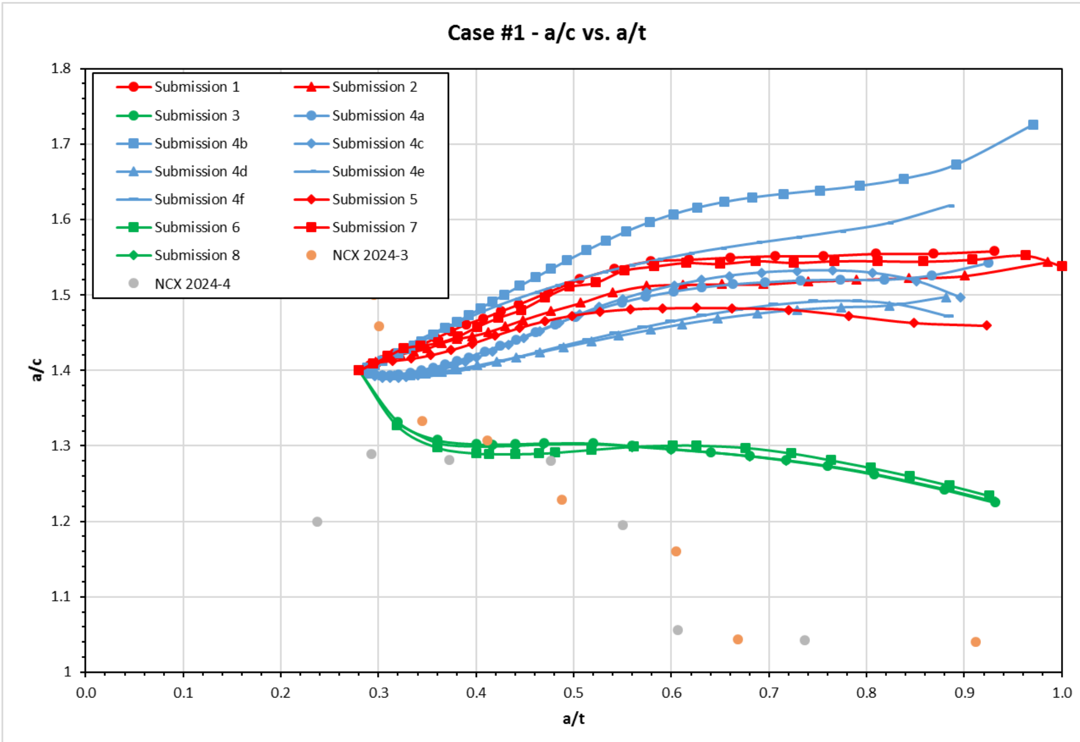

Figure 65 – Case #1 – Crack Aspect Ratio (a/c vs. a/t); Predictions vs. Test Data

19.3.2. *Case #2 results*

Table 6 – Case #2 Key Modeling Factors

Case #2 Key Modeling Factors												
	Software		Crack Definition			Stress Intensity		Material Model				
Submission #	**Lifing Software**	**FE Software**	**Crack Front Shape**	**# of Points Defining Crack Front**	**RS Incorporation Approach**	**Stress Intensity Calculation**	**Stress Intensity Incorporation**	**Material Model**	**R shift**	**Negative R Behavior**	**Growth Increment**	**Other**
1	CPAT	StressCheck	Multi-Point	30	B-Spline Crack Face Pressure	Contour Integral Method Loaded Cracks	Superposition Kres	Tabular	linear log-log	Rlo, Kmax	2%	
2	CPAT	StressCheck	Multi-Point	20	Legendre Polynomial Crack Face Pressure	Contour Integral Method - Loaded Cracks	Superposition Kres	Tabular	linear log-log	Rlo, Kmax	0.5-2.0%	
3a	AFGROW	N/A	Elliptical	2	2-D Gaussian Integration Free Surface	Standard, Classic Newman/Raju	Superposition	Tabular	Harter-T	Rlo, Kmax	cycle by cycle	
3b	AFGROW	N/A	Elliptical	2	2-D Gaussian Integration 5 degrees	Standard, Classic Newman/Raju	Superposition	Tabular	Harter-T	Rlo, Kmax	cycle by cycle	
3c	AFGROW	N/A	Elliptical	2	2-D Gaussian Integration 10 degrees	Standard, Classic Newman/Raju	Superposition	Tabular	Harter-T	Rlo, Kmax	cycle by cycle	
4g	NASGRO	N/A	Elliptical Straight Thru	2	Bivariant WF	NASGRO CC10/TC13 bivariant WF	Superposition	NASGRO Equation			10 cycles	Beta R extrapolated RS
4h	NASGRO	N/A	Elliptical Straight Thru	2	Bivariant WF	NASGRO CC10/TC13 bivariant WF	Superposition	NASGRO Equation			10 cycles	Beta R plateauing RS
4i	NASGRO	N/A	Elliptical Straight Thru	2	Univariant WF	NASGRO CC08/TC13 univariant WF	Superposition	NASGRO Equation			10 cycles	Beta R extrapolated RS
4j	NASGRO	N/A	Elliptical Straight Thru	2	Univariant WF	NASGRO CC08/TC13 univariant WF	Superposition	NASGRO Equation			10 cycles	Beta R plateauing RS
5	AFGROW-BAMF	StressCheck	Multi-Point	11	Polynomial Fit (15th order) Crack Face Pressure	Contour Integral Method - Loaded Cracks	Superposition Kres	Tabular	Harter-T	Rlo, Kmax	3%	
6	AFGROW	N/A	Elliptical Straight Thru	2	1-D Gaussian Integration ~ 0.05" from free surface	Standard, Classic Newman/Raju	Superposition	Tabular	Harter-T	Rlo, Kmax	5%	
7	CPAT	StressCheck	Multi-Point	15	Legendre Polynomial Crack Face Pressure	Contour Integral Method - Loaded Cracks	Superposition Kres	Tabular	Harter-T	Rlo, Kmax	5%	
8	AFGROW-BAMF	StressCheck	Multi-Point	10	Polynomial Fit (15th order) Crack Face Pressure	Contour Integral Method - Loaded Cracks	Superposition Kres	Tabular	Harter-T	Rlo, Kmax	3%	

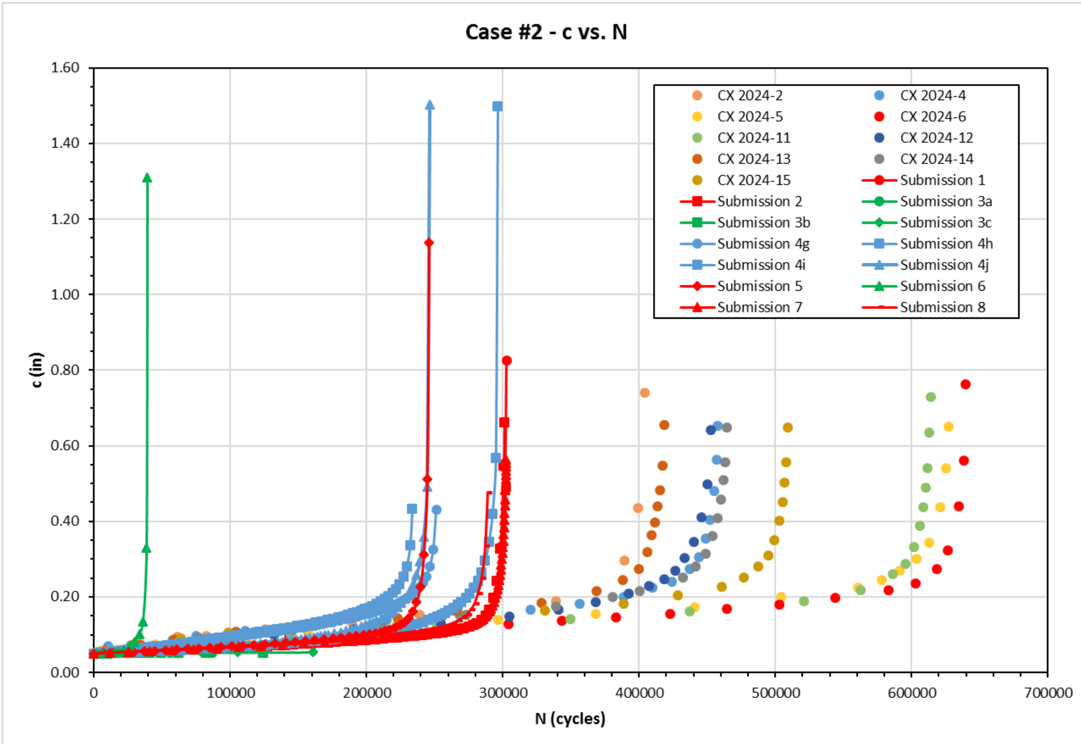

Figure 66 – Case #2 – Surface Crack Growth (c vs. n); Predictions vs. Test

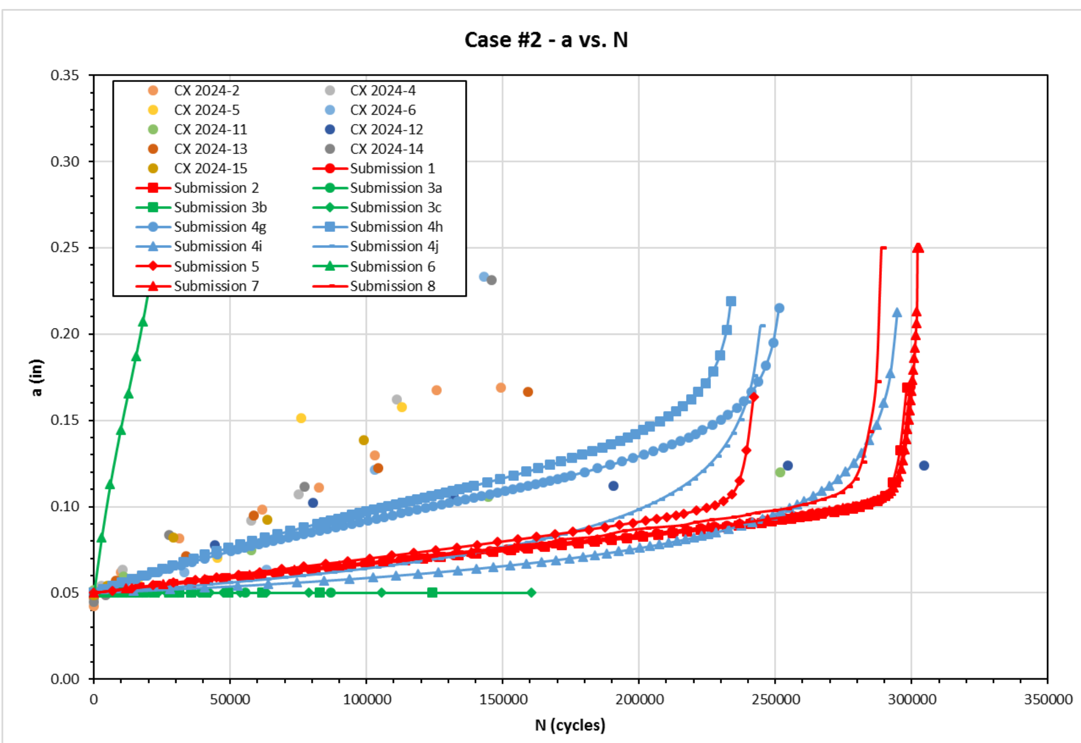

Figure 67 – Case #2 – Bore Crack Growth (a vs. n); Predictions vs. Test

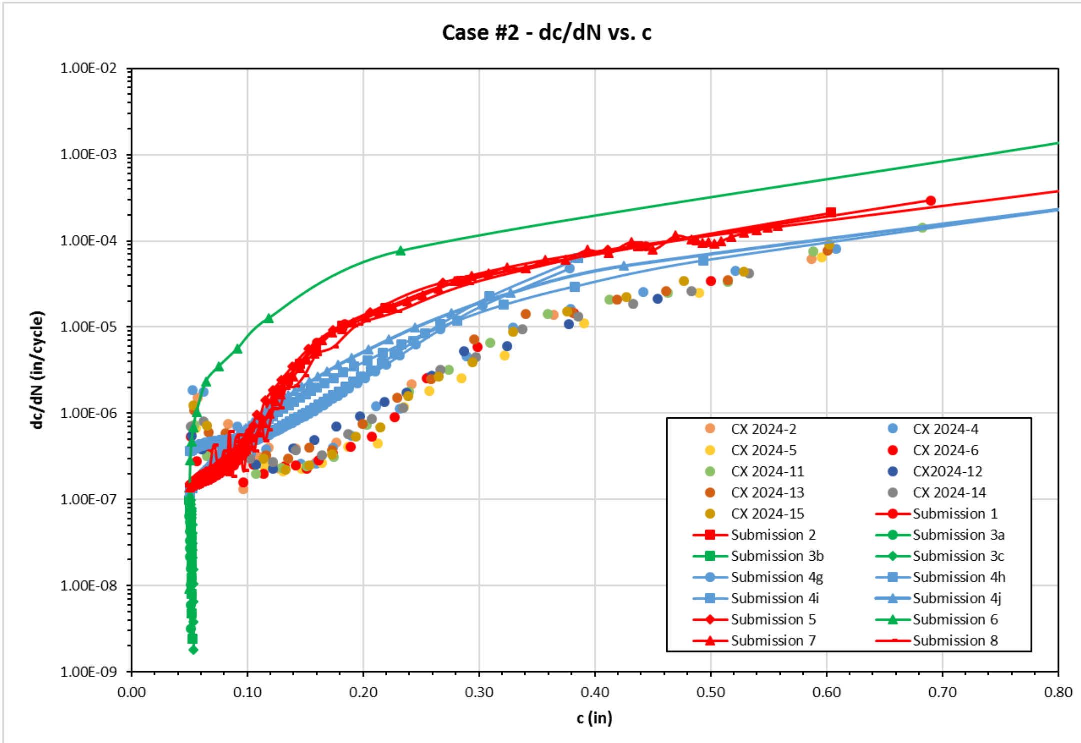

Figure 68 – Case #2 – Surface Crack Growth Rate (dc/dN vs. c); Predictions vs. Test

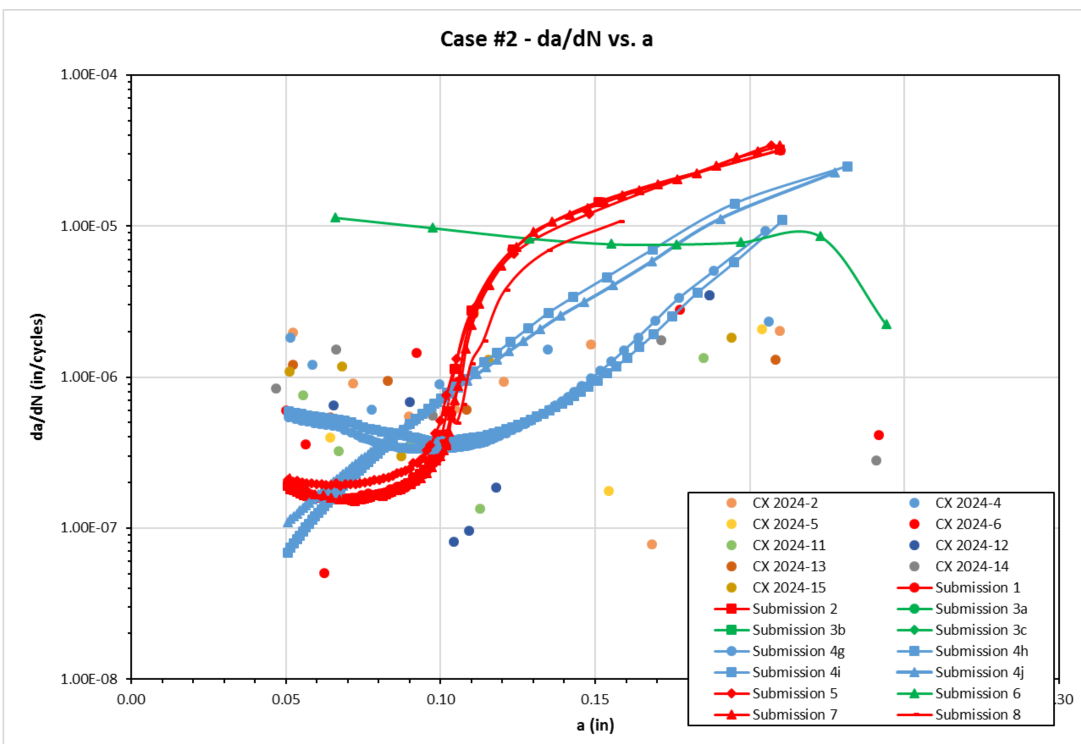

Figure 69 – Case #2 – Bore Crack Growth Rate (da/dN vs. a); Predictions vs. Test

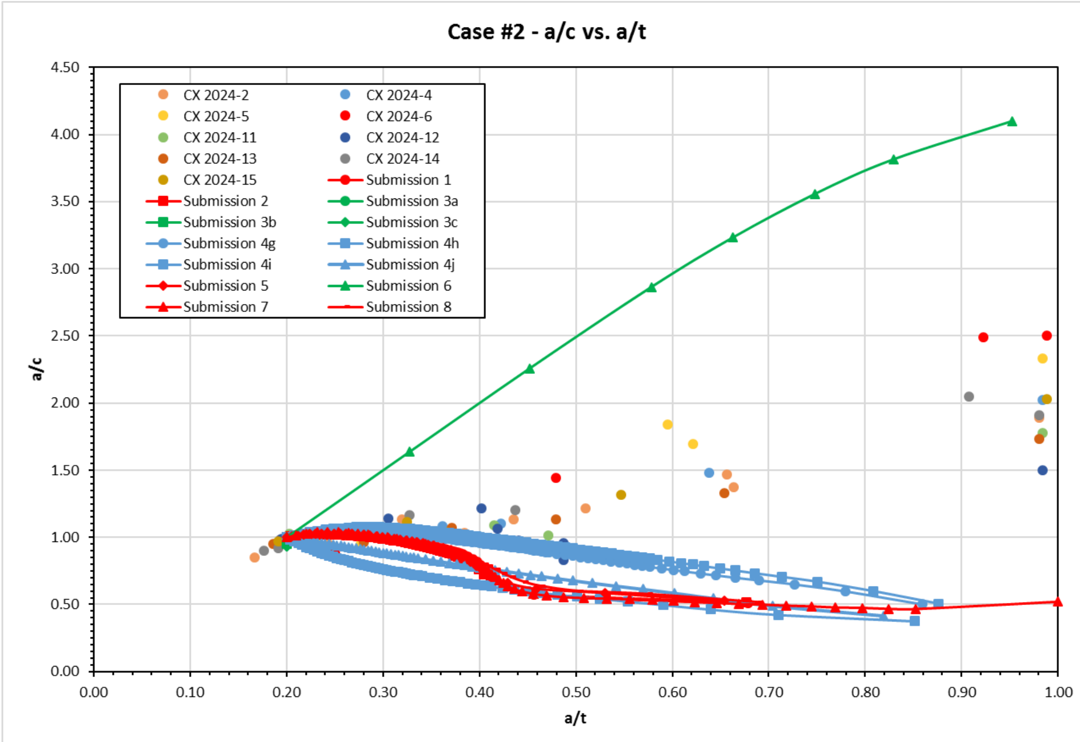

Figure 70 – Case #2 – Crack Aspect Ratio (a/c vs. a/t); Predictions vs. Test Data

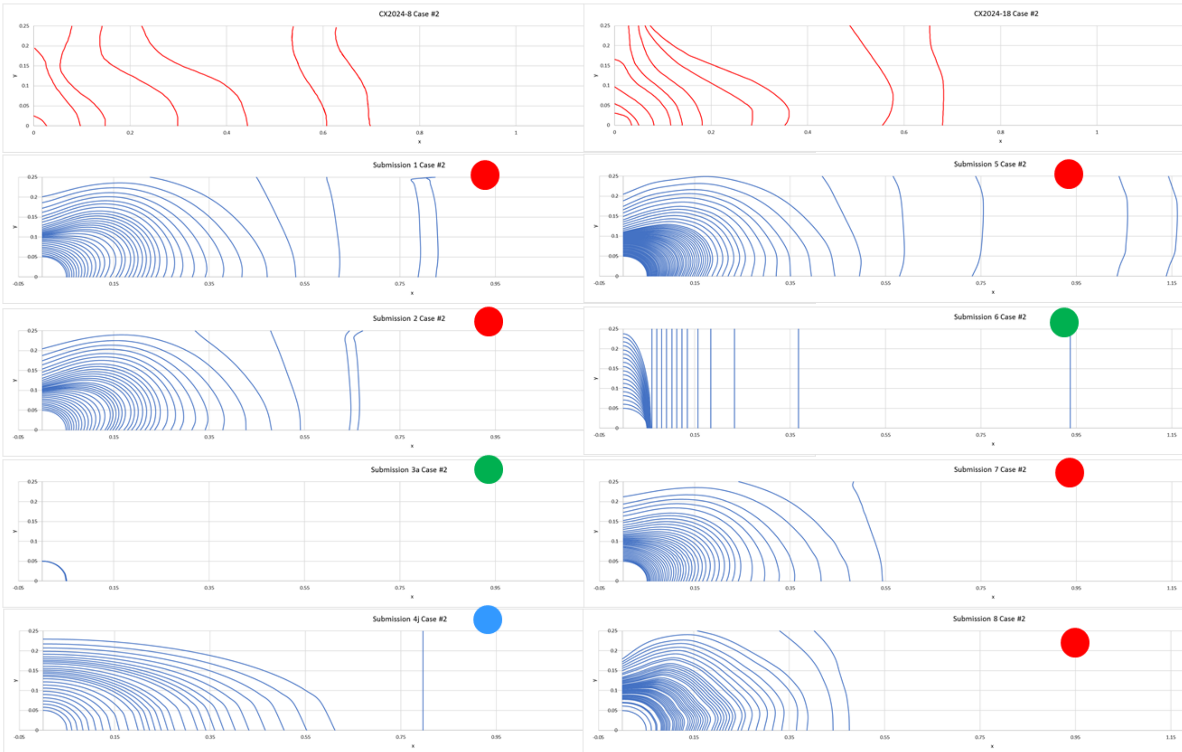

Figure 71 – Case #2 – Crack Shape Progression Differences between Test Coupons (Top, Red) and Predictions (Bottom, Blue)

CHAPTER V - CASE STUDIES

20. OVERVIEW OF CASE STUDIES

Case study examples are important to demonstrate different approaches for incorporation of engineered residual stress into “real life” scenarios as well as identify the lessons learned and best practices resulting from the programs. Several examples are provided with the long-term goal of adding examples as they become available.

21. CASE STUDY #1 – Laser shock peened F-22 wing attachment lugs[85, 86]

21.1. Background

During full-scale fatigue testing of the F-22, cracking was identified in the fracture critical wing attach lugs prior to reaching the full life requirements. The cracking was located adjacent to wing attach lugs, in the transition radius of the lug, in the wing carry through bulkheads (Figure 72 and Figure 73). The combination of the uniqueness of the geometry and the monolithic design of the bulkhead made reparability problematic, invasive, and expensive. As a result of these crack findings, design adjustments were cut into the production line and applied to the majority of the F-22 fleet. To reduce the long-term operational risk and inspection burden for already produced aircraft, a life extension retrofit program was initiated to investigate options to mitigate cracking.

Initially, Glass Bead Peening (GBP) was implemented “at risk” to impart beneficial residual stress at the cracking location. As a follow-on, an analysis and test program was initiated to evaluate GBP and Laser Shock Peening (LSP) fatigue benefits. To reduce risk, manage cost, and increase efficiencies, a building block approach was utilized to evaluate the repair options and optimize the final design.

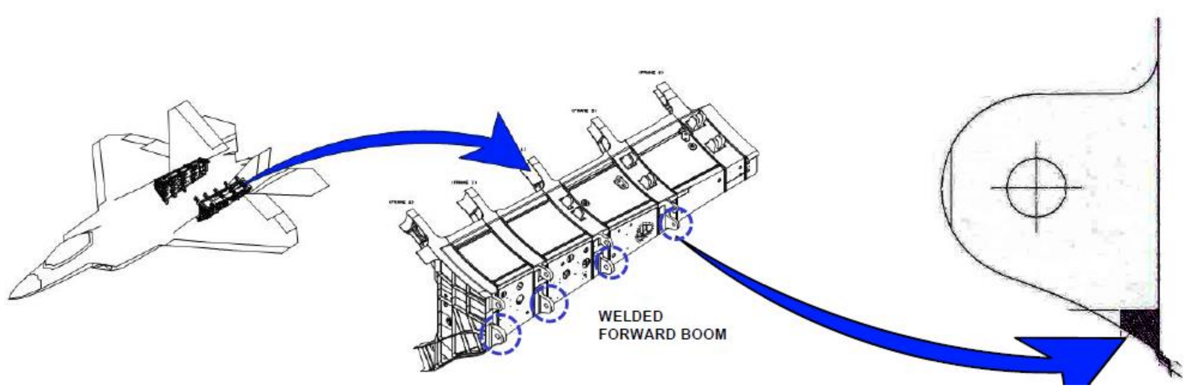

Figure 72 – F-22 cracking location, fracture critical wing carry-through structure

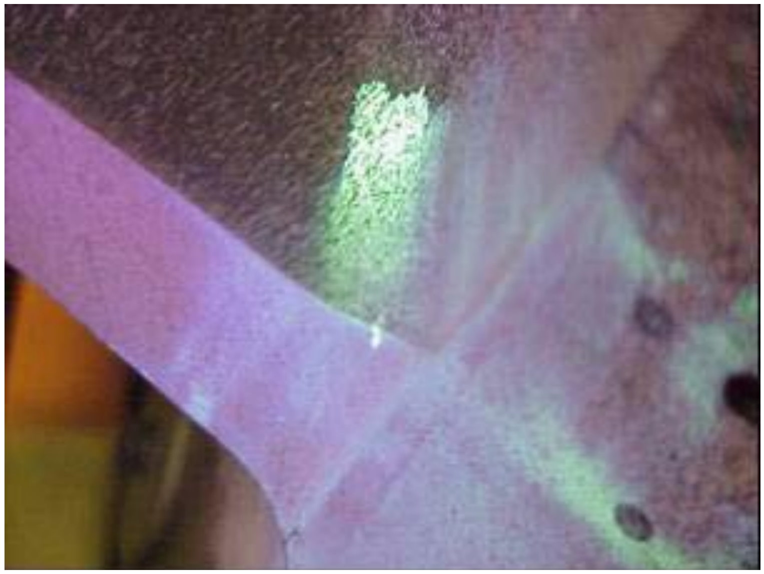

Figure 73 – F-22 cracking location, RHS Lower Fillet Crack Indication

21.2. *Building block approach*

As shown in Figure 74, a building block approach was utilized for the program to incrementally increase the similarity, cost, and scale of the testing. Of key importance was to optimize the LSP process while eliminating the risk of subsurface crack nucleation and controlling part distortion. The building block approach, starting with simple coupons and progressing with complexity through each phase of the program, provided sufficient coupons and data to evaluate different parameters while controlling cost and schedule. The results from each phase were utilized to fine tune the LSP process in progressive steps.

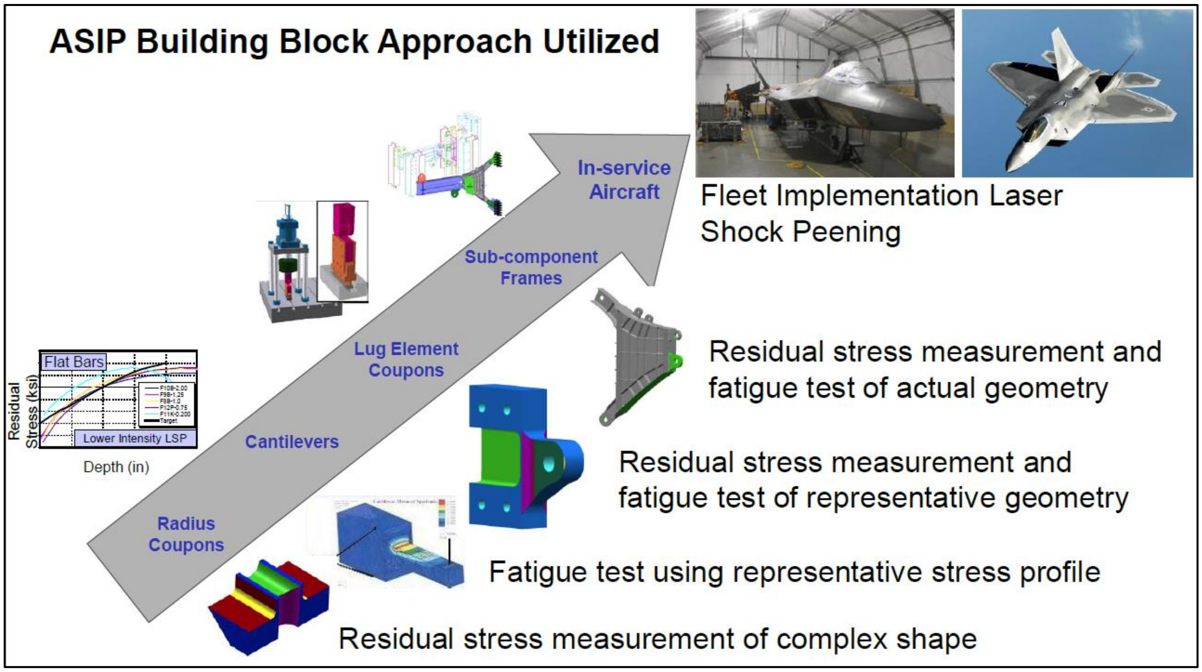

Figure 74 – Building block approach

21.3. *LSP optimization – residual stress engineering methods*

To complement the building block testing approach, residual stress engineering methods, including modeling and measurements, were utilized to drive efficiency and minimize costly coupon, component, and full-scale testing. Traditionally, key design variables are evaluated and honed with testing, driving up test replicates and costs, and limiting the ability to optimize the design. For the F-22 LSP program, new engineered residual stress tools were leveraged to quantify the residual stress and part distortion, iterating the LSP parameters, to efficiently optimize the design.

21.3.1. *Residual stress measurements*

Utilizing the contour method, residual stress profiles were determined for each progressive step throughout the building block approach. Figure 75 provides an overview of each step, with specific details on the geometry, the quantity of test articles, and the desired outcomes. Each step leveraged the findings from the previous steps and refined the LSP process to optimize the design.

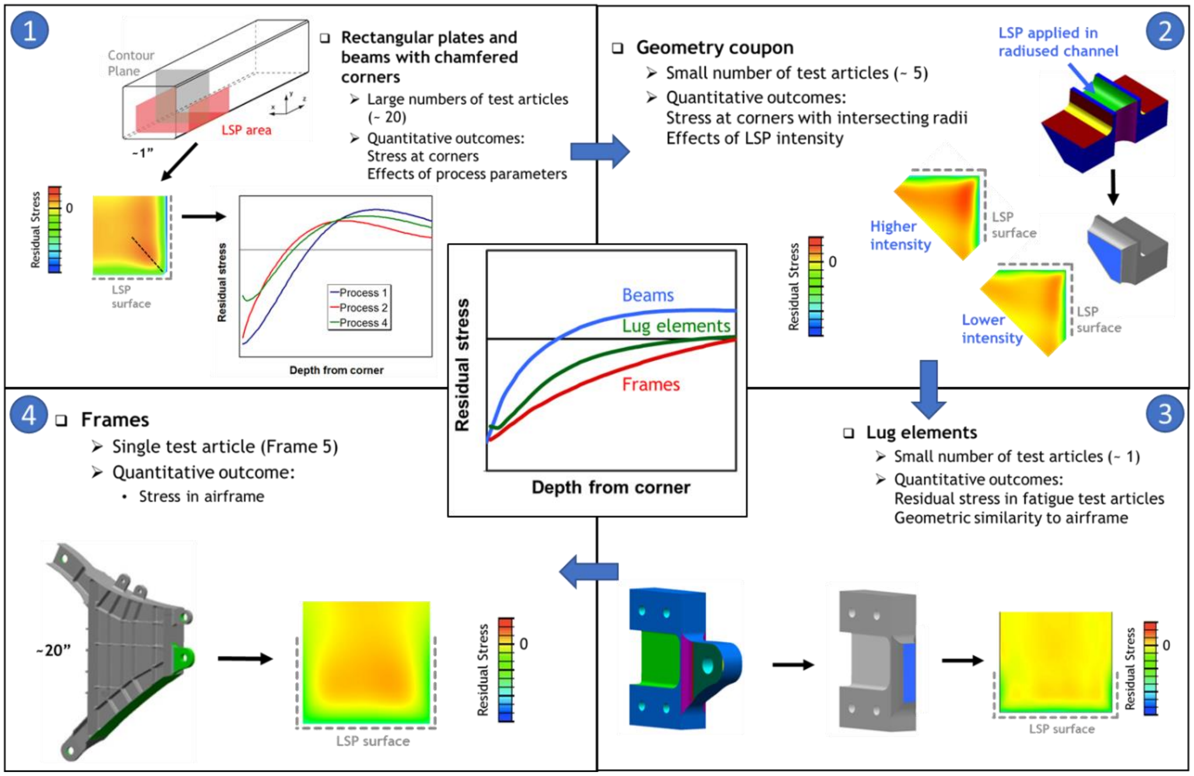

Figure 75 – Residual stress determination - building block approach

21.3.2. *Residual stress modeling*

Concurrent with the residual stress determination, residual stress predictions were completed utilizing an eigenstrain approach and the ERS-Toolbox^{TM}. Initial predictions, based on existing flat-plate residual stress characterizations, were blind for the geometry and lug element coupons. The modeling focused on identifying the key process parameters and their influence on the resulting residual stress profiles. Comparisons between the experimental evaluations and predictions enabled model updates to increase the accuracy of the eigenstrain approach. Figure 76 provides an example of the predicted versus measured residual stress. Ultimately, these predictions, coupled with the experimental residual stress characterizations, supported decisions for LSP parameters at each stage of testing and provided a framework to manage tradeoffs between more compressive stress (generally good) versus more tensile stress and distortion (generally bad). The predictions also facilitate efficient decisions on the optimum LSP intensities and processing areas.

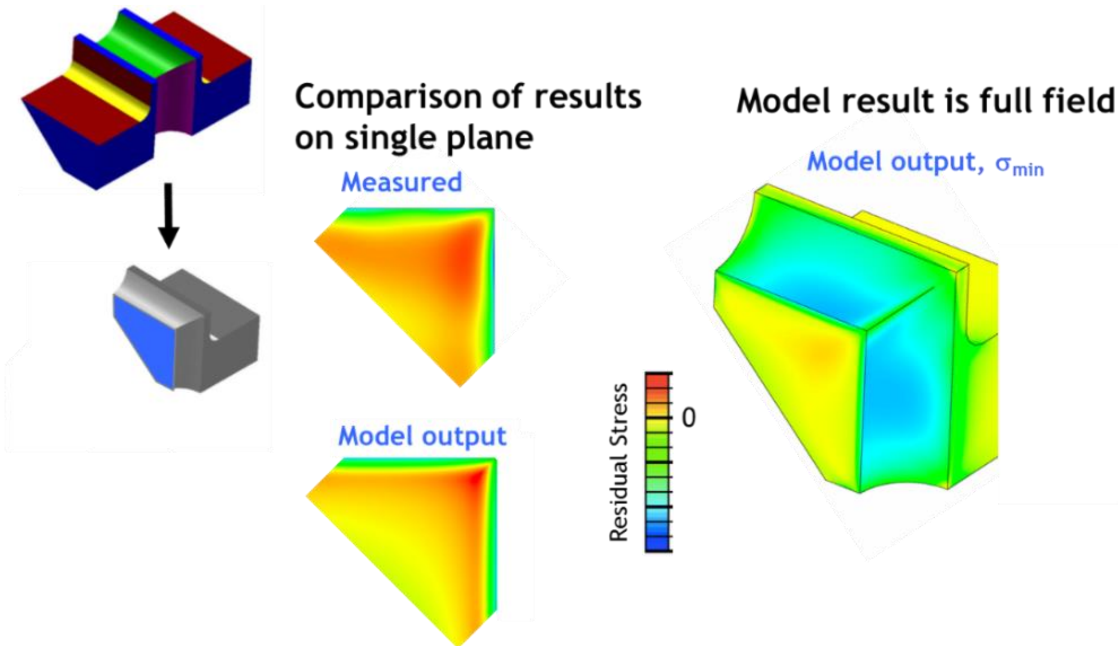

Figure 76 – Residual stress predictions versus measurement example

21.4. *Analytical prediction approach*

21.4.1. *Traditional analytical methods*

Concurrent with the testing and LSP parameter optimization, analytical methods and predictions were investigated to determine the analytical options for the problem. To establish a firm initial foundation, baseline crack growth life predictions were completed for the cracking locations. Traditional handbook models (corner-to-through crack in a plate) with idealized geometry and loading were utilized in the F-22 Damage Tolerance Assessment (DTA) and Force Structural Maintenance Plan (FSMP). These initial assessments significantly under-predicted the crack growth life and demonstrated the need for better analysis tools for complex geometry. Figure 77 provide an example of the modeling approach and baseline predictions versus experimental results.

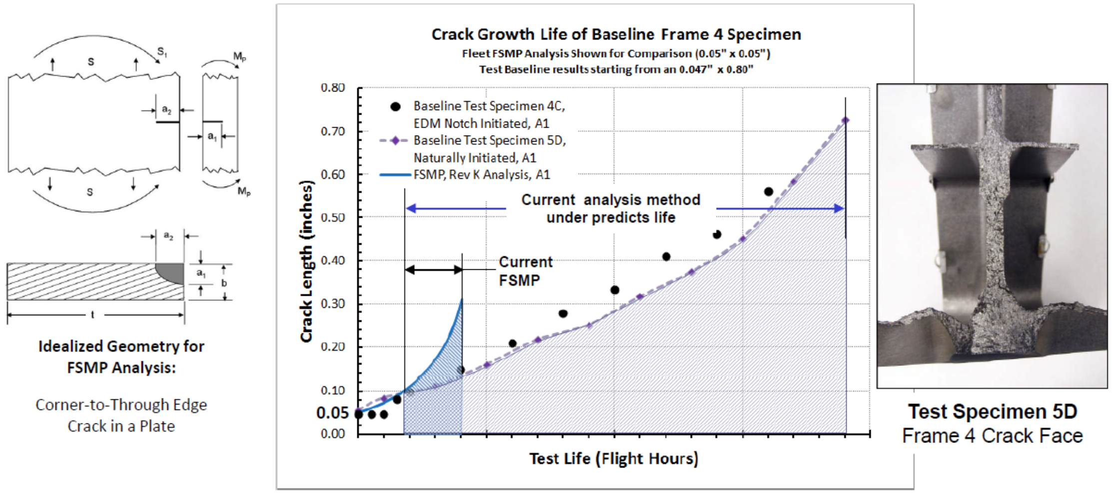

Figure 77 – Initial baseline crack growth predictions versus experimental results

21.4.2. ***Refined modeling approach***

Initial assessments made it evident that greater refinement in the analytical approach was necessary to accurately predict the baseline crack growth behavior, and ultimately, the LSP repair condition. The resulting approach focused on several key aspects, as shown in Figure 78. These aspects included: 1) utilizing BEASY, a 3D boundary element code, to model stress intensity factors with the capability to characterize 3D arbitrary crack shape evolution; and 2) direct inclusion of residual stress derived from the eigenstrain method (ERS Toolbox^{TM}) and validated with experimentally derived residual stress profiles utilizing the contour method. These aspects, combined with applied stress spectrum, material models, and assumed initial flaw, were utilized to predict stress, stress intensities, crack shape evolution, and crack growth life at the critical cracking locations. Load cases from remote loading and residual stress were combined using the linear superposition to calculated the net results.

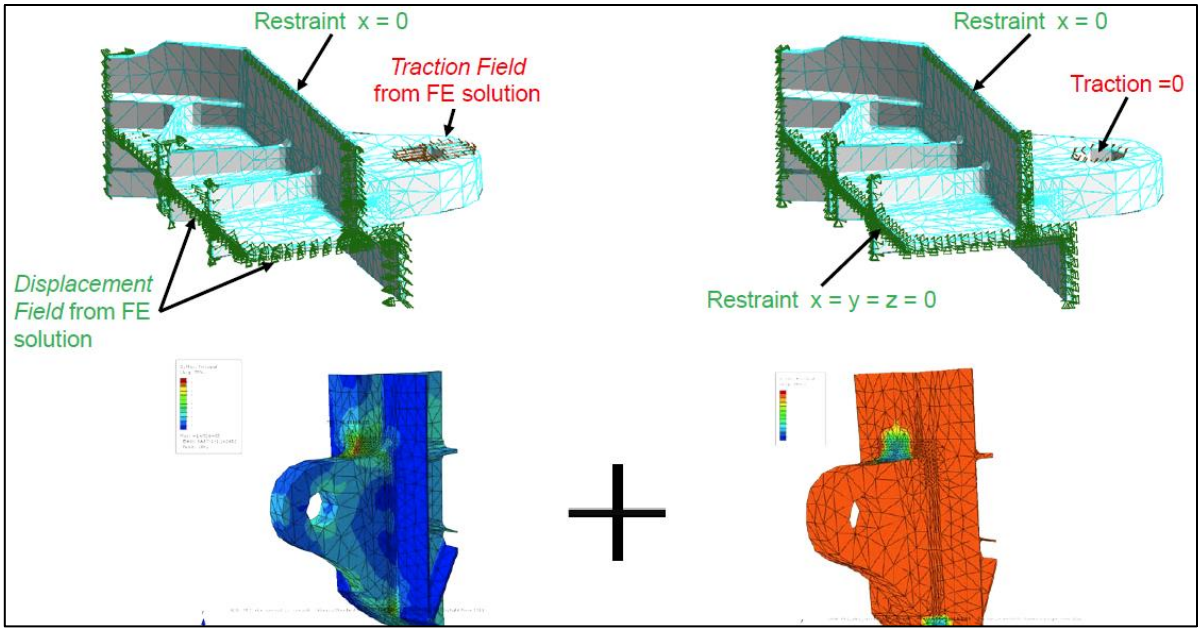

Figure 78 – (LH) Remote loading; (RH) residual stress loading

21.5. *Damage tolerance life results*

Damage tolerance comparisons between baseline and LSP were completed to assess the LSP benefits as well as understand the accuracy of the analytical predictions. Figure 79 provides an example comparison for a lug element condition, detailing baseline and LSP lives. One salient finding worth noting from the program was the influence of characterizing the crack shape evolution, and the influence on accurate predictions. Comparisons were completed for the new analysis approach and a classical analysis approach, assuming a quarter-ellipse crack shape, and incorporation of the residual stress with weight functions (see Figure 80). For the baseline predictions, the crack shapes observed in the tests and predictions were fairly consistent and nearly quarter-elliptical, resulting in accurate predictions for both analysis approaches. For the LSP condition, however, significant prediction differences were evident for the two analysis approaches. Because of the unique "ballooning" that occurs as a result of the greater residual stress at the surfaces, the classical approach assuming a quarter-ellipse crack front misrepresents the crack shape, and ultimately, significantly overpredicts the life observed in the tests. This is a primary example where the utility of multi-point capability is necessary to accurately characterize crack shape evolution and damage tolerant lives. Figure 81 details the predicted (new analysis approach) versus test crack shape evolution for the baseline and LSP conditions, with good agreement.

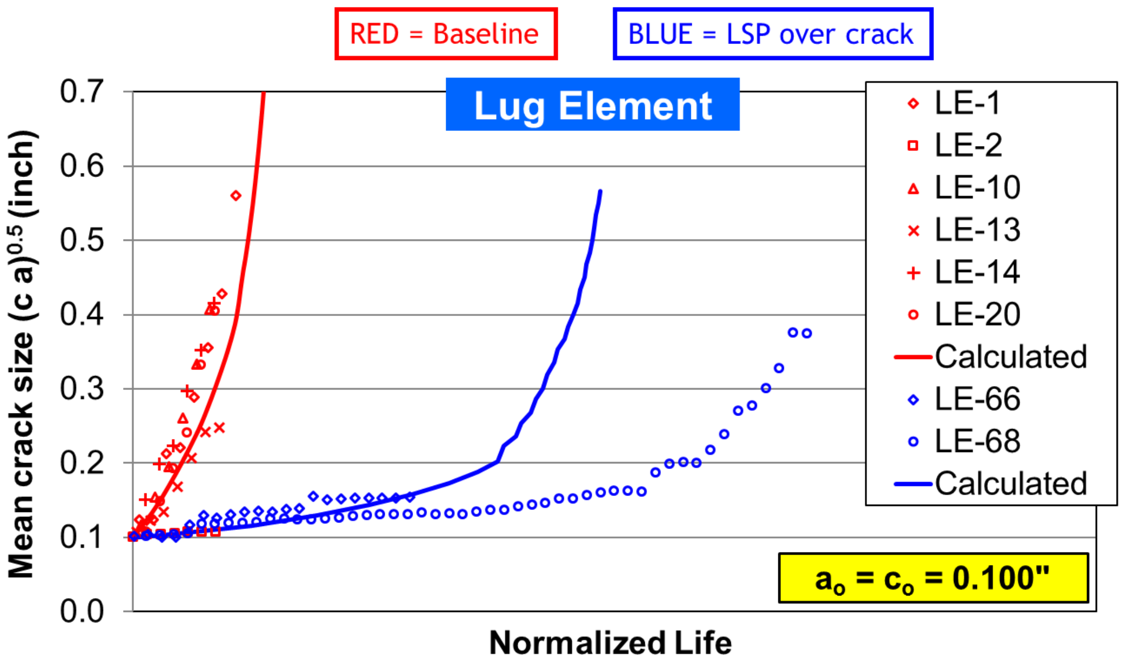

Figure 79 – Predicted versus test life examples

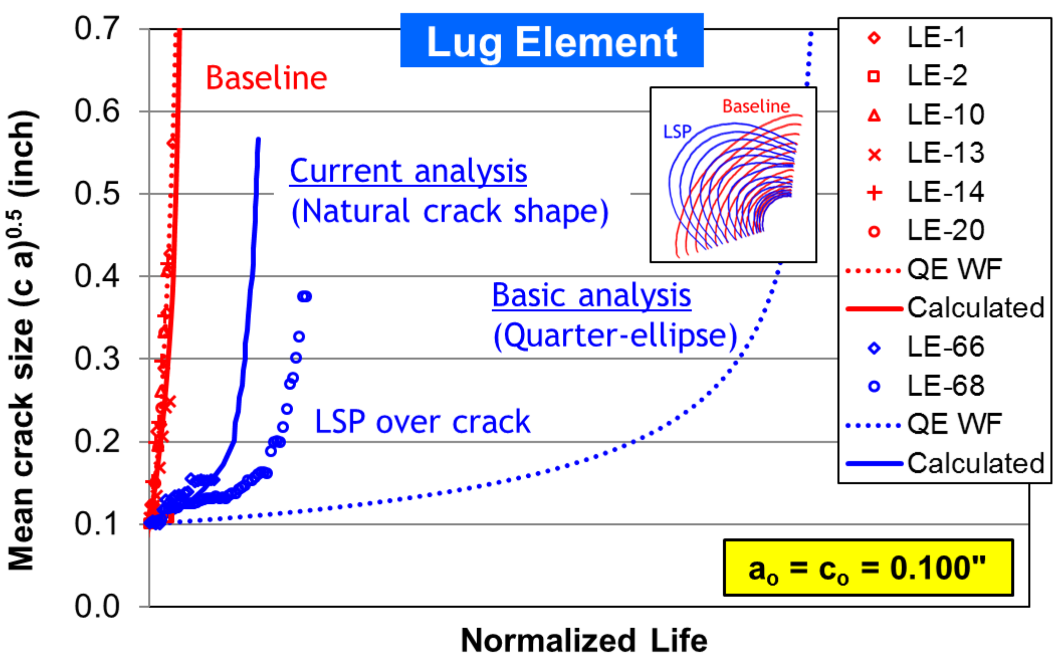

Figure 80 – Current versus typical handbook analysis

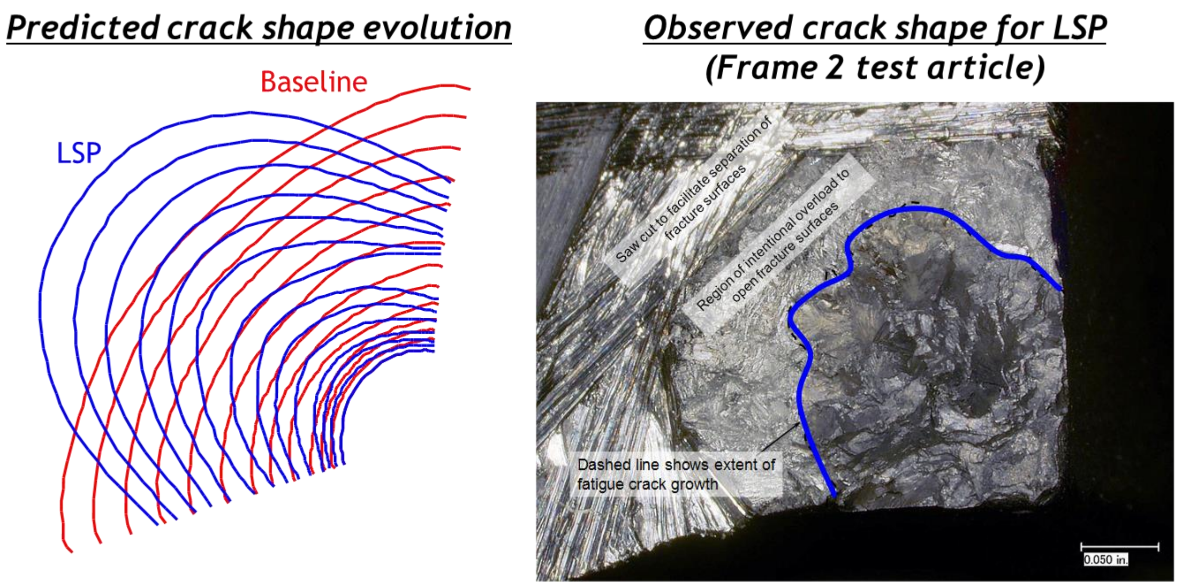

Figure 81 – Crack shape comparisons – prediction (new approach) versus test

21.6. *Results/conclusions*

The test, measurement, and analysis program successfully demonstrated the risk to the F-22 fleet is mitigated by LSP applied compressive stress. The building block approach demonstrated an efficient method to identify the key LSP processing parameters and ultimately certify the life improvement. The residual stress benefits were successfully quantified by eigenstrain predictions and residual stress measurements and validated with lug element and full-scale component tests. The end result, as shown in Figure 82, demonstrated significant inspection relief and maintenance cost savings for the F-22 fleet.

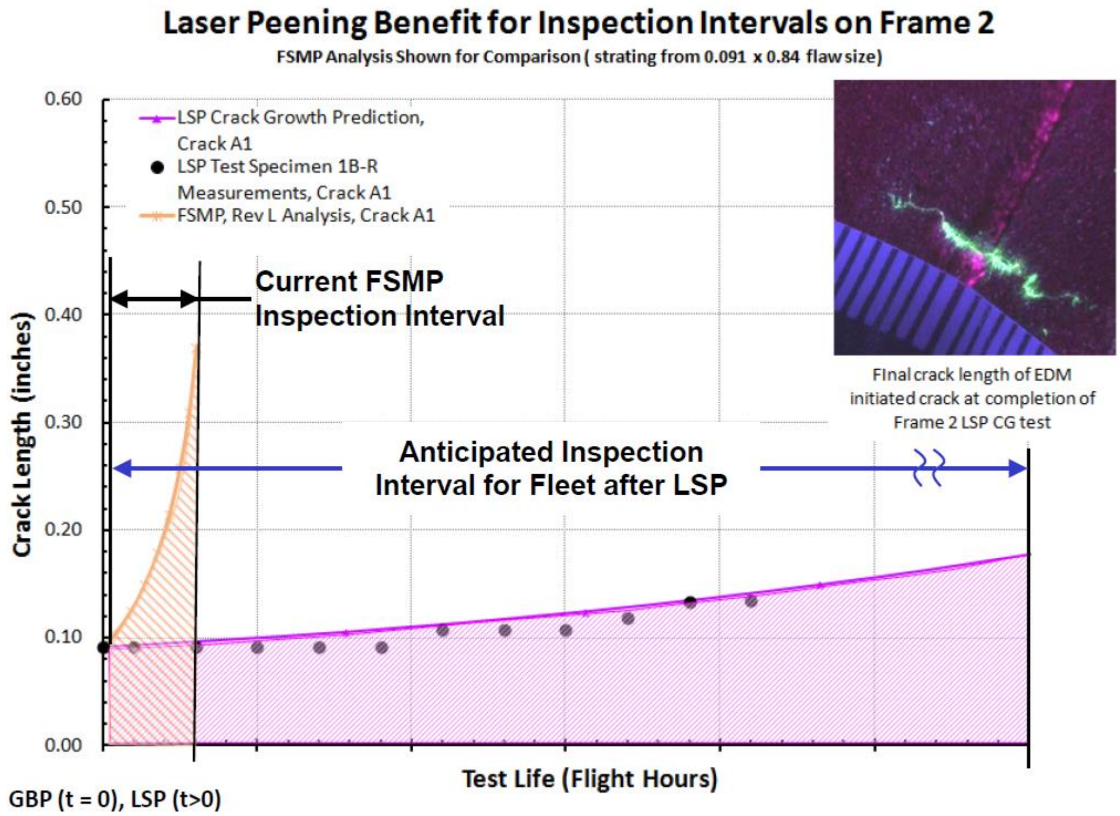

Figure 82 – Crack growth life and inspection interval benefits for F-22 LSP repair – test and prediction results.

22. *CASE STUDY #2 – A-10 Fuselage Upper Longeron Cold Expanded Holes*

22.1. *Background/issues*

The holes in the fuselage upper longeron strap on the A-10 are typically not cold expanded in production. In repair situations, some holes may be oversized. In order to restore the structure to equivalent strength, cold expansion was investigated as an option. In these scenarios, oversizing of the hole leads to edge distances well below the recommendations from FTI. This case study lays out the analytical and testing approach used to determine if cold expanding a short ED hole would provide enough of a life benefit.

22.2. *Highlights of analytical process*

The analytical process walks through several key components that should be considered when performing an analysis on a coldworked hole. Specifics on spectrum effects, load interaction, crack shape, multi-crack nucleation and residual stress development are discussed below.

22.3. *Spectrum loading and specimen design*

For this case study, the specimens were modified to accommodate existing tool sets and readily available materials. Key pieces of geometry were modified from the aircraft geometry to reduce the costs of the program (see Figure 83). The diameter and thickness were driven by available tools and materials and the edged distance was selected to keep the edge distance equivalent to the aircraft geometry. Two oversize repair scenarios were analyzed. For the repair diameter of 0.375-inch the coupons were modified to fall within the maximum and minimum values of the specification (~3 and 4% applied expansion). For the second oversize (0.4375-inch) only the maximum applied expansion was investigated.

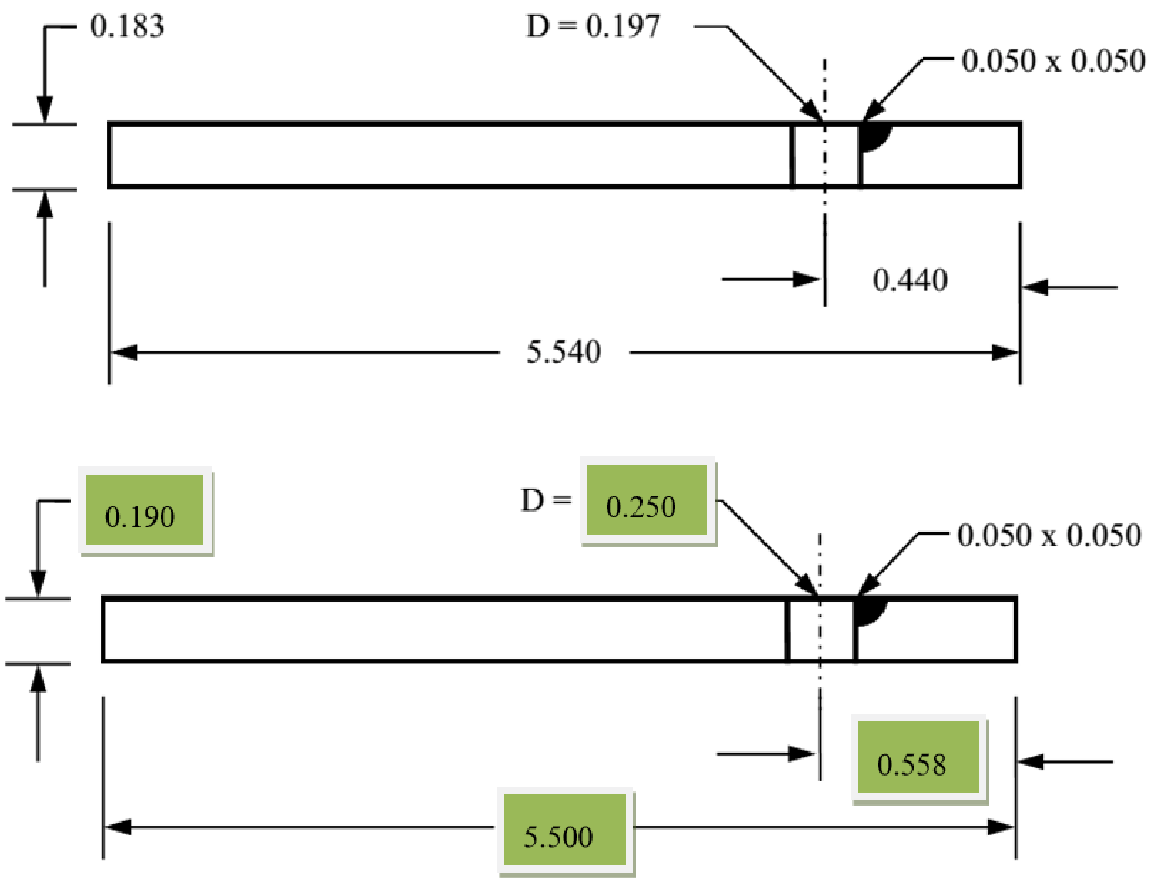

Figure 83 – Comparison of actual geometry (top) vs. specimen geometry (bottom)

The max spectrum stress identified for this case was 24.329 ksi. Previous tests showed some difficulty in generating fatigue failures from the hole, even with low edge margins. The decision was made to increase the spectrum to have a max peak stress of 28 ksi.

22.4. *Residual stress measurements/implementation*

Two contour method measurements for the different hole conditions were performed. These results were processed by adjusting the measurements so the data began at the origin (0,0), averaging left and right-hand side of each coupon, and then averaging similar specimens together. The processing method is outlined in section 4.6.1 of ref 60. All the data/fits are provided in the residual stress database discussed in Section 9.4.3.1.

The RS database outputs a multi-order polynomial which was applied to the StressCheck™ model using a normal crack face traction. Two load cases were built, one for the applied loads model and one for the residual stress.

22.5. *Crack shape comparisons*

Crack shape comparisons were made between the marker banded specimens and the analytical prediction. The marker banded specimens had several active secondary cracks growing during the test that are not modeled in the analytical predictions. Ignoring the complexities of secondary cracking the predictions matched the actual test shapes reasonably well.

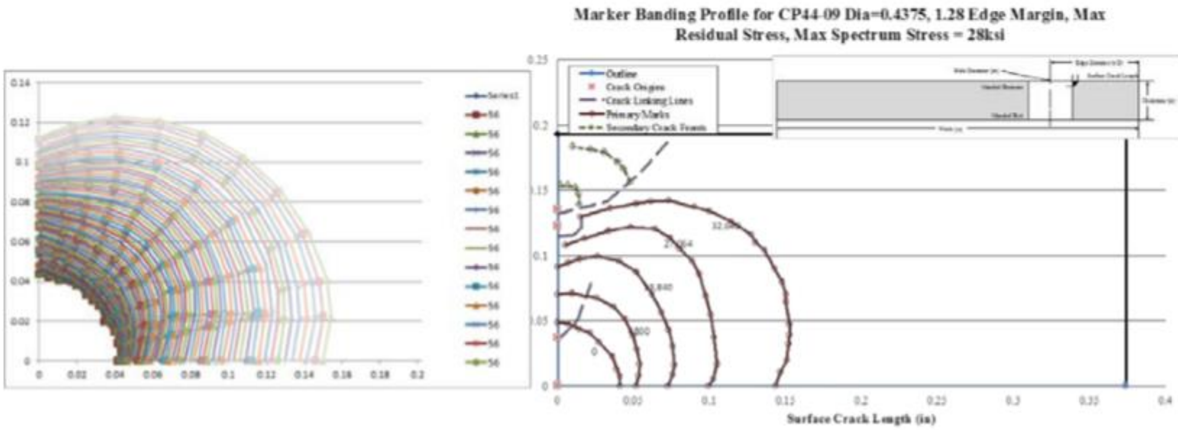

Figure 84 – (Left) Comparison of analysis crack growth and (right) marker banded specimen

22.6. *Legacy method comparisons*

Initial comparisons were made using legacy methods vs tests. For the max applied expansion on the 0.375-inch diameter hole, three analyses were performed: original geometry with no Cx, reduced IFS prediction (0.005” IFS), and a BAMF prediction. These comparisons are shown in Figure 85. The BAMF prediction outperformed the legacy analyses by a factor of 1.5 but did not used crack retardation.

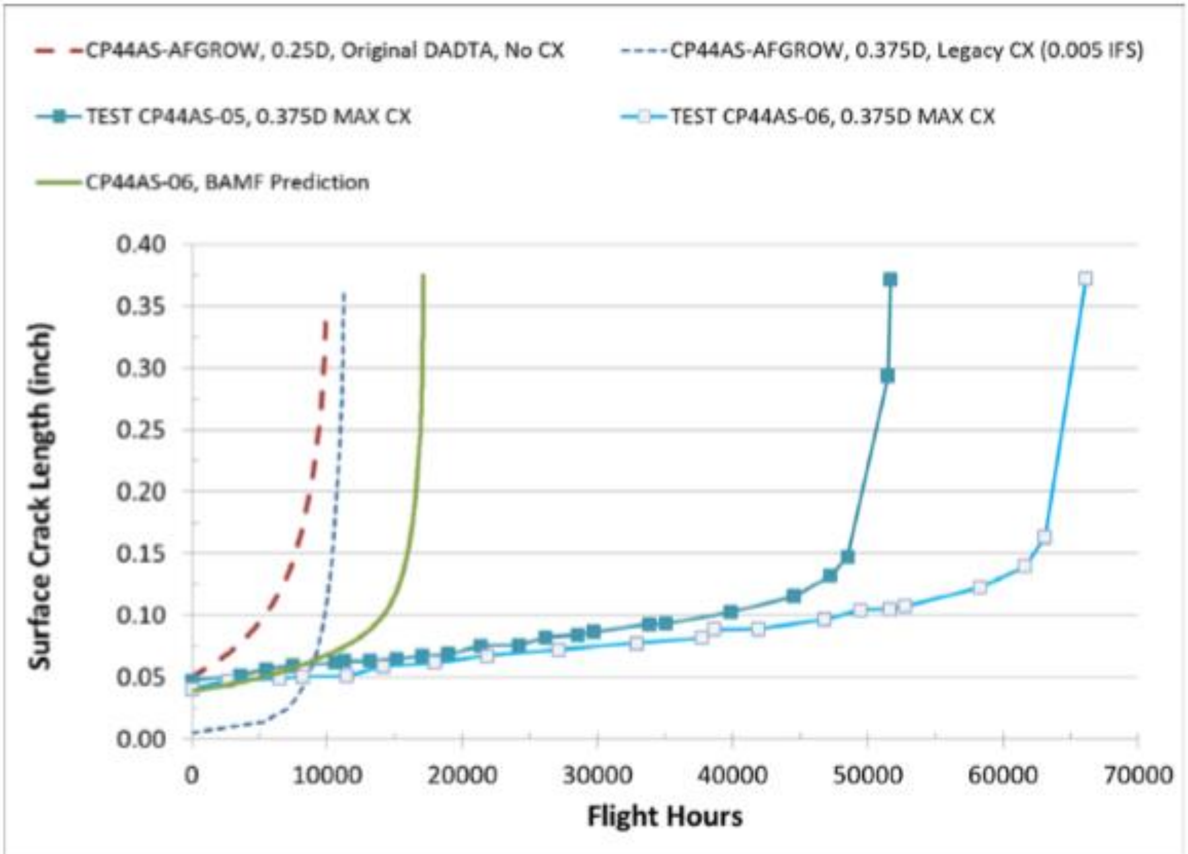

Figure 85 – Fatigue life comparisons and analytical predictions for max Cx condition

Similarly, evaluation was performed for the minimum applied expansion on the 0.375-inch diameter hole, which are documented in Figure 86. This time with (2) BAMF analyses performed. Each one showing different residual stress distributions. Again, neither of the BAMF analyses took account of crack retardation.

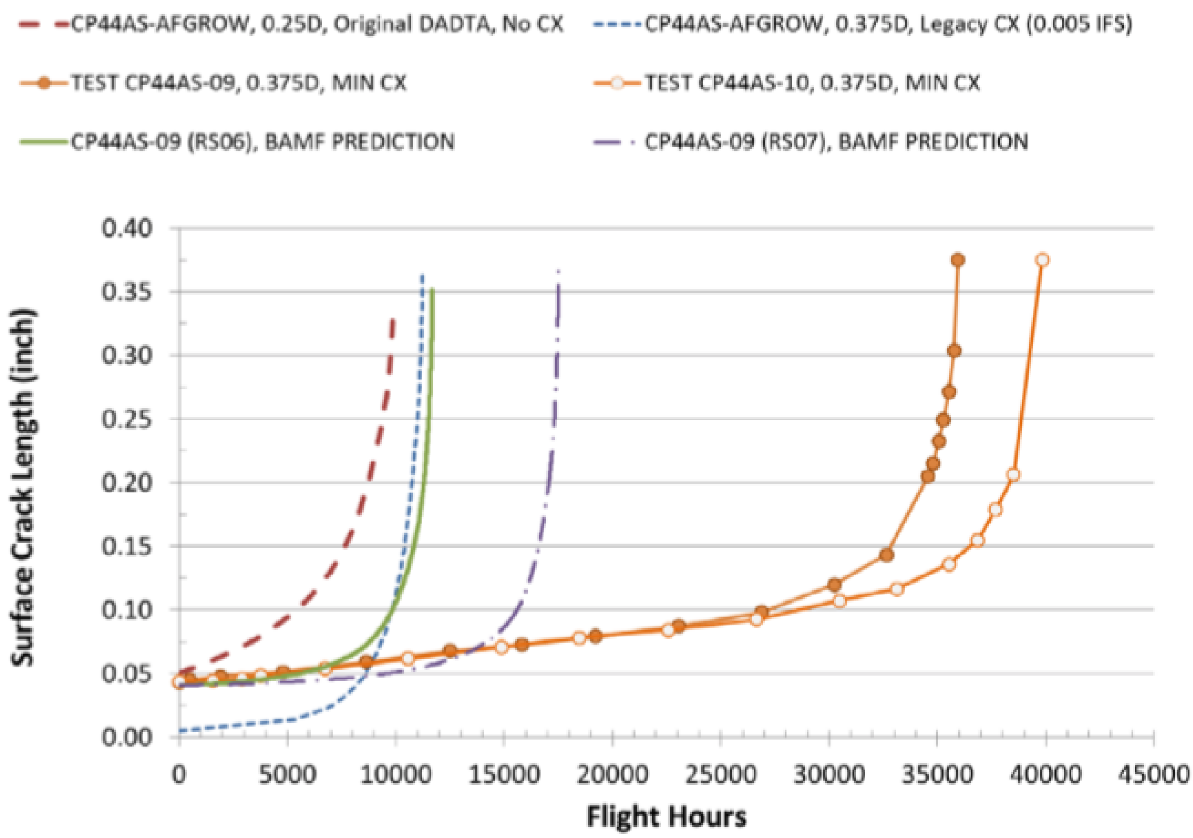

Figure 86 – Fatigue life comparisons and analytical predictions for min Cx condition

22.7. *Retardation effects*

The constant underpredicting of life led to investigating the inclusion of load interaction, or crack retardation, into the predictions. The betas developed in the baseline BAMF analysis were used in a User-Defined AFGROW model. This allowed the user to input the betas developed from the multi-point analysis into AFGROW and incorporate retardation into the prediction. It should be noted that load interaction would affect each point on the entire crack front differently and could affect how the shape of the crack evolves over time.

The pre-established Generalized Willenborg Shut-off Overload Ratio (SOLR) value for the baseline analysis (SOLR=1.6), which was previously developed from baseline spectrum fatigue tests, was utilized for the predictions. The results show good correlation with tests, however, a more detailed analysis directly incorporating retardation into the BAMF prediction should be investigated before making assessments regarding the validity of using established retardation models/values with residual stress are incorporated into damage tolerance assessments.

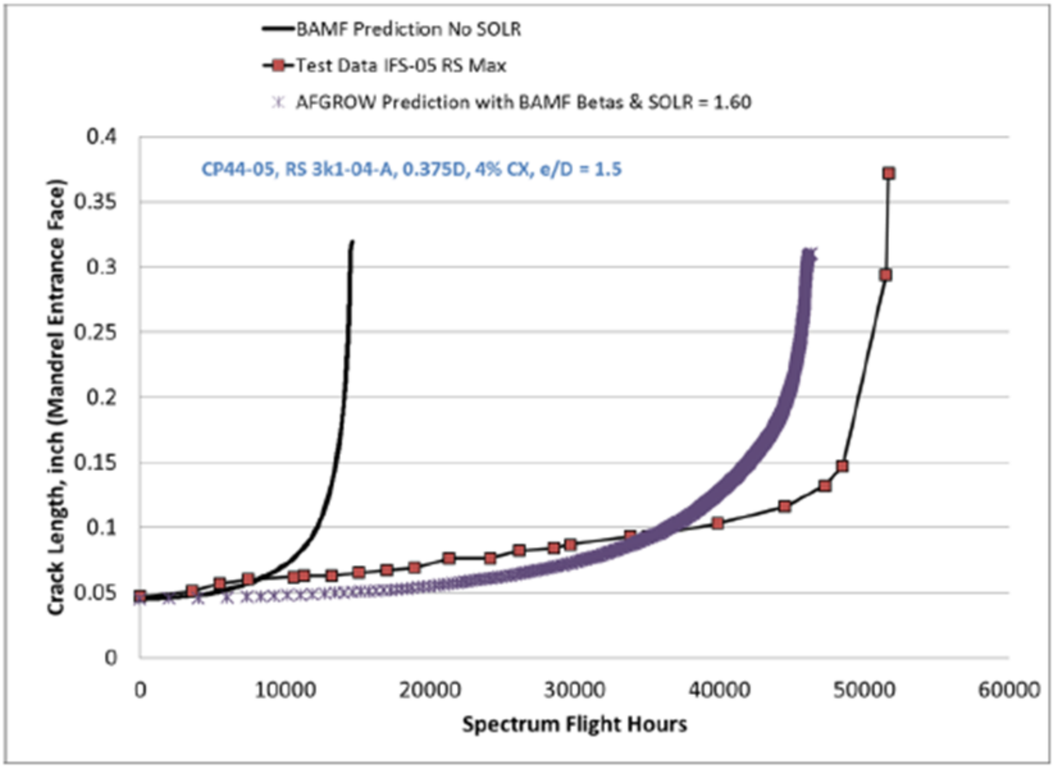

Figure 87 – Fatigue life comparisons and analytical predictions for max Cx condition with load interaction.

22.8. *Conclusions/findings*

The outlined approach demonstrated an approach to incorporate residual stress into damage tolerance assessments and provided comparisons to fatigue test results. Load interaction models with residual stress merit additional investigation to understand the appropriate applications. Often, the benefits of Cx holes relative to baseline lives are significant enough that accounting for crack retardation benefits isn't necessary. Nevertheless, this continues to be a key focus area to address in future research.

REFERENCES

1 Schutz, W. (1996). A History of Fatigue, Engineering Fracture Mechanics, Vol 54.

2 Albert, W. (1837). Uber Treibseile am Harz. Archiv fur Mineralogie, Georgnosie, Bergbau und Huttenknde 10, 215-234.

3 Braithwaite, F. (1854). On the fatigue and consequent fracture of metals. Institution of Civil Engineers, Minutes of Proceedings, Vol. XIII, pp. 463-474, London.

4 Smith, R. (1990). The Versailles railway accident of 1842 and the first research into metal fatigue, in Fatigue ’90, Vol. IV, EMAS, Birmingham.

5 Griffith, A. (1920). The Phenomena of Rupture and Flow of Solids, Trans. Roy. Soc., London, Vol. A221, p. 163.

6 Palmgren, A. (1924). Die Lebensdauer von Kugellagern, ZDVDI, Vol. 68, No. 14, p.339.

7 Langer, B. (1937). Fatigue failure from stress cycles of varying amplitude, Trans. ASME J. appl. Mech, 59, A160-A162.

8 Miner, M. (1945). Cumulative damage in fatigue. Trans. ASME J. appl. Mech. 12, A159-A164.

9 Irwin, G. (1957). Analysis of Stresses and Strains Near the End of a Crack Traversing a Plate, Trans. ASME, J. Appl. Mech. Vol. 24, p.361.

10 Paris, P. (1961). A Rational Analytical Theory of Fatigue, Trend Eng., Vol. 13, No. 9, p. 9.

11 HOLSIP (2017). Holistic Structural Integrity Process, http://www.holsip.com

12 Almen, J.; Black, P. (1963). Residual Stresses and Fatigue in Metals. New York: McGraw-Hill Book Company.

13 Stephens, R. (2001). Metal Fatigue in Engineering, Second Edition, Wiley Inter-science.

14 Schijve, J. (2001). Fatigue of Structures and Materials, Kluwer Academic Publishers.

15 Walz, K. (1941). Federfragen Insbesondere aus dem Gebiet der Zeitfestigkeit bei Sinusformiger und Schlagartiger Beanspruchung, Mauser.

16 Metal Improvement Company (2007). Shot Peening. http://metalimprovement.com/shot_peening.php

17 Haywood, R. (1962). Designing Against Fatigue of Metals, Reinhold, New York.

18 Migala, T.; Jacobs, T. Low Plasticity Burnishing: An Affordable, Effective Means of Surface Enhancement. Cincinnati: Surface Enhancement Technologies

19 Reid, L. ; Fatigue Technology Inc. Incorporating Hole Cold Expansion to Meet

Durability and Damage Tolerance Airworthiness Objectives.

20 West Cost Industries. (1997). Split Mandrel Coldworking-Holes (Aluminum) Engineering Handout WCI-9202-6.1.

21 Skeen, C.; York, C., (1968). Laser-induced "blow-off" phenomena, Applied Physics Letters, 12(11), pp. 369-371.

22 O'Keffe, J.; Skeen, C., (1972) Laser-induced stress-wave and impulse augmentation, Applied Physics Letters, 21(10), pp. 464-466.

23 Fairand, B.; Wilcox, B.; Gallagher, W.; Williams, D., (1972). Laser shock-induced microstructural and mechanical property changes in 7075 aluminum, Journal of Applied Physics, 43(9), pp. 3893-3895.

24 Hill, M.; DeWald, A.; Demma, A.; Hackel, L.; Chen, H.; Dane, C.; Specht, R.; and Harris, F., (2003). Laser peening technology, Advanced Materials and Processes, 161(8), pp. 65-67.

25 Peyre, P.; Fabbro, R.; Merrien, P.; Lieurade, H., (1996), Laser shock processing of aluminium alloys. Application to high cycle fatigue behaviour, Materials Science and Engineering A, 210(1-2), pp. 102-113.

26 Peyre, P.; Braham, C.; Ledion, J.; Berthe, L.; Fabbro, R., (2000), Corrosion reactivity of laser-peened steel surfaces, Journal of Materials Engineering and Performance, 9(6), pp. 656-662.

27 Zhuang, W.; Halford, G., (2001), Investigation of residual stress relaxation under cyclic load, International Journal of Fatigue, 23, pp. S31-S37.

28 Montross, C.; Florea, V.; Swain, M., 2001, "The influence of coatings on subsurface mechanical properties of laser peened 2011-T3 aluminum," Journal of Materials Science, 36, pp. 1801-1807.

29 Fabbro, R.; Fournier, J.; Ballard, P.; Devaux, D.; Virmont, J., (1990) Physical study of laser-produced plasma in confined geometry, Journal of Applied Physics, 68(2), pp. 775-784.

30 Schmidt-Uhlig, T.; Karlitschek, P.; Yoda, M.; Sano, Y.; Marowsky, G., (2000). Laser shock processing with 20 MW laser pulses delivered by optical fibers, The European Physical Journal - Applied Physics, 9, pp. 235-238.

31 DeWald, A.; Rankin, J.; Hill, M.; Lee, M.; and Chen, H., (2004). Assessment of tensile residual stress mitigation in Alloy 22 welds due to laser peening, Journal of Engineering Materials and Technology, 126(4), pp. 465-473.

32 Tenaglia, R.; Lahrman, D.; LSP Technologies Inc., (2003) Preventing Fatigue Failures with Laser Peening, AMPTIAC Quarterly, 2 ed.

33 Scientific Electronic Library Online, (2007). http://www.scielo.br

34 Prevey, P.; Lambda Research, The Effect of Cold Work on the Thermal Stability of Residual Compression in Surface Enhanced IN718.

35 Department of Defense (2006). DoD Joint Service Specification Guide, Aircraft Structures, USA.

36 Air Force Lifecycle Management Center, (2017). Testing and Evaluation Requirements for Utilization of an Equivalent Initial Damage Size Method to Establish the Beneficial Effects of Cold Expanded Holes for Development of the Damage Tolerance Initial Inspection Interval, EN-SB-17-001.

37 Babish, C., (2017). Aircraft Structural Integrity Program (ASIP) Perspective on Accounting for Engineered Residual Stress in Damage Tolerance Analysis, 2017 ASIP Conference, Jacksonville, FL.

38 Air Force Lifecycle Management Center, (2018). In-Service Inspection Crack Size Assumptions for Metallic Structures, EN-SB-08-012 Revision D.

39 Phillips, J., (1974). Sleeve Cold Working Fastener Holes, Vol. 1. AFML-TR-74-10, Air Force Materials Laboratory, Wright-Patterson AFB, OH.

40 Petrak, G.; Stewart R., (1974). Retardation of cracks emanating from fastener holes. Eng Fract Mech, 6(2):275-282.

41 Toor, P., (1976). Cracks emanating from precracked coldworked holes. Eng Fract Mech: 8; 391-395.

42 Ball, D., (1995). Elastic-plastic stress analysis of cold expanded fastener holes. Fatigue Fract Engng Mater Struct 1995;18(1):47-63.

43 Kokaly M.; Ransom J.; Jude B.; Restis, H.; Reid, L., (2005). Observations and analysis of fatigue crack growth from cold worked holes. Proceedings of the 8th Joint FAA/DoD/NASA Aging Aircraft Conference, Palm Springs, CA.

44 Carlson, S., (2008). Application of β corrections to model and predict fatigue crack growth at cold expanded holes in 2024-T351 aluminum alloys. M.S. Thesis, Univ of Utah.

45 Pilarczyk, R., (2008). Beta corrections to predict fatigue crack growth at cold expanded holes in 7075-T651 aluminum alloy. M.S. Thesis, Univ of Utah.

46 Reid, L.; Fatigue Technologies Inc., (2000). Incorporating Hole Cold Expansion to Meet Durability and Damage Tolerance Airworthiness Objectives. Fatigue Technologies Inc., Seattle, WA, USA.

47 Ozelton, M.; Coyle, T., (1983). Investigation of Fatigue Life Improvement by Cold Working of Holes in Aircraft Material, Northrop Corp. Final Report for Contract N00019-82-C-0364.

48 Warner, J., (2012). Cold Expansion Effects on Cracked Fastener Holes Under Constant Amplitude and Spectrum Loading in the 2024-T351 Aluminum Alloy, Master of Science Thesis, University of Utah.

49 Kokaly, M.; Ransom, J.; Restis, J.; Reid, L., (2002). Prediction fatigue crack growth in the residual stress field of a cold worked hole. Journal of Testing and Evaluation. **20**, 1-15.

50 Cathey, W.; Grandt, A., (1980). Fracture mechanics consideration of residual stresses introduced by coldworking fastener holes. Journal of Engineering Materials and Technology. **102**, 85-91.

51 Chandawanich, N.; Sharpe, W., (1979). An experimental study of fatigue crack growth initiation and growth from cold worked holes. Engineering Fracture Mechanics. **11**, 609-620.

52 Ball, D.; Lowry, D., (1998) Experimental Investigation on the effects of cold expansion of fastener holes. Fatigue Fract. Engng Mater. Struct. **21**, 17-34.

53 Underwood, J.; Pook, L.; Sharples, J., (1977). Fatigue-crack propagation through a measured residual stress field in alloy steel. Flaw Growth and Gracture, ASTM STP 631. American Society for Testing and Materials, pp. 402-215.

54 Kapadia, B. (1978). Influence of residual stresses on fatigue crack propagation in electroslag welds. Fatigue Testing of Weldments, ASTM STP 648, Hoeppner DW, editor. American Society for Testing and Materials, pp. 244-260.

55 Nelson, D. (1982). Effects of residual stress on fatigue crack propagation. Residual Stress Effects in Fatigue, ASTM STP 776. American Society for Testing and Materials, pp. 172-194.

56 Lam, Y.; Lian, K., (1989). The effect of residual stress and its redistribution on fatigue crack growth. Theor Appl Frac Mech;12(1):59-66.

57 Parker, A. (2004). A critical examination of Sachs' material-removal method for determination of residual stress. J Pressure Vessel Technol Trans ASME;126(2):234-236.

58 Saunder, T.; Grandt, A., (2000). The Effect of Edge Distance on Cold Working Fastener Holes. Proceeding of the Fourth Joint DoD/FAA/NASA Conference on Aging Aircraft, St. Louis, Missouri.

59 Jones, K., (2009). Predicting Fatigue Crack Growth Through Residual Stress Fields, PhD Dissertation, University of Colorado.

60 Mills, T.; Honeycutt, K.; Prost-Domasky, S.; Brooks, C., (2015). Integrating residual stress analysis of critical fastener holes into USAF depot maintenance, Air Force Life Cycle Management Center, AFLCMC/WWAEJ, Hill AFB, UT 84056.

61 Mura, T. (1987). Micromechanics of Defects in Solids, 2nd Edition. Lancaster, Martinus Nijhoff Publishers.

62 DeWald. A.; Hill, M., (2009). Eigenstrain based model for prediction of laser peening residual stresses in arbitrary 3D bodies: Part 1 model description. *The Journal of Strain Analysis for Engineering Design, 44*(1), pp. 1-11

63 DeWald. A.; Hill, M., (2009). Eigenstrain based model for prediction of laser peening residual stresses in arbitrary 3D bodies: Part 2 model verification. *The Journal of Strain Analysis for Engineering Design, 44*(1), pp. 13-27

64 Afazov S.; Becker A.; Hyde, T., (2012). Mathematical Modeling and Implementation of Residual Stress Mapping from Microscale to Macroscale Finite Element Models. *Journal of Manufacturing Science and Engineering*, 134(2), pp. 1-11.

65 Hill Engineering, Broad Application for Modeling Failure – User's Guide (2018),

Release 5.0.

66 Engineering Software Research & Development, Inc. (2017). StressCheck Master Guide, Release 10.3.

67 Pilarczyk, R.; Morrison, C.; Hodges, J. (2016). Benchmark Problems in Fatigue Crack Growth Analyses, AFGROW Workshop 2016, Layton UT.

68 Mills, T.; Fawaz, S. (2017). AFGROW Round Robin, Corner Crack at Center and Offset Holes, Proceedings from the 2017 AFGROW User Group Workshop.

69 Harter, J. (2018). Case Study on Test/Prediction Correlation for Corner Cracks at Holes, Proceedings from the 2018 Aircraft Airworthiness & Sustainment Conference, Jacksonville, FL.

70 Olson, M.; DeWald, A.; Hill, M., (2018). Validation of a Contour Method Single-Measurement Uncertainty Estimator, Experimental Mechanics.

71 Northrop Grumman Corporation, (2013). Residual Stress Measurements for the A-10 Thunderbolt Life-cycle Program Support (TLPS) ASIP Modernization III, Crack Growth Analysis in Residual Stress Fields, NG-0016-00030008-12-PLN.

72 Northrop Grumman Corporation, (2015). Residual Stress Measurements for the A-10 Thunderbolt Life-cycle Program Support (TLPS) ASIP Modernization V, Crack Growth Analysis in Residual Stress Fields, NG-0020-A10-00030014-15-RPT-A.

73 Northrop Grumman Corporation, (2018). Residual Stress Measurements for the A-10 Thunderbolt Life-cycle Program Support (TLPS) ASIP Modernization VI, Crack Growth Analysis in Residual Stress Fields, HE-R-050818.

74 Surface Engineering, Volume 5, ASM Handbook, (1994). Materials Park, OH, ASM International.

75 Mills, T.; Prost-Domasky, S.; Hodges, J. (2017). Residual Stress Redistribution and Applied Stress Ratio Effects, Proceedings from the 2017 Aircraft Airworthiness & Sustainment Conference, Phoenix, AZ.

76 Carlson, S. (2018). Quantifying the Effect of a Fatigue Crack on the Residual Stress Field Induced by the Split Sleeve Cold Expansion Process in 2024-T351 and 7075-T651 Aluminum Alloys, Doctor of Philosophy, Univ of Utah.

77 Pilarczyk et al. (2018). Residual Stress Evaluation in Legacy Aircraft Cold Expanded Fastener Holes, Proceedings from the 2018 Aircraft Airworthiness & Sustainment Conference, Jacksonville, FL.

78 Hill Engineering, LLC. (2017). Analytical Tools for Design/Life Prediction of Aircraft Structural Components with Engineered Residual Stress, Part II: Cold expanded hole teardown, HE-R-120717.

79 Harding, C.; Hugo, G.; Bowles, S. (2006); Model-Assisted POD for Ultrasonic Detection of Cracks at Fastener Holes, Presented at RPQNDE 2005. In ASIP Conference Proceedings (Vol. 820, p. 1862).

80 Fahr, A; Forsyth, D., (1997) Pod Assessment Using Real Aircraft Engine

Components, Review of Progress in QNDE, Vol. 17.

81 Brausch, J.; Stubbs, D., (2017) Effects of Laser Shock Peening (LSP) on Eddy Current, Fluorescent Penetrant and Ultrasonic Inspection of 7050-T7451 Aluminum (Nondestructive Evaluation), United States Air Force Research Lab, Report AFRL/RXS 17-038.

82 NDT Education Resource Center, (2001-2014). The Collaboration for NDT Education, Iowa State University, www.ndt-ed.org.

83 Department of Defense (2016) Aircraft Structural Integrity Program, USA.

84 Pilarczyk, R.; (2017); Analytical Methods Subcommittee: Overview of Recent Efforts, Proceedings from the 2017 Engineered Residual Stress Implementation Workshop 2017, Layton, UT.

85 Polin, L.; Bunch, J.; Caruso, P.; McClure, J., (2011). F-22 Program Full Scale Component Tests to Validate the Effects of Laser Shock Peening, 2011 ASIP Conference

86 Hill, M.; DeWald, A.; VanDalen, J.; Bunch, J.; Flanagan, S.; Langer, K. (2012). Design and analysis of engineered residual stress surface treatments for enhancement of aircraft structure, 2012 ASIP Conference